

(Title)

**The Effect of Pressure on
Arsenic Diffusion in Germanium**

A thesis presented

by

Salman Mitha

to

The Division of Applied Sciences
in partial fulfillment of the requirements
for the degree of
Doctor of Philosophy
in the subject of
Applied Physics

Harvard University
Cambridge, Massachusetts
June 1995

(Copyright)

© 1995 by Salman Mitha.
All rights reserved.

(Dedication)

Acknowledgments

I would like to thank my advisor Prof. Mike Aziz for assigning me this great project where I could play with all these wonderful toys, especially the SIMS. I am also very grateful to Mike for the many hours of insightful debate during group meetings, for his patience in explaining science, for constantly providing encouragement and for maintaining the funding for the project even when nothing seemed to work. I would like to thank Prof. Frans Spaepen for being such a great teacher and keeping me alert. Even though Frans's lectures seemed to go twice as fast as they should, I was always surprised how clear the material seemed afterwards. I would like to especially thank Prof. David Turnbull for always having time for me and for answering all those questions that nobody else would or could answer.

I would like to thank Dr. David Schiferl for teaching me the high temperature diamond cell technique; it is an honor to have been taught by a leading authority in the field. I am also grateful to Dave for his hospitality at Los Alamos and for the so many the wonderful stories. I would like to thank Dr. David Poker for the ion implanting he did for me and for his hospitality when I went to Oak Ridge to prepare samples.

I would like to thank Steve Theiss for his part in the setting up of the diamond cell. Steve is my good friend and lab partner and without his help this experiment would never have been completed. I am also very grateful to Bill Carter being a very good friend and a great help during the waning days of my thesis work, which included the proofreading of this thesis (except for the Acknowledgments).

I would like to thank my good buddy Guo-Quan Lu for introducing me to the secrets of life at McKay and making those first few years so much more pleasant than they otherwise would have been. I also would like to thank Jenny Devaud for teaching me the 'manly' art of operating the piston cylinder press. I am very grateful to Pat Smith and Dave Hoglund for being such

wonderful neighbors and allowing me to use their laser for my project. I also wish to thank all the other grad students and post-docs who made life at McKay so enjoyable.

I would like to thank the late John Martin for his tremendous help on the SIMS analysis, for taking the time to teach me how run the SIMS and for the rousing political debates. He will be sorely missed. I am also very grateful to Libby Shaw for her assistance during my trips to MIT. I would like to thank John Chervinsky for his assistance on the RBS. I am also grateful to Bob Graham for keeping things running smoothly at McKay.

I would like to thank Joe Bell and Frank Molea for the tremendous support they provided, technical and otherwise. Joe has been threatening to retire and I am glad that I finished before he left. I would like to thank Louis Defeo for making the diamond cell and then running the shop as it should be run. I would like to thank Ralph Genarazzo and Joan for running what is probably the best purchasing department I will ever see.

I would like to thank Barbara Sewall for all her assistance and her great attitude towards life. I would like to thank Pauline Mitchell and Sandra Godfrey for truly caring about the students and for protecting us from the vagaries of Holyoke Center.

I would like to thank my parents for their never-ending support even when the thesis seemed never-ending. Finally I want to thank my wife for her love and support during it all.

Abstract

We have measured the effects of pressure on arsenic diffusion in crystalline germanium. For this purpose we developed and built a high temperature high pressure diamond anvil cell (DAC) system. The samples are prepared by ion implantation and crystallinity is restored by solid phase epitaxial growth (SPEG). The samples were annealed in the DAC with fluid argon as the pressure medium. All the anneals were done at a temperature of 575 °C and pressures ranging from 0.1 GPa to 4 GPa. The pressure was measured at the anneal temperature by using the peak shift of Sm:YAG fluorescence as the pressure indicator. Diffusivity was measured by sputter sectioning using a secondary ion mass spectrometer (SIMS). We find that pressure slightly enhances the diffusivity of arsenic in germanium and measure an activation volume of $-1.7 \pm 1.4 \text{ cm}^3/\text{mole}$ or $-0.12 \pm 0.1 \Omega_{\text{Ge}}$ where Ω_{Ge} is the atomic volume of germanium. The implications of this result on the diffusion mechanisms in germanium are discussed and we conclude that it is unlikely that arsenic diffuses in germanium via the simple vacancy mechanism.

Table of Contents

Acknowledgments.....	iv
Abstract.....	vi
Table of Contents.....	vii
List of Figures	ix
List of Tables	xi
1. Introduction.....	1
2. Theory of Diffusion Mechanisms	5
2.1 The Phenomenology of Diffusion.....	5
2.2 Diffusion Mechanisms.....	6
2.3 Basic Rate Theory.....	10
2.4 Effect of Pressure on Diffusion.....	15
3. Survey of Diffusion in Silicon and Germanium.....	20
3.1 Ambient pressure diffusion in Silicon and Germanium.....	20
3.2 First-principles calculations for diffusion in Silicon.....	26
3.3 The Effect of pressure on self-diffusion in Germanium.....	28
3.4 Effect of Pressure on diffusion in Silicon.....	32
4. Experimental Techniques	36
4.1 Introduction.....	36
4.2 Early work.....	37
4.3 Sample Preparation.....	41
4.3.1 Goals	41
4.3.2 Preparation Technique.....	41
4.4 Generating Pressures	44
4.4.1 Design Goals	44
4.4.2 DAC.....	46
4.4.3 Furnace.....	52
4.5 Measuring Pressure	57
4.5.1 Goals	57
4.5.2 Optical Setup	58
4.5.3 Sm:YAG Spectrum Analysis	61
4.6 Measuring Diffusion.....	67
4.6.1 Goals	67
4.6.2 SIMS.....	68

4.6.3 Analysis of SIMS Data..... 76

4.7 Future Directions.....	78
4.7.1 Improvements in Sample Preparation and Analysis	79
4.7.2 Enhancements to the Pressure System.....	81
5. Results and Discussion.....	84
6. Summary.....	100
Appendix A. The Correlation Factor for Vacancy Mechanism in Diamond Cubic Structures with Vacancy Impurity Binding	102
Appendix B. The effect Vacancy Impurity Binding on Vacancy Mediated Diffusivity in Diamond Cubic Structures.....	106
References	111

List of Figures

Figure 2.1. Direct interchange mechanism.....	7
Figure 2.2. Vacancy mechanism.....	7
Figure 2.3. Interstitialcy mechanism with interstitialcies.....	8
Figure 2.4. Interstitialcy mechanism with interstitials.....	9
Figure 2.5. Interstitial mechanism.....	9
Figure 2.6. Free Energy Surface.....	11
Figure 2.7. Defect Formation.....	13
Figure 2.8. Arrhenius plot.....	14
Figure 2.9. Vacancy Mechanism; Formation and Migration Volumes.....	17
Figure 2.10. Interstitialcy Mechanism; Formation and Migration Volumes.....	18
Figure 3.1. Dopant and self-diffusion in Germanium.....	22
Figure 3.2. Dopant diffusion in silicon.....	24
Figure 4.1. Boyd-England Piston Cylinder.....	37
Figure 4.2. High Pressure Gas Cell.....	40
Figure 4.3. Sample Preparation.....	42
Figure 4.4. DAC Pressure Chamber.....	46
Figure 4.5. Diamond Anvil Cell.....	48
Figure 4.6. Cryogenic Argon Loader.....	52
Figure 4.7. Furnace.....	53
Figure 4.8. Furnace Temperature Control.....	54
Figure 4.9. Typical Temperature Profile.....	55
Figure 4.10. Plot of effective time.....	57

Figure 4.11. Optical setup.	59
Figure 4.12. Sm:YAG spectrum with a 7 Lorentzian fit.	62
Figure 4.13. Sm:YAG Spectrum at 575 °C.	63
Figure 4.14. Sm:YAG at 575 °C fit to a 3 peak 5 parameter model in the region 612 nm to 634 nm.	66
Figure 4.15. Sm:YAG at 25 °C with a 3 peak fit in the region 609 nm to 634 nm.	67
Figure 4.16. SIMS Technique.	69
Figure 4.17. The VG Ionex 1170S SIMS Instrument.	71
Figure 4.18. Crater Shape.	72
Figure 4.19. Sample Gating.	73
Figure 4.20. Function used to fit SIMS data.	77
Figure 4.21. SIMS Depth Profiles of Annealed and Unannealed Samples.	78
Figure 5.1. Diffusion of Arsenic in Germanium at 575 °C.	86
Figure 5.2. Diffusion of arsenic in germanium with the diffusion coef. for 4200s anneals reduced by a factor of 2.3.	88
Figure 5.3. Plot to exclude regions in DV_f and DV_m space for the vacancy mechanism.	92
Figure 5.4. Double defect diffusion mechanism compared with data.	94
Figure 5.5. 3-Fold arsenic trapped in a 4-fold germanium lattice.	96
Figure 5.6. Direct Tarzan mechanism.	98
Figure 5.7. Migration volume of the direct Tarzan mechanism.	98
Figure 5.8. Indirect Tarzan mechanism.	99
Figure A.1. Sites next to diffusing atom.	104
Figure B.1. Enhancement to diffusivity from vacancy impurity binding at 575 °C.	107
Figure B.2. Multiplier to the binding volume vs. free energy of binding at 575 °C.	108

Figure B.3. Region in DG_b vs. DV_b space where the correction to the activation volume is insignificant at 575 °C.....	109
---	-----

List of Tables

Table 3.1. Diffusion coefficients in germanium.....	21
Table 3.2. Diffusion coefficients in silicon.....	23
Table 3.3. Self-diffusion coefficients in silicon.....	25
Table 3.4. Dopant diffusion in silicon under Oxidation and Nitridation.....	26
Table 3.5. First Principles calculations of Formation Enthalpies reported by Nichols <i>et al.</i>	27
Table 3.6. First Principles calculations of Formation Volumes reported by Antonelli <i>et al.</i>	28
Table 3.7. Activation volume for Ge self diffusion measured by Werner <i>et al.</i>	29
Table 3.8. Activation volumes for Arsenic Diffusion in Silicon measured by Nygren <i>et al.</i>	32
Table 3.9. Activation Volumes of B, Ga and Ge diffusion in Silicon measured by Södervall <i>et al.</i>	34
Table 4.1. Constants used in the model to fit spectra.....	65
Table 5.1. Diffusion Coefficient of Arsenic in Germanium at 575 °C.....	85
Table 5.2. Comparison of Activation volumes in Germanium.....	90
Table A.1. Calculation of Probabilities for different Diffusion Paths.....	104

1. Introduction

This thesis is a contribution towards the understanding of diffusion in semiconductors. Diffusion is the macroscopic transport that results from the random motion of atoms. The macroscopic transport equations contain a single temperature dependent number, the *diffusion coefficient*, that contains all the microscopic information. In the simplest case the diffusion coefficient is independent of position, time and the concentration of the diffusing species. Atomic motion in solids is geometrically constrained because the crystal lattice must maintain its integrity. All atomic motion in solids can be reconstructed from individual steps that are jumps from one lattice site to a neighboring one. The exact path that the diffusing atom takes is called the *diffusion mechanism*. This mechanism may involve atoms located between lattice sites, vacant lattice sites (both called *point defects*), or a direct interchange of atoms on neighboring lattice sites. Though each diffusion mechanism is considered to be a uniquely defined path, multiple diffusion mechanisms may coexist. For example in an elemental solid with a small impurity concentration, there may be one diffusion mechanism for the solvent atom and another for the solute atoms. Even the solute atoms may have multiple diffusion mechanisms operating in parallel. In compounds, each of the different types of atoms may have their own set of diffusion mechanisms operating in parallel. Finally in all systems there may be a chemical driving force superimposed on the random motion of atoms. In these cases the diffusion coefficient may depend on position or concentration. Nevertheless the identification of the path for random motion of atoms is the foundation on which the understanding of diffusion is built.

In the elemental solids, diffusion mechanisms are an intrinsic property of the material and are of fundamental scientific interest. In manufacturing, the knowledge of diffusion mechanism assists in predicting and controlling diffusion. Diffusion related phenomena become very important during manufacture of very small physical features. In such cases, the atoms have to move only very small distances to destroy the desired features. For example, in the case of manufacturing of semiconductor devices, the electrical circuits are made by introducing impurity atoms in the silicon in a specified pattern. As the impurity atoms diffuse a distance comparable to the circuit dimensions these circuits are destroyed. The semiconductor industry continues to develop smaller and smaller circuits and the understanding of diffusion becomes increasingly important in the fabrication and design of microchips. Of particular importance is the transient diffusion that occurs after ion-implantation during microchip manufacturing. However neither this transient diffusion nor the underlying basic diffusion is well understood. Hence diffusion in semiconductors has been a heavily studied topic because it is interesting from both the basic and applied perspectives. Despite all the effort, if the different sets of published data for self-diffusion in silicon are extrapolated to room temperature the extrapolated diffusion coefficients vary by five orders of magnitude!! Clearly the understanding of diffusion in semiconductors is a scientific problem worth pursuing.

The most widely used general technique to study diffusion is to measure the temperature dependence of the diffusion coefficient. A quantity called an *activation energy* is derived from such an experiment. The activation energy, which is discussed in greater detail later, represents the sum of the energy of the individual jump and formation of the point defect associated with it. First

principles calculations have also been done to calculate the activation energy of self diffusion and impurity diffusion in silicon². All the experiments and numerical calculations to date have not convincingly demonstrated which diffusion mechanism predominates at the high temperatures at which these experiments are done. Nor have they allowed reliable extrapolation of the resulting research data to regimes that are relevant to integrated circuit fabrication³. Complementary techniques are needed.

The study of the effect of pressure on the diffusion coefficient is another widely applicable general technique and the resulting measurement is called an *activation volume*. The activation volume, which is discussed in detail later, is the sum of the volume changes associated with the atomic jump and with the formation of the relevant point defect. Unlike activation energies, which are always positive, activation volumes are expected to have different signs for different types of diffusion mechanisms. Hence a measurement of the activation volume can be a more revealing test for distinguishing between potential diffusion mechanisms. The identification of diffusion mechanisms is a key step in developing theoretical models of the diffusion process. The pressure effects on the diffusion coefficient have been extensively studied for metals^{4,5,6} and have assisted in understanding the diffusion mechanisms. The first experiment on the effects of pressure on diffusion in germanium was performed for self-diffusion⁷, and is the only measurement of the activation volume for diffusion in germanium that preceded this work. This work is discussed in Section 3.4. As silicon is economically a more important material than germanium, accurate measurements of activation volumes in silicon would generate more interest. The first reported measurement of an activation volume in silicon was performed by Nygren *et al.*⁸ They measured the

activation volume of arsenic diffusion in silicon. Aziz *et al.*⁹ measured the activation volume of self-diffusion in silicon. But both these studies were performed in the high pressure piston cylinder cell described in Section 4.2. It is possible that chemical contamination from the solid pressure medium and the application of non-hydrostatic stresses may have affected those results. Södervall *et al.*¹⁰ have measured the activation volume of boron, gallium and germanium diffusion in silicon using a gaseous pressure medium. The measurements of activation volumes in silicon are discussed in Section 3.4.

This work is a part of a program to systematically study the pressure effects on diffusion in semiconductors. A comparison of activation volumes for various dopants in silicon and germanium would be very helpful in developing detailed models for the diffusion process. This thesis concerns itself with the development of the experimental apparatus for this purpose and its first use in the measurement of the activation volume of arsenic diffusion in germanium.

2. Theory of Diffusion Mechanisms

2.1 *The Phenomenology of Diffusion*

Macroscopic diffusion is the transport of matter resulting from a concentration gradient. Consider a material with a concentration profile $c(x)$. Its flux J will be¹¹:

$$J = -D \frac{\partial c}{\partial x} \quad (2.1)$$

where D , is called the *Diffusion Coefficient*. Eq. 2.1 can be taken as the definition of the diffusion coefficient.

Mass conservation requires that the rate of change of the concentration in a volume element should equal the net flux entering that volume element. In one dimension,

$$\frac{\partial c}{\partial t} = -\frac{\partial J}{\partial x} \quad (2.2)$$

Incorporating Eq. 2.1 into Eq. 2.2 gives,

$$\frac{\partial c}{\partial t} = \frac{\partial}{\partial x} \left(D \frac{\partial c}{\partial x} \right) \quad (2.3)$$

which is called the *Diffusion Equation*.

For the special case where D is concentration independent, Eq. 2.3 becomes

$$\frac{\partial c}{\partial t} = D \frac{\partial^2 c}{\partial x^2} \quad (2.4)$$

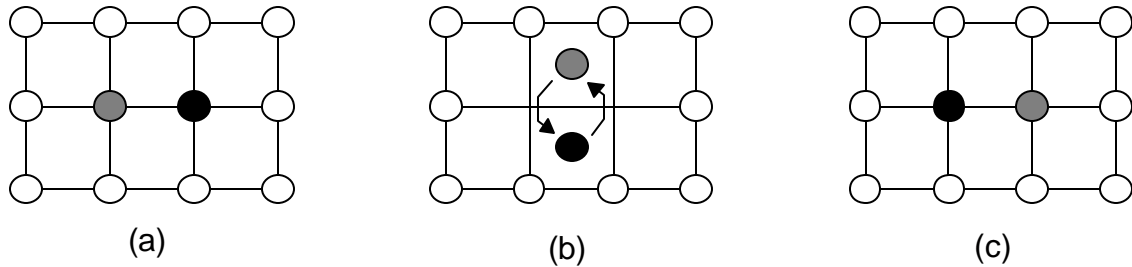
and is referred to as the *Linear Diffusion Equation*. We show later that linear diffusion results when atomic motion is an unbiased random walk. Empirically, linear diffusion exists for dilute solutions of the diffusing species. Eq. 2.4 is a well studied differential equation with standard numerical and analytical solutions for a variety of initial and boundary conditions. Its

solutions will be used to calculate D from the measured concentration versus depth profiles.

2.2 *Diffusion Mechanisms*

The first step in understanding diffusion is to identify the predominant diffusion mechanism. We discuss the geometry of the most important types of diffusion mechanisms. These basic types are independent of the crystal structure; here we represent them schematically in two dimensions.

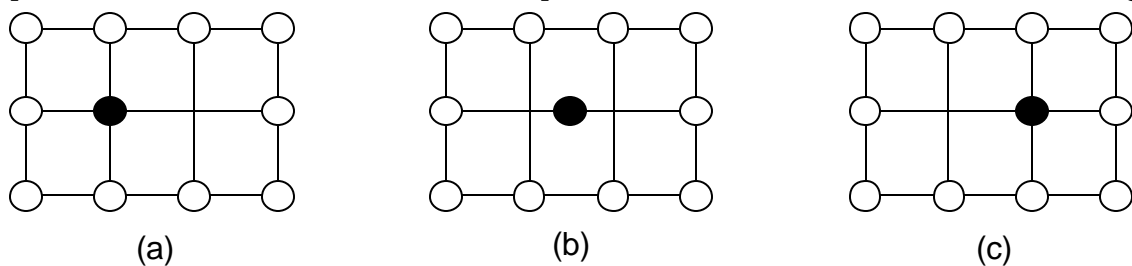
In an ideal crystal with all atoms on lattice sites and all sites occupied, an atom cannot jump to neighbouring site unless that neighboring atom simultaneously jumps back to the first site. A two dimensional schematic of such a *direct interchange mechanism* for diffusion is shown in Fig. 2.1. The atoms merely switch positions. Note that the two atoms are shaded differently for identification only: the diffusing atoms need not be impurities. For the jump to take place, there must be enough localized energy to drive the jump. The energetics of jumping are discussed in greater detail in Section 2.3. The direct interchange mechanism requires that there be enough localized energy for moving two atoms simultaneously, and hence in most cases it is thought to be unlikely as the predominant mechanism. Furthermore in close packed structures such as metals, the energy required to move apart the adjoining atoms to allow enough room for passage may also be prohibitively high. However in silicon, which is an open network structure, an direct interchange mechanism is considered plausible¹².



{tc "Figure 2.1 Direct interchange mechanism" \f f}Figure 2.1 Direct interchange mechanism.
(a) Initial Configuration. (b) Saddle point Configuration. (c) Final Configuration.

However, if a lattice site is vacant then a neighboring atom can easily jump into the vacant site. It is generally believed that in metals, vacant lattice sites, called *vacancies*, mediate diffusion¹³. This diffusion mechanism, called the *vacancy mechanism*, is shown in Fig. 2.2. Because only one atom must move and the adjoining atoms move very little, the energetics of the jump for the vacancy mechanism are thought to be favorable compared to the direct interchange mechanism; however, the vacancy must be present for the mechanism to operate. The vacancy is a one type of a lattice *point defect*. Point defects are lattice imperfections that require energy to form but due to global entropy considerations they exist in thermodynamic equilibrium in the crystals. The energetics of point defect formation and their equilibrium concentrations are discussed in Section 2.3.

The inverse point defect of a vacancy is an *interstitialcy*, where two atoms share a single lattice site. In metals, the self-interstitialcy is not considered plausible because metals are closed packed structures and there is not enough



{tc "Figure 2.2 Vacancy mechanism. " \f f}Figure 2.2 Vacancy mechanism.
(a) Initial Configuration. (b) Saddle point Configuration. (c) Final Configuration.

volume between lattice atoms for the additional atom. However in the four fold coordinated open structures such as silicon or germanium the self-interstitialcy may be the dominant point defect at high temperatures¹⁴. The interstitialcy diffusion mechanism is shown in Fig. 2.3. The black atom moves from one interstitialcy site to another. Both atoms are considered equivalent and after the state in Fig. 2.3 (c) either atom may move.

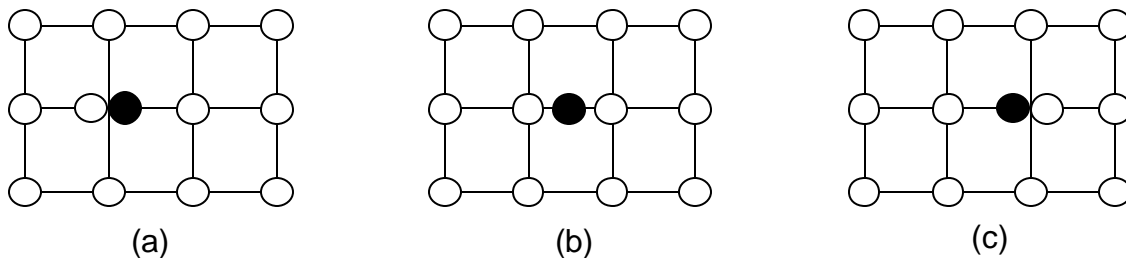
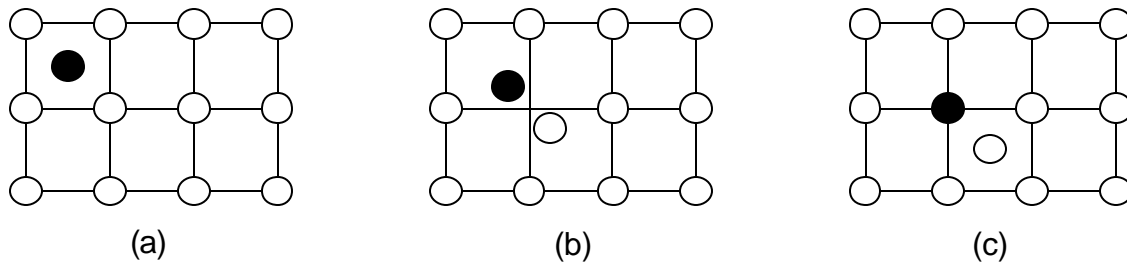


Figure 2.3 Interstitialcy mechanism with interstitialcies.

(a) Initial Configuration. (b) Saddle point Configuration. (c) Final Configuration.

The additional atom need not share a lattice site, but may reside in the interstitial spaces of the lattice. Such an atom is called an *interstitial* atom. The interstitial atom is equidistant from several lattice sites and is not associated with any particular site. Interstitial atoms cause another type of interstitialcy mechanism¹⁵ shown in Fig. 2.4. The black interstitial atom pushes an atom off a lattice site. The other atom now becomes an interstitial and it will in turn push another atom off a lattice site. The common feature of both interstitialcy mechanisms is that the equilibrium position for the diffusing atom is a lattice site. An impurity atom with an equilibrium position on a lattice site is called a *substitutional* impurity. The interstitialcy mechanism can work for both substitutional impurity diffusion or self-diffusion. However, the distinction between interstitial and interstitialcy point defects is difficult to make from an experimental perspective. The distinction between silicon self interstitialcy and self-interstitial is rarely made

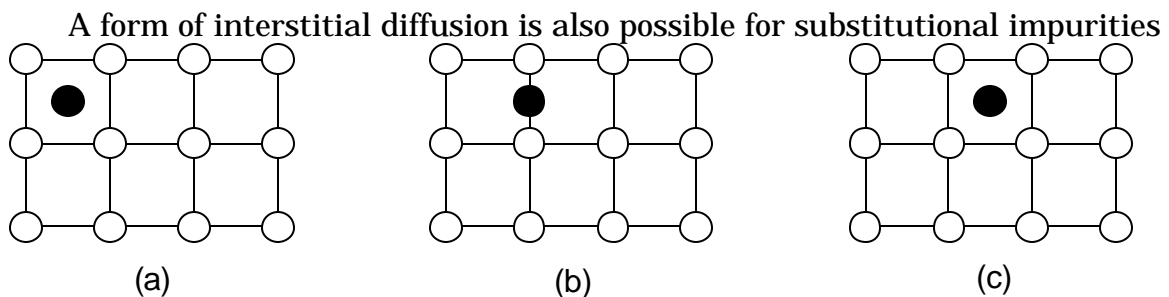


{tc "Figure 2.4 Interstitialcy mechanism with interstitials." \f f}Figure 2.4 Interstitialcy mechanism with interstitials.

(a) Initial Configuration. (b) Saddle point Configuration. (c) Final Configuration.

in the literature **Error! Bookmark not defined.** and both are often referred together as interstitials or interstitial-type point defects. For substitutional atoms, the distinction may be meaningless because the actual defect can be a hybrid of the two cases. The impurity atom may be associated with a lattice point but not be equidistant to it with the host matrix atom. In this thesis we will refer to both types as interstitial-type point defects.

If the equilibrium position of an impurity atom is an interstitial site, then it can move between lattice sites as shown in Fig. 2.5. Such a mechanism is called the *interstitial mechanism* and it does not require a thermally generated point defect or an direct interchange. Atoms diffusing via the interstitial mechanism are usually very fast diffusers. Note in the interstitialcy mechanism described previously the diffusing atom does not directly jump from one interstitial site to another.



{tc "Figure 2.5. Interstitial mechanism." \f f}Figure 2.5. Interstitial mechanism.
(a) Initial Configuration. (b) Saddle point Configuration. (c) Final Configuration.

that are very mobile as interstitials. The impurity atom leaves a lattice site and makes several jumps as an interstitial before jumping back onto a lattice site. Such a mode of diffusion is called a *dissociative* mechanism¹⁶ or a *kick-out*¹⁷ mechanism depending on how the impurity interstitial was created. For the kick-out mechanism the impurity interstitial is created by self-interstitials by the reaction:



where A_I is the impurity interstitial, A_S is the impurity substitutional and I is the self-interstitial. In the Frank-Turnbull, or dissociative, mechanism the substitutional impurity atom creates a vacancy and an impurity interstitial by the reaction



where V is a vacancy.

2.3 **Basic Rate Theory**

The diffusion coefficient D , using the statistics of a random walk with a fixed jump distance l is¹⁸:

$$D = gl^2G \quad (2.7)$$

where G is the jump rate and g is a geometric factor accounting for the crystal structure and the diffusion mechanism. ($g = 1/6$ for the vacancy mechanism in all cubic and isotropic systems.)

Consider all the diffusion mechanisms described in Section 2.2. The atom, originally in a site that is a local free energy minimum for the crystal, moves into another site. In the Figs. 2.1 to 2.5, (a) and (c) are the initial and final states of the diffusion jump. They are equivalent and are equilibrium states of the crystal, provided the defect does not annihilate on the crystal surface. The

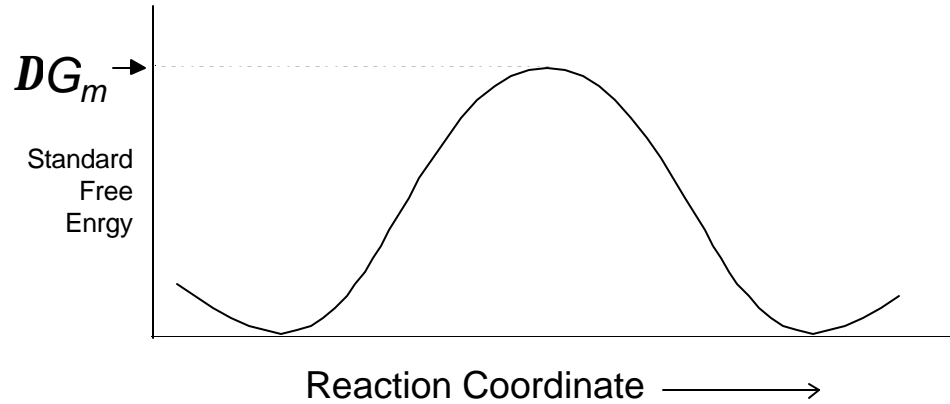


Figure 2.6 Free Energy Surface.

middle state, Figs. 2.1 to 2.5 (b) is an intermediate non-equilibrium state called the *transition state*. The transition state is higher in standard free energy than the adjacent sites, and hence represents a barrier. The standard free energy surface for the crystal during the jump is represented in Fig. 2.6.

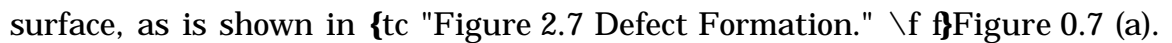
The rate with which the atom crosses the barrier is proportional to the attempt frequency times the probability that an attempt is successful. The attempt frequency is governed by the thermal vibrations of the atoms about their lattice positions and is related to the Debye frequency. The number of successful attempts comes from fluctuation theory in statistical mechanics. A third term is due to the availability of a site to which the atom can jump.

Hence the rate by which the atom gets over the barrier is given by¹⁹:


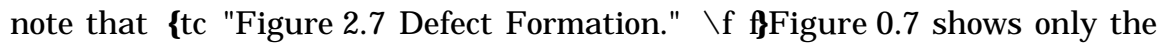
$$G = Pn \exp(-DG_m/kT) \quad (0.8)$$

where DG_m is the height of the standard free energy barrier, and will be called the *free energy of migration*, n is the attempt frequency and P is the probability that a site is available for that particular diffusion mechanism. For example, in the vacancy mechanism P is the probability that there is a vacancy next to the atom under consideration. Likewise for the interstitialcy

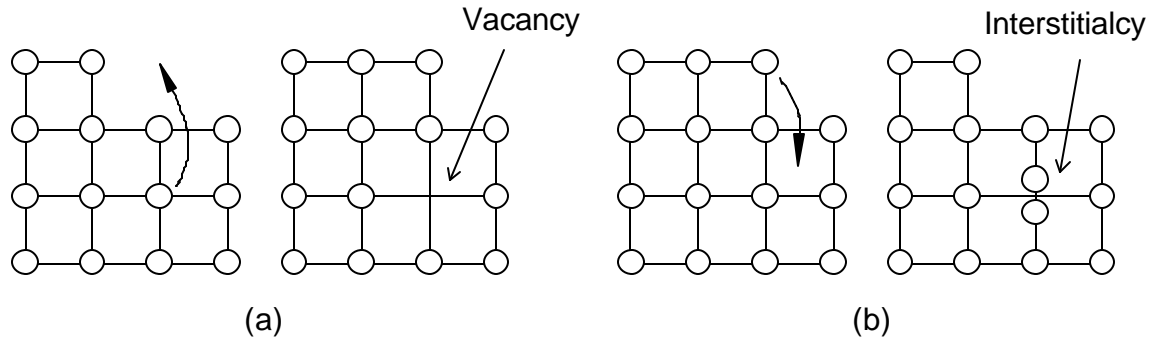
mechanism, P is the probability that an interstitial is suitably positioned next to the atom under consideration. The probability that a point defect is next to the jump site depends on the concentration of that particular point defect. For the direct interchange mechanism P is unity, because the direct interchange mechanism is always possible and no defect is involved.

Point defects exist in a crystal lattice in thermodynamic equilibrium and hence will always exist except in very unusual circumstances. The concentration of the defect depends on the free energy of formation of the defect. To create a vacancy one must move an atom from a lattice site to the surface, as is shown in  Figure 0.7 (a). This step requires additional energy, but there is a gain in configurational entropy because now N atoms are on $N + 1$ sites. From global free energy minimization we get

$$N_d = N \exp(-DG_f^0/kT) \quad (0.9)$$

where N_d is the number of defects, and N is the total number of atoms, and DG_f^0 is the *standard free energy of formation* of the defect. Similarly  Figure 0.7 (b) shows an interstitialcy formation by moving an atom from the surface to an interstitialcy site. We note that  Figure 0.7 shows only the initial and final configuration and should not be interpreted as depicting the physical mechanisms for defect formation. The physical mechanisms for defect formation involve surfaces and extended defect structures such as dislocations and grain boundaries.

In the preceding paragraph we have assumed that the crystal is uniform and that the diffusing atoms are indistinguishable from the matrix atoms. If



{tc "Figure 2.7 Defect Formation." \f}Figure 0.7 Defect Formation.

the diffusing atom is an impurity there may be some type of energetic attraction or *binding* between the impurity atom and point defect. This binding could be either attractive or repulsive and will affect the formation energy of the point defect next to impurity atoms. The effects of vacancy impurity binding on vacancy mediated diffusion in diamond cubic crystals, the particular case relevant to this work, and its consequences are discussed in Appendix B.

From Eq. 2.9, the probability that a defect exists next to the jump site is:

$$P = \exp(-DG_f^0/kT). \quad (2.10)$$

Using Eq. 2.7, Eq. 2.8 and Eq. 2.10 we get

$$D = gnI^2 \exp(-DG^*/kT) \quad (2.11)$$

where

$$DG^* = DG_f^0 + DG_m \quad (2.12)$$

and DG^* is the *free energy of activation* for the diffusion mechanism. Eq. 2.11 is valid when at the atomic level the diffusing species executes a random walk. Point defects execute a random walk but the motion of the impurity atoms is correlated with motion of the point defects. This correlation is accounted for by introducing a *correlation factor* f . Therefore, for impurity diffusion mediated by point defects, the resulting diffusivity is given by²⁰

$$D = fgnl^2 \exp(-DG^*/kT). \quad (2.13)$$

For self-diffusion f is purely a geometrical factor based on the diffusion mechanism and the lattice geometry and is calculated from the statistics of a random walk²¹. However, any binding between the impurity atom and defect will affect the correlation factor. In Appendix A we calculate the correlation factor for vacancy mediated diffusion in a diamond cubic crystal with impurity vacancy binding and in Appendix B we consider its effects on the diffusivity.

We can use the thermodynamic identity, $DG^* = DH^* - TDS^*$ to reduce Eq. 2.11 to the Arrhenius form of the diffusion coefficient

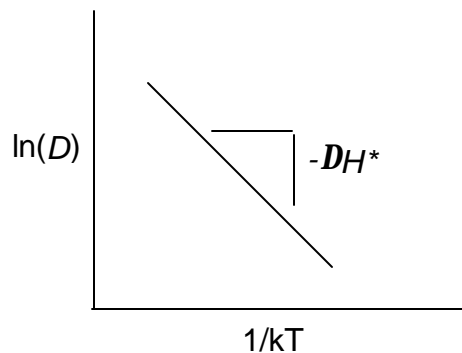
$$D = D_0 \exp(-DH^*/kT) \quad (2.14)$$

where D_0 is called the pre-exponential factor and is given by

$$D_0 = gnl^2 \exp(-DS^*/k) \quad (2.15)$$

and DH^* is the activation enthalpy, often called the activation energy in the literature for atmospheric pressure diffusion experiments. Like DG^* , DH^* can be also be separated into DH_f^0 , the enthalpy of formation, and DH_m , the enthalpy of migration. A plot of the Arrhenius equation is shown in {tc "Figure 2.8. Arrhenius plot." \f f}Figure 0.9. The slope gives the activation enthalpy.

Note that the direct interchange mechanism does not have any formation



{tc "Figure 2.8. Arrhenius plot." \f f}Figure 0.9. Arrhenius plot.

energy. However it is likely to have a large migration energy because two atoms need to simultaneously move off their lattice sites. The proposed direct interchange mechanism for silicon self-diffusion is plausible because the migration energy is comparable to the sum of the formation and migration energies for the vacancy and interstitialcy mechanisms **Error! Bookmark not defined.**

Studying the effects of temperature on the diffusion coefficient is the principal experimental technique used to study diffusion. Data are analyzed using Eq. 2.13 and the results are reported as an activation enthalpy and a pre-exponential factor. Values of DH^* and D_0 calculated for a variety of mechanisms are compared to experimental values.

2.4 Effect of Pressure on Diffusion

Consider the thermodynamic identity

$$V = \left. \frac{\partial G}{\partial p} \right|_T \quad (2.16)$$

The rate of change in the free energy with pressure results in a volume term; hence from the pressure dependence of the free energy of activation we derive an *activation volume*. Expressing the free energy of activation using Eq. 2.11 we get

$$DG^* = -kT \ln(D) + kT \ln(fgnl^2). \quad (0.17)$$

Using Eq. 2.16 we get:

$$DV^* = -kT \left. \frac{\partial \ln D}{\partial p} \right|_T + kT \left. \frac{\partial \ln(fgnl^2)}{\partial p} \right|_T. \quad (0.18)$$

The magnitude of the second term of Eq. 2.18 is typically regarded as small in

the literature and is ignored²². The pressure dependences of f , n , g and I are now discussed.

g is a geometrical term hence its pressure derivative is exactly zero for a given crystal structure and diffusion mechanism.

Jeffery and Lazarus^{Error! Bookmark not defined.} have proved that if the concentration profile is measured after the pressure is released, the effective pressure derivative of I , the jump distance, is exactly zero. They show that the pressure derivative of I need only be considered if the concentration profiles are measured while the solid is still under pressure.

Werner *et al.*^{Error! Bookmark not defined.} have approximated the pressure derivative of the attempt frequency n by assuming that it is equal to the pressure derivative of the Debye frequency. Then, using a Gruneisen model for a perfect crystal gives

$$\frac{\partial \ln n}{\partial P} \approx g_G c \quad (2.19)$$

where g_G is the Gruneisen constant and c is the isothermal bulk compressibility. They estimate the correction to the activation volume from this term to be less than 1% of the atomic volume of germanium. Hence we will ignore it.

For self-diffusion the correlation factor f is of only geometrical origin and hence its pressure derivative is exactly zero. However, for impurity diffusion, a possible free energy of binding between the impurity atom and defect may be pressure dependent thus making f pressure dependent. In Appendix B we calculate the contribution to the activation volume from the pressure

derivative of f for vacancy diffusion in diamond cubic lattices and show that for arsenic diffusion in germanium it is very unlikely that this contribution is significant. Because the predominant point defects in germanium are thought to be vacancies^{Error! Bookmark not defined.}, we can ignore the pressure derivative of f . We note that for any other diffusion mechanism the effect of pressure on impurity defect binding energy and hence f will need to be reconsidered.

Because all four pressure derivatives are taken to be negligible, the second term of Eq. 2.18 is also negligible. We then write the activation volume as:

$$DV^* \cong -kT \left. \frac{\partial \ln D}{\partial P} \right|_T \quad (0.20)$$

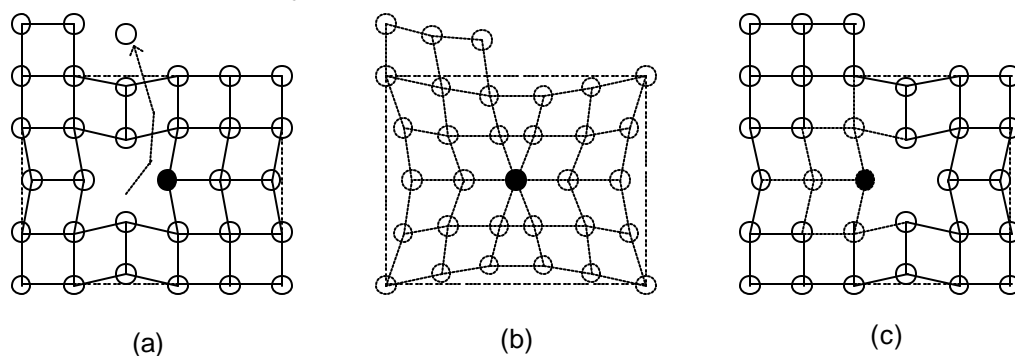
Eq. 2.20 is used to calculate the activation volume from the experimental data.

Using Eq. 2.16 to take the derivative of Eq. 2.12 we get

$$DV^* = DV_f^0 + DV_m \quad (0.21)$$

where DV_f^0 is called the formation volume and DV_m is called the migration volume of the point defect.

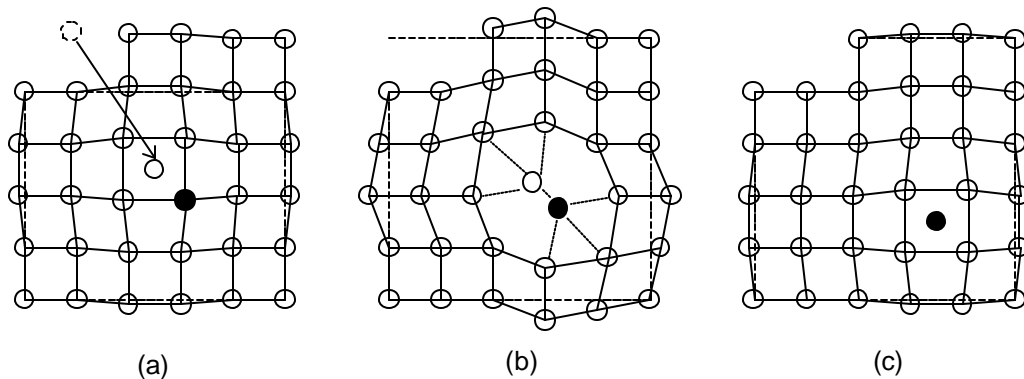
{tc "Figure 2.9. Vacancy Mechanism; Formation and Migration Volumes." \f}Figure 0.11 shows a pictorial representation of migration and formation volumes for the vacancy diffusion mechanism in an open structured lattice.



{tc "Figure 2.9. Vacancy Mechanism; Formation and Migration Volumes." \f}Figure 0.11. Vacancy Mechanism; Formation and Migration Volumes.

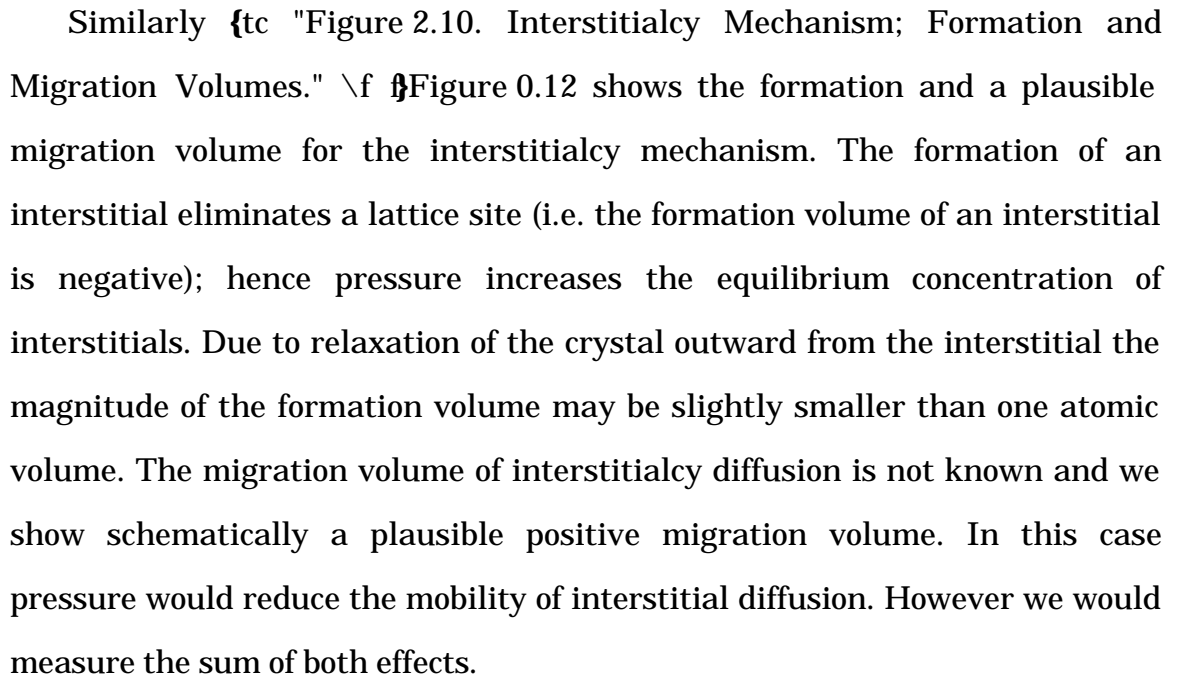
From Fig. 2.9 (a), the formation of the vacancy creates an additional lattice point. The formation volume for this diffusion mechanism will be the volume of one lattice point, Ω , minus the relaxation volume of the atoms around the vacancy. Note that the relaxation propagates to the free surface. The figure shows the lattice relaxing inwards, which is the generally accepted direction, though some authors believe it may relax outwards^{23,24,25,26}. In either case the amount of relaxation is expected to be small compared to Ω and the formation volume for the vacancy is therefore expected to be close to $+1\Omega$.

{tc "Figure 2.9. Vacancy Mechanism; Formation and Migration Volumes." \f }Figure 0.11(b) depicts the transition state for migration. This state is the least understood. We show a plausible situation where the lattice comes together to assist during the transition stage. During the transition stage where the free energy goes through a maximum, the volume may go through a minimum. This diffusion mechanism would then have a negative migration volume. With the formation and migration volumes depicted in {tc "Figure 2.9. Vacancy Mechanism; Formation and Migration Volumes." \f }Figure 0.11, pressure would reduce the concentration of the defects but would enhance the defect mobility. We would measure the sum of both these effects. Note that



{tc "Figure 2.10. Interstitialcy Mechanism; Formation and Migration Volumes." \f }Figure 0.12. Interstitialcy Mechanism; Formation and Migration Volumes.

these negative migration volumes are plausible only if the lattice has an open structure that can be compressed at the transition state. The diamond cubic structures of silicon and germanium fulfill this requirement.

Similarly  Figure 0.12 shows the formation and a plausible migration volume for the interstitialcy mechanism. The formation of an interstitial eliminates a lattice site (i.e. the formation volume of an interstitial is negative); hence pressure increases the equilibrium concentration of interstitials. Due to relaxation of the crystal outward from the interstitial the magnitude of the formation volume may be slightly smaller than one atomic volume. The migration volume of interstitialcy diffusion is not known and we show schematically a plausible positive migration volume. In this case pressure would reduce the mobility of interstitial diffusion. However we would measure the sum of both effects.

Point defects that mediate diffusion can exist in several charged states and thus their concentrations may be effected by changes in the Fermi level of the crystal. To account for the effect of pressure on the Fermi level, the different charged states of the point defects are treated as separate point defects. We then define the formation volume to include all the physical effects through which pressure changes the concentration of point defects. The migration volume associated with these charged defects is similarly defined. Thus, the effect of pressure on the Fermi level that in turn affects the concentration of the charged point defects or their migration energy is incorporated into the activation volume for that point defect. Werner *et al.* **Error! Bookmark not defined.** also use this formalism.

3. Survey of Diffusion in Silicon and Germanium

3.1 *Ambient pressure diffusion in Silicon and Germanium.*

Diffusion in silicon and germanium have been extensively studied and have been reviewed in detail elsewhere^{Error! Bookmark not defined.,Error! Bookmark not defined.}^{27,28}. The study of this topic is driven by the needs of the semiconductor industry and vast amounts of data have been accumulated. This section provides a brief introduction to the topic.

The pre-exponential factor and the activation enthalpy for dopant and self-diffusion in germanium are tabulated in Table 3.1 and the Arrhenius plots are shown in Fig. 3.1. The most outstanding feature in Table 3.1 is that the activation enthalpies separate out into two classes. All the Group V dopants diffuse with activation enthalpies that are approximately 2.5 eV. Diffusion for all the Group III dopants and self-diffusion have activation enthalpies that are 3 eV or higher. This trend is clearly visible in Fig. 3.1 where the Arrhenius plots for the Group III and Group V dopants separate out into two distinct bands, with Group V dopants being the faster diffusers. A proposed explanation for this fast diffusion of Group V dopants is discussed in the next paragraph.

Copper is a substitutional impurity in germanium that is very mobile as an interstitial^{Error! Bookmark not defined.}. Copper diffusion in germanium has been studied by Stolwijk²⁹ and they show that copper diffuses in germanium by the dissociative mechanism. Frank uses the copper diffusivity data to calculate the vacancy concentration and from that he calculates the vacancy component of self-diffusion in germanium. By comparing his calculated

vacancy component of self diffusion to published self-diffusion data he concludes that self diffusion in germanium occurs predominantly via the vacancy mechanism. Werner *et al.* have studied the effect of pressure and doping on self diffusion on germanium. They conclude that self-diffusion in germanium is mediated by neutral and negative vacancies. Their work is described in greater detail in Section 0. This negative vacancy would be attracted to the positively charged Group V dopants in germanium. Frank **Error! Bookmark not defined.** concludes that this Coulomb attraction between the dopant and the vacancy would enhance the probability of a vacancy being next to the dopant and explain the enhanced diffusion of Group V dopants. However in Section 5 we show that a Coulomb attraction or any other kind of binding between a vacancy and a diffusing species in a four-fold coordinated system would reduce the correlation factor that would offset the enhanced probability and would not lead to enhanced diffusion.

The pre-exponential factor and activation enthalpies for dopants in silicon are tabulated in Table 3.2 and the Arrhenius plots are shown in Fig. 3.2. Note that the trend in the activation enthalpies for dopant diffusion is opposite to that in germanium. In silicon the Group III dopants are faster diffusers than

Dopant	Pre-exponential Factor D_0 (cm ² /sec)	Activation Enthalpy DH^* (eV)
Ge	18.5	3.07
B	1.1×10^7	4.54
Al	1.6×10^2	3.24
Ga	40	3.15
In	33	3.03
P	2.5	2.49
As	10.3	2.51
Sb	3.2	2.42

{tc "Table 3.1. Diffusion coefficients in germanium. " \f t}Table 0.1. Diffusion coefficients in germanium. (After Casey and Pearson³⁰)

Ge Diffusion

{tc "Figure 3.1. Dopant and self-diffusion in Germanium." \f f}Figure 0.1. Dopant and self-diffusion in Germanium. (After Casey and PearsonError! Bookmark not defined.)

Group V dopants but the differences in the activation enthalpies are not as great as for the case of germanium. Some implications of this observation are discussed below.

Gold and platinum have been shown to be substitutional impurities in silicon that are very mobile as interstitials³¹ and can be used to study point defect concentrations. Experimental studies of gold and platinum diffusion in silicon show that they both diffuse via the kick-out mechanism^{Error! Bookmark not defined.}. From the gold diffusivity, Frank calculates the interstitial concentration and then an interstitialcy component of self-diffusion in silicon. By comparing his calculated interstitialcy component of self diffusion to published self-diffusion data he concludes that self diffusion in silicon occurs predominantly via the interstitialcy mechanism at approximately 1000 °C and

greater. But at lower temperatures his calculated interstitialcy component of self-diffusion falls short of the published data and he concludes that the vacancy mechanism must also make a significant contribution to self diffusion. Theoretical calculations from Blount³² and Watkins *et al.*³³ show that the silicon self-interstitial can exist in a negatively charged, positively charged or neutral state depending on the doping level. Experiments by Watkins *et al.*^{34,35} show that under typical conditions the silicon vacancy exists in a neutral or negatively charged state. Frank^{Error! Bookmark not defined.} uses a combination of coulomb and elastic interactions between the dopants and point defects to explain dopant diffusion in silicon. He concludes that small size or Group III membership favors the interstitialcy mechanism and larger size or Group V membership favors the vacancy mechanism. This explanation is consistent with the results of oxidation enhanced diffusion studies described later in this section. At this point it should be noted that these conclusions are not universally accepted. For further details the reader is referred to the review articles^{Error! Bookmark not defined.,Error! Bookmark not defined.,Error! Bookmark not defined.}

Dopant	Pre-exponential Factor D_0 (cm ² /sec)	Activation Enthalpy DH^* (eV)
B	5.1	3.70
Al	8.0	3.47
Ga	3.6	3.51
In	16.5	3.91
P	10.5	3.69
As	60.0	4.20
Sb	3.2	3.98
Bi	1.03×10^3	4.63

{tc "Table 3.2. Diffusion coefficients in silicon. " \f t}Table 0.2. Diffusion coefficients in silicon. (After Casey and Pearson^{Error! Bookmark not defined.})

Table 3.3 lists the values of the silicon self-diffusion coefficient from different experiments. There is no clear explanation as to why the self-diffusion numbers in silicon vary so much. There is much better agreement between the results from different experiments for studies of diffusion in metals^{Error! Bookmark not defined.}. One explanation is that poor control over the concentration of oxygen in the samples is responsible for this effect^{Error! Bookmark not defined.}^{Error! Bookmark not defined.} because it has been shown that oxygen dissolved in silicon affects diffusion³⁶. Other elements such as carbon may play a similar role^{Error! Bookmark not defined.}. Frank^{Error! Bookmark not defined.} has also suggested that part of the discrepancy may be due to the switching of the diffusion mechanism at approximately 1000 °C resulting in different numbers for the different temperature ranges.

Si Diffusion

{tc "Figure 3.2. Dopant diffusion in silicon." \f f}Figure 3.2. Dopant diffusion in silicon. (After Casey and Pearson^{Error! Bookmark not defined.})

Pre-exponential Factor D_0 (cm^2/sec)	Activation Enthalpy DH^* (eV)	Temperature Range $^{\circ}\text{C}$
1800	4.77	1200-1400
1200	4.72	1178-1300
9000	5.13	1100-1300
154	4.65	855-1175
1460	5.02	1047-1387
8	4.1	900-1100
20	4.4	857-1200

{tc "Table 3.3. Self-diffusion coefficients in silicon. " \f t}Table 3.3. Self-diffusion coefficients in silicon.
(After Borg *et al.* **Error! Bookmark not defined.**)

Oxidation and nitridation of the silicon surface are known to inject point defects into the substrate below **Error! Bookmark not defined.**. This has been established by the study of oxidation induced stacking faults³⁷. These stacking faults grow with interstitials being injected from the surface and shrink with vacancies being injected from the surface. Under typical conditions, oxidation has been shown to inject excess interstitials and nitridation has been shown to inject excess vacancies **Error! Bookmark not defined.**. These excess point defects enhance or retard the dopant diffusion. The semiconductor industry has been using oxidation enhanced diffusion (OED) to diffuse implanted dopants at temperatures below those at which they would diffuse without oxidation. Oxidation and nitridation can be used to establish the diffusion mechanism for diffusion. If the diffusion of a dopant is enhanced by the injection of excess interstitial and retarded by the injection of excess vacancies then it must predominantly diffuse via the interstitialcy mechanism. However if the injection of both vacancies and interstitials enhances diffusion then the dopant can diffuse via either mechanism. Table 3.4 lists the results of oxidation and nitridation on dopant diffusion in silicon. The anomalous behavior of Sb under oxidation has not been explained.

Process	Oxidation Interstitials Injected	Nitridation Vacancies Injected
P, B diffusion Intrinsic Extrinsic	Enhanced Enhanced	Retarded Retarded
Sb diffusion Intrinsic	Enhancement then Retardation	Enhanced
As diffusion Intrinsic Extrinsic	Enhanced Retarded	Enhanced Enhanced
Ga diffusion Intrinsic	Enhanced	Retarded

{tc "Table 3.4. Dopant diffusion in silicon under Oxidation and Nitridation." \f t}Table 3.4. Dopant diffusion in silicon under Oxidation and Nitridation. (After Fahey *et al.*^{Error! Bookmark not defined.})

3.2 *First-principles calculations for diffusion in Silicon.*

Nichols *et al.*^{Error! Bookmark not defined.} have used first principles to calculate the activation enthalpies for the interstitialcy, vacancy and concerted exchange mechanism for B, P, As, Sb and self diffusion in silicon. They find that under equilibrium conditions the vacancy and the interstitialcy mechanisms have comparable activation energy for B, P, As and self diffusion. For Sb diffusion the vacancy mechanism has the lowest energy. They find, however, that for all these diffusing species, the concerted exchange mechanism proposed by Pandey^{Error! Bookmark not defined.} does not play a significant role.

The results of the calculation are presented in Table 3.5. Note that only the enthalpies of formation for vacancy and interstitialcy and the activation enthalpy for concerted exchange have been calculated. The enthalpies of migration for the vacancy and interstitialcy mechanism are experimental results³⁸ except for the B values which are estimates. The experimental enthalpies of migration were determined from studies of dopant diffusion in silicon supersaturated with point defects. The supersaturation of point defects

was created by electron irradiation. The enthalpies of formation are calculated for the dopant point defect complex associated with each respective mechanism. They effectively treat the dopant point-defect complex as a single entity. For the vacancy mechanism in the diamond cubic lattice the dopant point-defect complex must dissociate for any diffusion to take place. Nichols *et al.* are aware of this fact but their formalism does not allow them to explicitly incorporate it into their calculations. We note that the Group V vacancy complexes have a lower calculated formation energy than the silicon vacancy pair, thus implying that they are stable. We also note that the reported experimental migration energy for vacancy Group V dopant diffusion is higher than that for vacancy self-diffusion. Therefore in their formalism, where the dopant point-defect complex migrates as a single entity, the stable complex manifests itself by having a lower formation energy, but has a higher 'migration' energy because it is forced to dissociate in order to move. These effects in the formation and 'migration' terms offset each other and the total activation enthalpy for diffusion is not greatly affected by the stability of the complex. We come to a similar conclusion in Appendix B.

Species	DH^* (eV)	DH_f (eV) Calculated	DH_m (eV) Experimental
B_i	3.9	3.9	0.0
BV	not stable	3.0	1.0
B(CE)	4.9		
P_i	3.8	3.0	0.8
PV	3.4	2.5	0.94
P(CE)	4.6		
As_i	3.6	3.2	0.4
AsV	3.4	2.3	1.07
As(CE)	3.9		
Sb_i	4.9	4.7	0.2
SbV	3.6	2.3	1.28
Sb(CE)	4.6		
Si_i	4.0	3.6	0.4
SiV	3.8	3.5	0.3
Si(CE)	4.3		

{tc "Table 3.5. First Principles calculations of Formation Enthalpies reported by Nichols *et al.*" \f t}Table
3.5. First Principles calculations of Formation Enthalpies reported by Nichols *et al.*Error! Bookmark not defined.

Antonelli *et al.*³⁹ have used first principles to calculate the effect of pressure on self-diffusion in silicon. They have calculated the formation volumes for several charge states of the vacancy, the tetrahedral interstitial and the bond-centered interstitial. They have also calculated the activation volume of the concerted exchange mechanism. Their results are presented in Table 3.6. Note that the charge state of the point defect affects the formation volume for vacancies and tetrahedral interstitials but not for bond centered interstitials.

Defect	Formation Volume DV_f (Ω_{Si})	
Vacancy:	V^0	0.76
	V^{2+}	0.60
Tetrahedral Interstitial:	I_T^0	-0.28
	I_T^{2+}	-0.24
Bond-Centered Interstitial:	I_B^0	
	I_B^+	-0.56
	I_B^{2+}	-0.56
Concerted Exchange: (Activation Volume)	(CE)	-0.04

{tc "Table 3.6. First Principles calculations of Formation Volumes reported by Antonelli *et al.*"\f t}Table
 3.6. First principles calculations of Formation Volumes reported by Antonelli *et al.*Error! Bookmark not defined.

3.3 The Effect of pressure on self-diffusion in Germanium.

Werner *et al.*Error! Bookmark not defined. have measured the activation volume for self-diffusion in germanium as a function of temperature and doping. Their results for the activation volume versus temperature experiment are shown in Table 3.7 From the positive sign of the activation volume they conclude that vacancies are mediating self-diffusion. By studying the effect of doping they conclude that self-diffusion in germanium is mediated by neutral and singly negatively charged vacancies and at 700°C, that 77% of the self-diffusion is mediated by the negative vacancy. Finally by studying effects of pressure and doping simultaneously they conclude that at 700°C the negative vacancy diffusion has an activation volume of $+0.28\Omega_{Ge}$ and the neutral vacancy diffusion has an activation volume of $+0.56\Omega_{Ge}$. A synopsis of their experimental technique and their analysis follows.

Temperature (°C)	Activation Volume (Ω_{Ge})
813	0.41
752	0.36
700	0.35
643	0.28
603	0.24

{tc "Table 3.7. Activation volume for Ge self diffusion measured by Werner *et al.*" \f t}Table 3.7.
Activation volume for Ge self diffusion measured by Werner *et al.*³⁹

Self-diffusion was measured by tracking the radioactive tracer ^{71}Ge . The radioactive tracer was prepared by neutron irradiation of natural germanium, converting ^{70}Ge into ^{71}Ge . The samples were prepared by vapor deposition of the radioactive material onto the surface of polished germanium wafers resulting in a thin film diffusion source for each sample. The samples were annealed in a high pressure high temperature gas cell⁴⁰. This cell uses gaseous argon as the pressure medium and is capable of achieving pressures up to 0.6 GPa, temperatures up to 900°C and anneal times of several days. The samples were then sputter sectioned by an Ar ion beam. The sputtered material was deposited onto a moving polymer ribbon. The radioactivity profile along the polymer ribbon was converted into a depth profile of the radioactive tracer in the sample. These radioactive tracer depth profiles were used to calculate the diffusion coefficient for the various pressures and doping conditions. The activation volumes were then calculated in a manner identical to that used in this thesis, that is by using Eq. 2.20.

The doping dependence of self-diffusion was used to deduce the charge states of the defects. The doping dependence data showed that n-doping increased self-diffusion and therefore Werner *et al.* concluded that negative vacancies and perhaps neutral vacancies are mediating self-diffusion. For singly charged negative vacancies⁴¹, **Error! Bookmark not defined.**

$$c_{-}^{dop} / c_{-} = n^{dop} / n_i \quad (0.1)$$

where c_-^{dop}, c_- are the concentrations of negatively charged point defects and n^{dop}, n_i are the conduction electron concentrations in doped and intrinsic material respectively. For diffusion mediated by neutral and negatively charged vacancies

$$D = D_x + D_- \quad (0.2)$$

where D is the intrinsic self-diffusion coefficient and D_x, D_- are the contributions from the neutral and negatively charged vacancies in the intrinsic material. For the negatively charged vacancy mediated diffusion mechanism, Eq. 2.11 is written as

$$D_- = fgl^2 c_- G_- \quad (0.3)$$

where G_- is the jump rate for the negative vacancy. Using Eqs. 3.1 and 3.3 gives

$$D_-^{dop} = \left(n^{dop} / n_i \right) D_- \quad (0.4)$$

for doped material. Note that the contribution of neutral vacancies in the doped material is given by

$$D_x^{dop} = D_x \quad (0.5)$$

because the concentration of neutral vacancies is independent of doping. For doped material Eq. 3.2 becomes

$$D^{dop} = D_x^{dop} + D_-^{dop} \quad (0.6)$$

and then using Eqs. 3.4, 3.5 and 3.6 gives

$$\frac{D^{dop}}{D} = \frac{D_x}{D} + \left(\frac{n^{dop}}{n_i} \right) \frac{D_-}{D} \quad (0.7)$$

where D_x/D and D_-/D are the relative contributions to self-diffusion in the intrinsic material from the neutral and negative vacancies respectively. Values for n^{dop}/n_i are determined from the level of doping and D^{dop}/D is experimentally measured. Eq. 3.7 shows a linear relationship between n^{dop}/n_i

and D^{dop}/D because by definition D_x/D and D_-/D are independent of doping. Therefore D_x/D and D_-/D are easily calculated from a plot of n^{dop}/n_i versus D^{dop}/D . The linear relationship breaks down for doubly charged vacancies because Eq. 3.1 becomes **Error! Bookmark not defined.,Error! Bookmark not defined.**

$$c_{\pm}^{dop}/c_{\pm} = \left(n^{dop}/n_i\right)^2 \quad (0.8)$$

resulting in a quadratic relationship between n^{dop}/n_i and D^{dop}/D . Werner *et al.* found that their doping dependence data clearly showed a linear relationship between n^{dop}/n_i and D^{dop}/D and therefore concluded that the negative vacancies were singly charged.

Werner *et al.* used the following approach to separate the activation volumes for the two types of vacancy diffusion. From Eq. 3.2,

$$\frac{\int \ln(D)}{\int p} = \frac{\int \ln(D_x + D_-)}{\int p} \quad (0.9)$$

where p is the pressure. Using Eq. 2.20, the total activation volume can be shown to be the weighted average of the individual components:

$$DV^* = DV_x^* \frac{D_x}{D} + DV_-^* \frac{D_-}{D}. \quad (0.10)$$

Similarly by using Eqs. 3.4, 3.5 and 3.10 the activation volume for doped material

$$DV^{*,dop} = DV_x^* \frac{D_x}{D^{dop}} + DV_-^* \frac{D_-}{D^{dop}} \left(\frac{n^{dop}}{n_i}\right). \quad (0.11)$$

which can be rewritten as

$$DV^{*,dop} = \frac{DV_x^* \left(\frac{D_x}{D}\right) + DV_-^* \left(\frac{D_-}{D}\right) \left(\frac{n^{dop}}{n_i}\right)}{\left(\frac{D_x}{D}\right) + \left(\frac{D_-}{D}\right) \left(\frac{n^{dop}}{n_i}\right)} \quad (0.12)$$

Note that D_x/D and D_-/D are constants at a given temperature and are experimentally determined. Werner *et al.* fit Eq. 3.12 to a plot of n^{dop}/n_i versus $DV^{*,dop}$ to determine DV_x^* and DV_-^* .

3.4 Effect of Pressure on diffusion in Silicon.

Nygren *et al.*^{Error! Bookmark not defined.} measured the activation volume of arsenic diffusion in silicon. Their results are listed in Table 3.8. Their experiment was performed in the high pressure piston cylinder, described Section 4.1, using NaCl as their pressure medium. The samples were prepared by ion implantation and the diffusivity was measured with Rutherford Backscattering spectrometry (RBS). From the negative values of their activation volumes they concluded that arsenic diffusion in silicon probably occurs via the interstitialcy mechanism.

Temperature (°C)	Activation Volume (W_{Si})
850	0.48±0.19
900	0.62±0.08
950	0.43±0.10
1000	0.39±0.11

{tc "Table 3.8. Activation volumes for Arsenic Diffusion in Silicon measured by Nygren *et al.*" \f t}Table 3.8. Activation volumes for Arsenic Diffusion in Silicon measured by Nygren *et al.*^{Error! Bookmark not defined.}

Concern remains however, that the results may have been affected by chemical contamination from the pressure medium, including oxidation, and by the non hydrostatic stresses. The piston cylinder device, discussed in greater detail in Section 4.2, is not air-tight and uses a solid medium to transmit pressure, allowing shear stresses to be applied to the sample. The pressure medium can only be used in the temperature pressure regimes in which it remains a solid. At the anneal temperatures of this experiment NaCl, the pressure medium, becomes molten at ambient pressures. Therefore all the zero pressure anneals were done in a vacuum furnace. This may have allowed additional cross calibration temperature uncertainties to affect the results.

Aziz *et al.*^{Error! Bookmark not defined.} studied self diffusion of silicon in the same high pressure piston cylinder apparatus and reported that pressure enhances silicon self diffusion. They used ion implantation of ^{30}Si to prepare the samples and measured diffusivity with secondary ion mass spectroscopy (SIMS). However at anneal temperatures high enough for measurable silicon self diffusion there is a very small window between the melting pressure of NaCl and the instrument's maximum pressure. This meant that they could not achieve a sufficient pressure range for their experiment. The zero pressure anneals were done in a vacuum furnace that may have allowed the cross calibration temperature uncertainties to affect the results.

Södervall *et al.*^{42, Error! Bookmark not defined.} have measured activation volume for boron, gallium and germanium diffusion in silicon. Their results are tabulated in Table 3.10. The boron diffusion samples were prepared by ion implantation. The gallium and germanium diffusion samples were prepared by vapor deposition of a thin film of the respective material. The high pressure anneals were done in a high temperature gas cell capable of reaching pressures of up to 1.4 GPa and used argon as the pressure medium. The diffusivity measurements were made using SIMS. A summary of their conclusions is presented below.

Dopant	Temperature (°C)	Activation Volume (V_{Si})
Boron	1054	+0.41±0.05
	1056	+0.48±0.12
	1056	-0.03±0.06
	1154	+0.52±0.13
	1230	+0.02±0.15
Gallium	1050	-0.85±0.25
	1050	-0.45±0.20
Germanium	1050	-0.52±0.03
	1170	-0.46±0.11
	1230	-0.28±0.13

{tc "Table 3.9. Activation Volumes of B, Ga and Ge diffusion in Silicon measured by Södervall *et al.*" \f t}Table 3.9. Activation Volumes of B, Ga and Ge diffusion in Silicon measured by Södervall *et al.*^{Error!}
Bookmark not defined.

From the negative values of the activation volumes of germanium and gallium, they conclude that the interstitial is the predominant defect mediating diffusion. For a normal substitutional impurity, if interstitials mediated diffusion, then the interstitialcy mechanism, shown in Figs. 2.3 and 2.4, would operate. Boron diffusion, on average, has a positive activation volume that does not seem to be consistent with the interstitialcy mechanism. Also boron and gallium, being trivalent substitutional impurities, are expected to diffuse by the same mechanism. Therefore to account for the difference in sign of their activation volumes they propose that both dopants diffuse via the kick-out mechanism. They base their claim on the following argument. From Eq. 2.5 the kick-out mechanism involves a matrix self-interstitial replacing a substitutional impurity on a lattice site; the substitutional impurity then becomes mobile. When the matrix interstitial replaces the substitutional impurity there is a volume change given by

$$DV^* = (V_{mat}^{subs} - V_{imp}^{subs}) - (V_{mat}^{int} - V_{imp}^{int}) \quad (3.13)$$

where V_{mat}^{subs} and V_{imp}^{subs} are the volumes associated with the matrix and impurity atoms as substitutionals, that is their covalent volumes. V_{mat}^{int} and V_{imp}^{int} are the volumes associated with the matrix and impurity atoms as interstitials.

Södervall *et al.* argue that the result of Eq. 3.13 is the measured activation volume for kick-out mechanism and that the term $(V_{mat}^{subs} - V_{imp}^{subs})$ always dominates. Therefore, boron, with a smaller covalent radius than silicon, would have a positive activation volume of diffusion. Gallium with a larger covalent radius than silicon would have a negative activation volume. They conclude that both boron and gallium diffuse by the kick-out mechanisms. However, for germanium diffusion, and hence, by analogy for silicon self-diffusion, they do not rule out the interstitialcy mechanism.

Södervall *et al.* only provide a qualitative derivation of the activation volume for the kick-out mechanism. No formal or quantitative arguments are presented and the information that is summarized in Eq. 3.13 was provided entirely without any derivation. Their activation volume seems to be the formation volume of the point defect, the defect being the mobile impurity. However, for this point defect to form, an interstitial must be located next to the dopant. Therefore the activation volume for the kick-out mechanism must include the formation volume of the interstitial. They are aware of a migration term in the activation volume but assume that all migration volumes are small and positive. But from Section 2.4, we see that in diamond cubic crystals, large and negative migration volumes are also plausible. No quantitative comparison was made between the covalent volumes of the dopants and their respective activation volumes of diffusion. Indeed the scatter in their data, especially for boron and germanium activation volumes, is indicative of the extraordinary difficulty in measuring activation volumes in silicon.

4. Experimental Techniques

4.1 *Introduction*

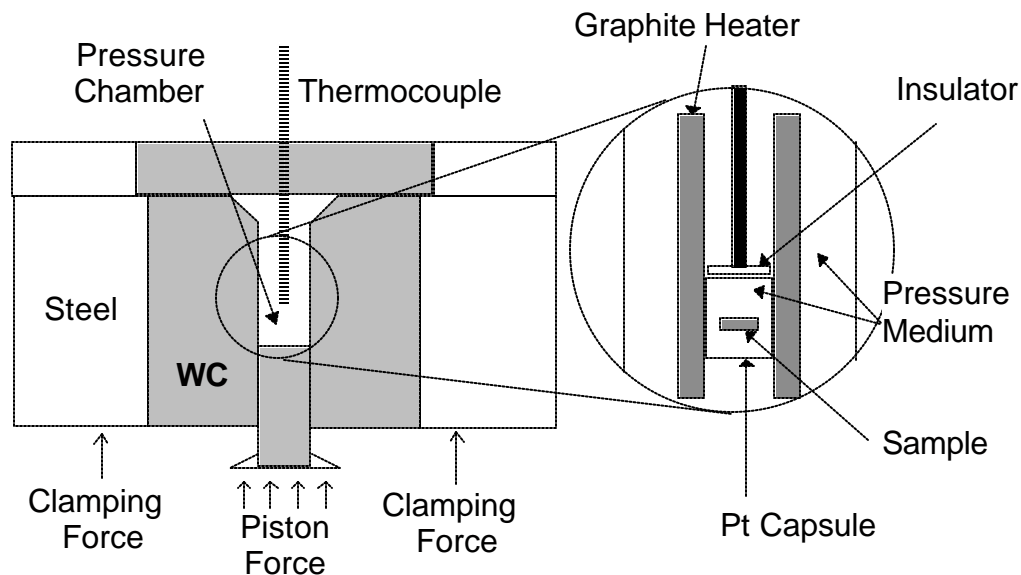
This thesis is the first part of a project to do a systematic measurement of the activation volume of dopant diffusion in germanium and silicon, and of silicon self-diffusion. The activation volume for silicon self-diffusion is theoretically the most interesting and experimentally the most difficult to measure. The principal experimental difficulty is due to the high temperatures required for self-diffusion in silicon. We have designed the experimental procedure to ultimately attain this goal.

Measurement of the activation volume requires the following steps. A sample with a known concentration profile is prepared. It is annealed under pressure at a temperature such that measurable diffusion takes place in a convenient length of time. Then, diffusion is measured by comparing the dopant profiles before and after the anneal. These steps are performed for different pressures and the activation volume is computed using Eq. 2.20. For this thesis, samples are prepared by ion implantation, annealed in an externally heated diamond anvil cell and then analyzed using Secondary Ion Mass Spectrometry (SIMS).

Ion implantation and SIMS are well-known commercial techniques and their applications to this project are described in Section 0 below. High temperature diamond anvil cells are still rare research instruments. The DAC used was developed for this thesis, and we used a newly developed technique for in-situ pressure measurement at high temperature. The detailed design for the cell and the pressure measurement technique are described in Section 0.

Before the diamond anvil cell was developed, this project was attempted in a piston cylinder high pressure apparatus. We convincingly demonstrated that solid medium pressure instruments such as the piston cylinder cannot be used for this project. A summary of our findings is described in the next section.

4.2 *Early work.*



{tc "Figure 4.1. Boyd-England Piston Cylinder." \f f}Figure 4.1. Boyd-England Piston Cylinder.

Our first attempt to study the effect of pressure on diffusion employed a Boyd-England⁴³ type piston cylinder press, located in the Harvard University Geology Department. A schematic is shown in {tc "Figure 4.1. Boyd-England Piston Cylinder." \f f}Figure 4.1. The pressure vessel is a thick walled tungsten carbide chamber with a tungsten carbide lid. A clamping force keeps the lid in place and pre-stresses the side walls compressively to increase their effective strength. A soft steel ring around the pressure vessel absorbs the shock if the pressure vessel cracks. Pressure is generated by forcing a tungsten carbide piston into the pressure chamber by a hydraulic ram. In the press used for this experiment, the clamping force is achieved with a 600 ton hydraulic

ram and the piston is forced using a 50 ton hydraulic ram. It has a pressure chamber 12 mm in diameter and 25 mm high and is capable of reaching 4 GPa.

The pressure chamber is filled with a soft deformable solid that acts as a pressure transmitting medium. Sodium chloride was used as the principal pressure medium. The sample was heated with a graphite heater inside the pressure chamber. The heater is a graphite tube with the top and bottom electrically connected to the piston and top plate. By passing a current through the heater the inner section can be heated to up to 1400 °C. A thermocouple through a hole in the top plate monitors the temperature. The tungsten carbide pieces are water cooled to keep from overheating. The sample itself is set inside a sealed platinum capsule. The capsule also contains a second pressure medium that is in physical contact with the sample. This physical contact is the source of the problem for this experiment.

The pressure chamber in the piston cylinder is not air-tight, so the pressure medium must be a solid. At temperatures needed to achieve measurable diffusion, both silicon and germanium become chemically very reactive. Besides being deformable, the pressure medium must also be chemically inert. However, we could find no solid that would not react with the samples at the temperatures and pressure of interest. Because the ion implanted layer of the sample is less than 500 nm deep, only a slight chemical reaction was enough to destroy the sample. Sodium chloride was the most inert medium for the silicon samples but it existed as a solid for a very small pressure window at the relevant temperature. Melting of the pressure medium

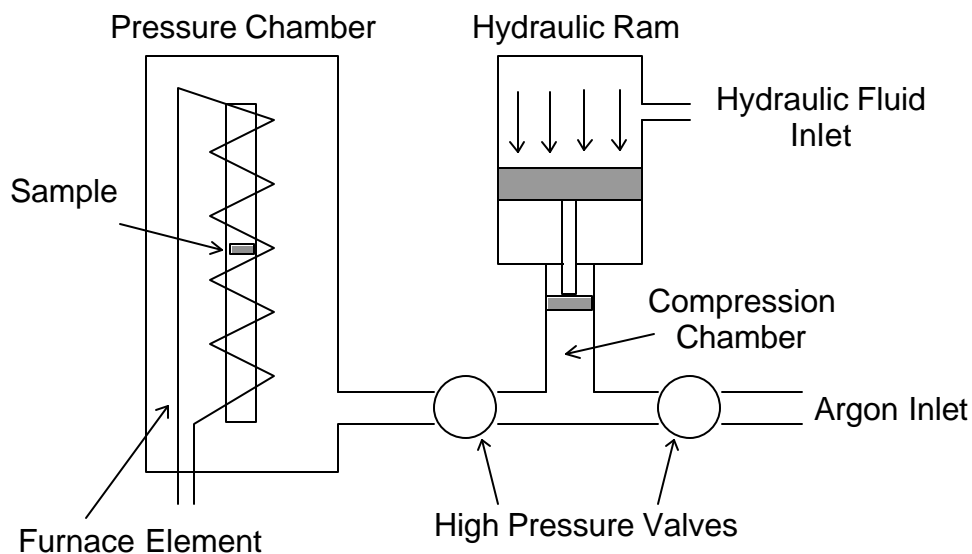
resulted with sample coming in contact with the platinum capsule and reacting.

Another effect from lack of sealing of the pressure chamber was presence of atmospheric oxygen and nitrogen. Oxidation and nitridation are known to inject non-equilibrium concentrations of point defects that effect diffusion in addition to the effects of pressure **Error! Bookmark not defined.**. In order to study the effects of pressure on diffusion, chemical activity on the surface must be suppressed. Gettering with silicon powder and using the most inert pressure medium, salt, still resulted in surface damage that was easily visible in a 60X microscope. Even when the surface layer survived, these samples were found to be useless for the experiment.

A third problem with piston cylinder apparatus concerns the temperature gradients that are present inside the pressure chamber. The cooling water and furnace are only few centimeters apart. One measurement showed temperature gradients of 40 K per mm⁴⁴. Uncertainties in the diffusivity resulting from 10 K uncertainty in the temperature will effectively hide the anticipated effects of pressure.

Due to the problems with the piston cylinder apparatus we attempted this project with a High Pressure Gas Cell located in Cornell University, a schematic of which is shown in {tc "Figure 0.2. High Pressure Gas Cell." \f f}Figure 0.2. The pressure is generated by compressing argon gas with a hydraulic ram by a multi-step process. The gas is introduced into the compression chamber by opening the outer valve. The hydraulic ram then compresses the gas, and the compressed gas in introduced into the pressure

chamber via the inner valve. The pressure chamber is a thick walled vessel with a metal furnace element inside it. The instrument used for this experiment was capable of reaching 0.7 GPa and 1400 °C.



{tc "Figure 0.2. High Pressure Gas Cell." \f}Figure 0.2. High Pressure Gas Cell.

The principal problem with the gas cell was the limited pressure range. Even attempting to reach the rated pressure of 0.7 GPa made pressure chamber prone to explode. This particular instrument was located in a separate room with steel door to protect the operator. The first few attempts to anneal silicon at 0.6 GPa showed that an oxidation problem would have to be overcome. However, the pressure chamber exploded before a fix could be found. Because pressures on the order 3 GPa would be optimal for this experiment, the gas cell was clearly a very difficult instrument to use for very little gain and we did not pursue it any further.

The experiences with these high pressure instruments prompted us to design and build the high temperature diamond anvil cell (DAC) described in Section 0.

4.3 **Sample Preparation**

4.3.1 **Goals**

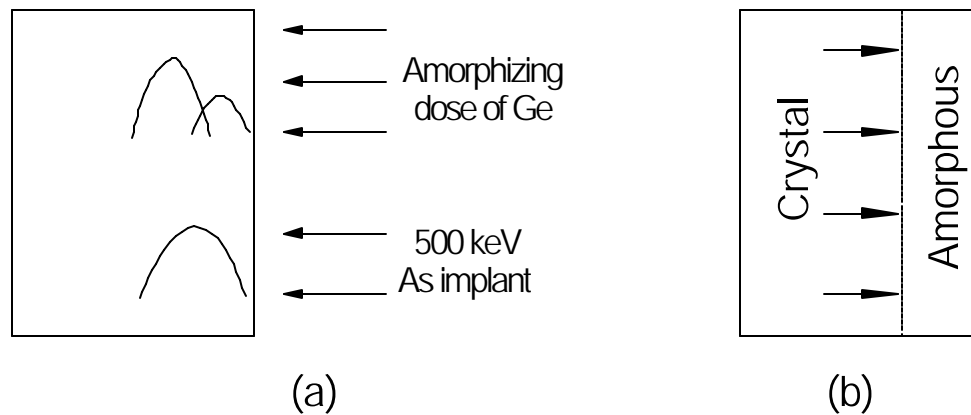
To measure diffusion in crystalline germanium, samples need to be undamaged germanium crystals with negligible concentrations of dislocations and grain boundaries. These extended defects are conduits for fast diffusion that will overshadow the diffusion from the bulk. Arsenic needs to be introduced in a sufficiently localized depth profile in order to measure diffusion. The concentration of arsenic should be sufficiently high to be measurable with SIMS but in the safest experiments should be lower than the solubility limit at the experimental temperature. The final samples should fit in the diamond anvil cell and should be approximately 200 μm by 200 μm and 50 μm thick. Finally, the surface of sample should be protected from chemical reaction to prevent the doped layer from reacting away.

4.3.2 **Preparation Technique.**

We start with 50 μm thick intrinsic germanium wafers polished on both sides, purchased from Semiconductor Processing Company, Boston MA. The germanium is intrinsic at room temperature and has a resistivity of 40 Ωcm . The arsenic is introduced by ion implantation. Thin germanium wafers are mounted onto thicker germanium wafers with a thin layer of lubrication oil, WD-40. The surface tension is strong enough to keep the thin wafers adhered to the backing wafers during the implant. The thin wafers are very fragile and oil is used instead of glue to allow the thin wafers to expand or contract without shattering. The backing layer is also germanium to minimize the effects from thermal expansion mismatch. The wafer is then implanted with 500 keV 75As^+ with a dose of 2×10^{14} atoms/ cm^2 at liquid nitrogen temperature. The resulting concentration profile is approximately a Gaussian

with a peak at a depth of 215 nm and a width of 67 nm. The peak concentration of arsenic is 1×10^{19} atoms/cm³ or 0.02 atomic percent. This peak concentration is about 10% of the solubility limit of arsenic in germanium at 575 °C, the temperature of the experiment. The implanted layer is then completely amorphized with a double self implant of ⁷⁴Ge⁺, with energies of 500 keV and 250 keV and doses of 1×10^{15} atoms/cm² and 5×10^{14} atoms/cm² respectively, at liquid nitrogen temperatures. The ion implantation was done at Oak Ridge National Laboratory.

Note that the implant profile characteristics were determined by performing a Monte-Carlo simulation with the TRIM89 computer program.



{tc "Figure 0.3. Sample Preparation. " \f f}Figure 0.4. Sample Preparation.
(a) Ion Implantation. (b) Restoring Crystallinity with SPEG.

Complete amorphization of the implanted layer is necessary for restoring a damage free crystal. The initial arsenic implant creates damaged crystal that cannot be directly transformed into defect-free crystal. Only complete amorphization allows the transformation to defect free crystal by Solid Phase Epitaxial Growth (SPEG)⁴⁵. SPEG is a well-characterized process by which a crystal grows into an amorphous layer. SPEG occurs at temperatures too low for measurable diffusion to take place, and at the anneal temperature all the

material is crystalline. For this experiment the samples undergo SPEG inside the DAC during temperature run-up for the diffusion anneal to ensure that handling does not create extended defects in the crystal. Pressure is known to enhance SPEG in germanium⁴⁶, which means that the amorphous layer transforms into crystal at even lower temperatures. We have calculated that all the amorphous material has been completely transformed by 400 °C, well below the diffusion temperature of 575 °C. A schematic of the sample preparation is shown in {tc "Figure 0.3. Sample Preparation. " \f f}Figure 0.4.

The implanted germanium wafer is coated with a sputter deposited SiO₂ film 2 - 4 nm thick in order to protect the surfaces from chemically reacting and volatilizing as GeO. This is the minimum thickness that can be sputter deposited reliably and a thicker layer will interfere with the SIMS analysis. The bottom surface is coated with 120 nm thick film such that it develops a blue luster allowing the bottom layer to be distinguished from the top. In both cases the film was simultaneously deposited on a glass substrate to check the stoichiometry. In each case the film was transparent indicating that the SiO₂ film is close to the proper stoichiometry; SiO₂ that is off stoichiometry is black.

The wafer is then cleaved into small pieces that fit inside the DAC. The resulting pieces have linear dimensions from 50 μm to 300 μm and are irregularly shaped.

4.4 ***Generating Pressures***

4.4.1 ***Design Goals***

The high pressure instrument for this project instrument should be designed to operate at pressures from 0 to 8 GPa.. A larger pressure span

would result in a more accurate measurement of the activation volume, but pressures beyond 8 GPa cannot be used because germanium melts at approximately 6 GPa and silicon melts at approximately 7 GPa at typical diffusion temperatures⁴⁷. Note that the ambient pressure solid phases of silicon and germanium are less dense than the liquid and hence they melt at lower temperatures under high pressure than at ambient pressure.

The instrument must be capable of attaining temperatures such that measurable diffusion occurs in a few hours or less. The specific temperature required is dependent on the diffusion system being studied, but an ultimate capability of achieving 1100 °C will allow us to study the diffusion of all the substitutional dopants in germanium and silicon, including self-diffusion. For this thesis we study the effect of pressure on arsenic diffusion in germanium and a capability of achieving 600 °C is adequate.

The temperature effects of the diffusion are typically much greater than the pressure effects. A temperature uncertainty of 10 °C is enough to overshadow the anticipated pressure effect. The instrument must have a temperature accuracy of ± 5 °C and a repeatability of ± 2 °C or better.

Both germanium and silicon become chemically very reactive at the temperature necessary for the experiment. They rapidly oxidize; they also react with or form eutectics with most metals. Even slight amounts of chemical activity can cause problems by injecting non-equilibrium quantities of point defects into the matrix. Hence, a chemically inert pressure medium is necessary.

It has been shown that for SPEG, non-hydrostatic stresses and hydrostatic pressure have very different effects⁴⁸. If the mechanism for SPEG and diffusion are in any way related, non-hydrostatic stresses will introduce an error in the measurement of activation volume. In addition to affecting the activation volume, non-hydrostatic stresses may create dislocations. Therefore the pressure instrument must have a hydrostatic pressure environment.

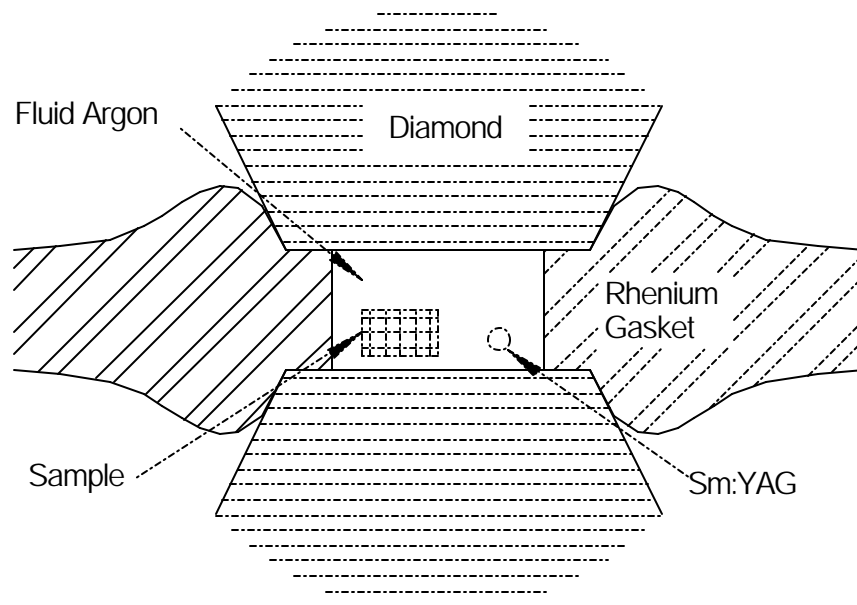
Preliminary work at ambient and high pressures also suggested that the overall experimental design should allow for a fast turn around in collecting individual diffusion measurements. Each individual measurement is prone to error and a large number of measurements may be necessary to achieve statistical significance.

As described in Section 0, we rejected the piston cylinder and gas cells as suitable instruments for this project and chose to develop an externally heated diamond anvil cell instead.

4.4.2 DAC

The diamond anvil cell (DAC) is a widely used high pressure instrument⁴⁹. Schiferl⁵⁰ has developed a very high temperature externally heated DAC system to study high temperature phase diagrams and develop pressure calibrants. This DAC was used for preliminary work for this project but proved to be unsatisfactory. The pressure medium was not adequately oxygen free, the vertical plane of culet surface caused the sample to sink into contact with the gasket and the optical system did not collect enough light for the data collection time to be short compared to the anneal durations. However, we were able to demonstrate that with modification it could be used for this

project. We designed and developed a DAC system for this project based on Schiferl's design.

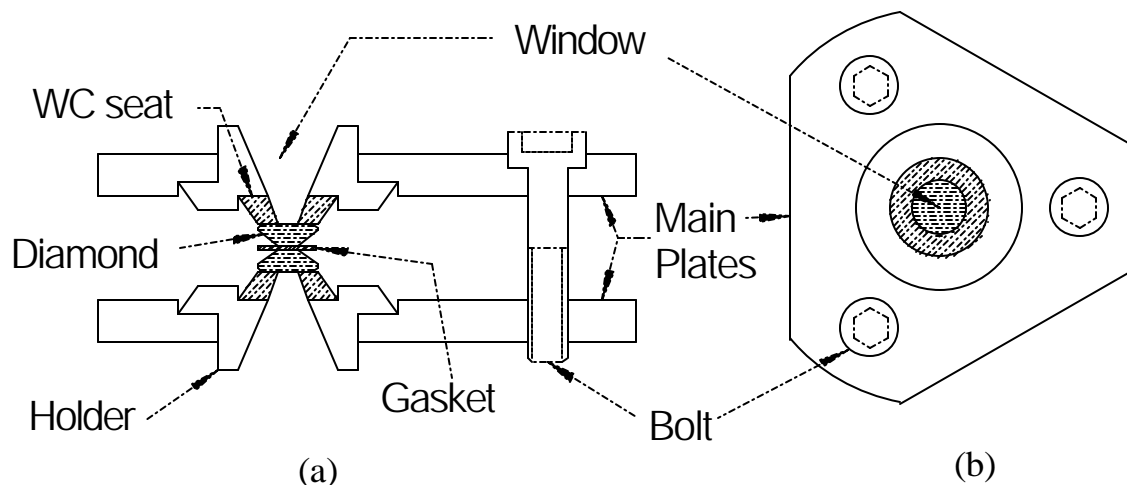


{tc "Figure 0.4. DAC Pressure Chamber." \f}Figure 0.5. DAC Pressure Chamber.

{tc "Figure 0.4. DAC Pressure Chamber." \f}Figure 0.5. shows the pressure chamber of the DAC. The top and bottom of the chamber are the anvils and the side walls are formed by a metal gasket. The metal gasket is a sheet of metal with a hole in it. The pressure is generated by forcing the two anvils together on the hole, which becomes the pressure chamber. The gasket then deforms plastically, sealing the pressure chamber. The pressure chamber is filled with a pressure medium, the sample and a pressure indicator. Diamond is used as anvil material because it is the hardest material currently known. It is also transparent and provides a window into the pressure chamber. The metal gasket is made from rhenium, which is a very strong yet ductile material. The ductility is necessary for the gasket to deform and seal the pressure chamber, and the strength is necessary to contain the high

pressure. Rhenium has the added advantage that it has a very high melting point, 3000 °C and retains its strength at high temperatures. Argon is used as a pressure medium because it is chemically inert and provides a hydrostatic environment. For this experiment the temperatures and pressures of different anneals were always above the argon melting curve. Even if the argon were solid, as a van der Waals solid it has a very low shear strength and provides an almost hydrostatic environment under pressure. The pressure indicator is piece of samarium doped YAG (Sm:YAG) and its function will be described in Section 0. The diamonds used in this experiment have a culet (front flat) diameter of 1 mm. The resulting pressure chamber has a diameter of about 300 μm to 400 μm with a height of 100 μm to 150 μm .

The main body of the DAC provides the structural support for the diamonds and the force necessary to generate the pressure. Generating a pressure of 5 GPa with 1 mm culets requires a force of approximately 5 kN on the diamonds, equivalent to a weight of 500 kg. Such a force can be generated with a palm sized instrument, and the DAC used in this experiment is 2.25" in diameter and less than 1" thick. A schematic of it is shown in {tc "Figure 0.5.



{tc "Figure 0.5. Diamond Anvil Cell. " \f}Figure 0.6. Diamond Anvil Cell.
(a) Cross Section. (b) Top View.

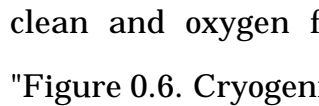
Diamond Anvil Cell. " \f f)Figure 0.6. It is a modified Merrill-Bassett⁵¹ design that is constructed from Haynes 230[®], a nickel based superalloy manufactured by Haynes International Inc. of Kokomo, Indiana. The main body consists of two triangular plates that are forced together by three bolts. The force on the diamonds is generated by tightening these bolts by hand, one at a time. The plates are flexible and the elastic bending of the plates allows the pressure to be built up gradually instead of a increasing sharply. The table (back flat) of the diamonds used in this experiment has an area about 10 times the culet. With the DAC operating at 5 GPa, the tables still transmit a pressure of 0.5 GPa and need to be seated on very hard material. The diamond seat is made from tungsten carbide (WC), and is tapered to further reduce the stress. The seats are then mounted on the holder, which is also made from the Haynes 230[®] superalloy. The holder is separate from the main plates to allow flexibility in aligning the diamonds before pressure loading. The seats and diamonds are held on the holder by a sodium silicate based high temperature furnace cement. The cement does not bear any load, but merely keeps the diamonds in position when the DAC is not under load. The holder is held in place by set screws that also do not bear any load. The DAC is designed such that under load, friction keeps all the alignments intact.

The DAC is constructed to be heat resistant and to operate inside an inert atmosphere furnace. This furnace is designed to eliminate temperature gradients around the pressure chamber and allow for an accurate measurement of temperature. The furnace and the temperature measurement are described in Section 0. Schiferl's DAC is constructed from rhenium metal and is designed be operated at temperatures up to 1600 °C. Unfortunately, rhenium is an expensive material and is very difficult to fabricate because it

must be machined using EDM (spark cutting). The materials and machining costs make fabrication of rhenium parts very expensive. The Haynes 230[®] alloy which we used for the main body of the DAC was manufactured to operate at temperatures up to 1200 °C for an indefinite length of time and is amenable to normal machining techniques. Other common super alloys such as the various Inconels[®] suffer significant microstructural damage at temperatures above 800 °C⁵². Haynes 230's principal limitation is its low strength, which was overcome by making the DAC physically large. This DAC is designed to achieve 10 GPa at 800 °C or lower temperatures with the 1 mm culet diamonds. The bolts are the weakest component, and if replaced with stronger (e.g. rhenium) bolts, the rest of the cell can achieve 10 GPa at 1100 °C. The diamond seat is made from tungsten carbide, a material that retains its strength up to 1100 °C in an inert atmosphere⁵³.

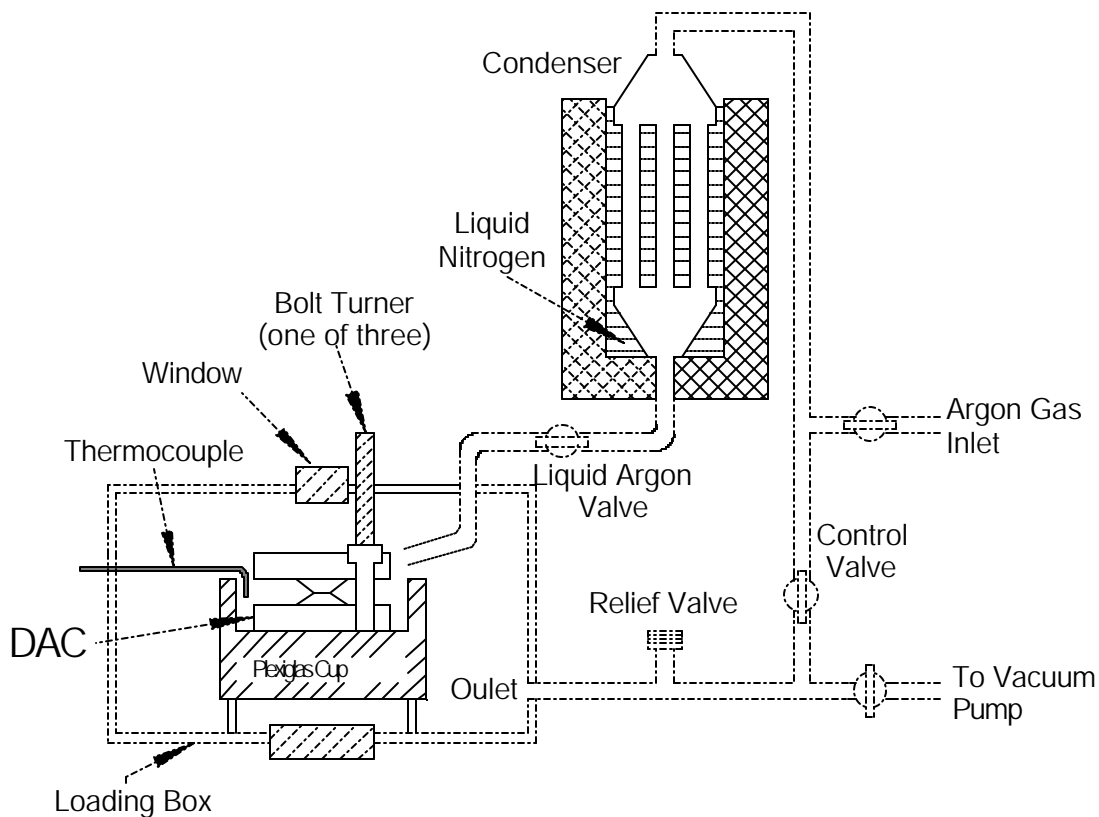
The diamonds also must be protected from heat related damage. In a vacuum or in an inert atmosphere, the diamonds will not graphitize up to 1600 °C⁵⁴. Air or oxygen will graphitize diamonds above 600 °C and hence the DAC is heated in an inert atmosphere furnace. Solids in contact with the diamond can also react with the diamonds or catalyze graphitization, and the gasket material must be chosen with care. Our experience has shown that the Inconel X750[®] alloy, a commonly used as gasket material, reacts with diamond at about 575 °C. Some data points were acquired using Inconel gaskets but such use resulted in the loss of the diamonds within three anneals. Our experience has also shown that rhenium gaskets do not affect diamonds up to at least 750 °C and were used for all the remaining anneals. All the anneals for this thesis were conducted at 575 °C and the diamonds used with the rhenium gaskets lasted for an indefinite number of anneals.

The samples have to be transferred into the pressure chamber of the DAC without getting them dirty. The samples are too small for normal laboratory tweezers but it has been found that they can be easily handled by attaching to pin points with surface tension and residual electrostatic attraction. The samples are cleaned with methanol in filter paper lined petri dishes. Just before all the methanol dries out, a sample can be attached to a clean pin point with the surface tension of the methanol. It is then transferred to the DAC pressure chamber, and by that time the methanol has evaporated and the sample is held by what is presumably residual electrostatic attraction. It is very easily shaken loose from the pin point into the pressure chamber. A similar technique is used to load a small piece, about 30 μm in diameter, of Sm:YAG. The DAC is then closed and argon is loaded into the pressure chamber by opening and closing the DAC under liquid argon.

Argon, the pressure medium, is introduced into the pressure chamber as a liquid at cryogenic temperatures. Care needs to be taken to keep the argon clean and oxygen free. A schematic of the argon loader is shown in  Figure 0.7. The DAC is loaded with argon inside an enclosed box. Before the loading process the loading box and the condenser are pumped out to remove all the oxygen. Clean gaseous argon is then passed through the condenser which sits in a bath of liquid nitrogen. Because the boiling point of nitrogen is below the freezing point of argon attempting to liquefy the argon may freeze it inside the condenser. Hence, the condenser walls are smooth and vertical in order to allow the argon snow to fall to the bottom of the condenser, melt and then flow out. Nevertheless, preliminary attempts failed because the solid argon probably blocked the exit of the condenser. A technique to generate liquid argon was then discovered

empirically. The gaseous argon inlet had to be connected to the gas outlet of the loading box. The valve connecting these two became a control valve, which is then used to regulate the liquid argon flow. Note that during loading the valve to the vacuum pump is closed, the gaseous argon valve is always open, the liquid argon valve is always open and the excess pressure is released by the relief valve.

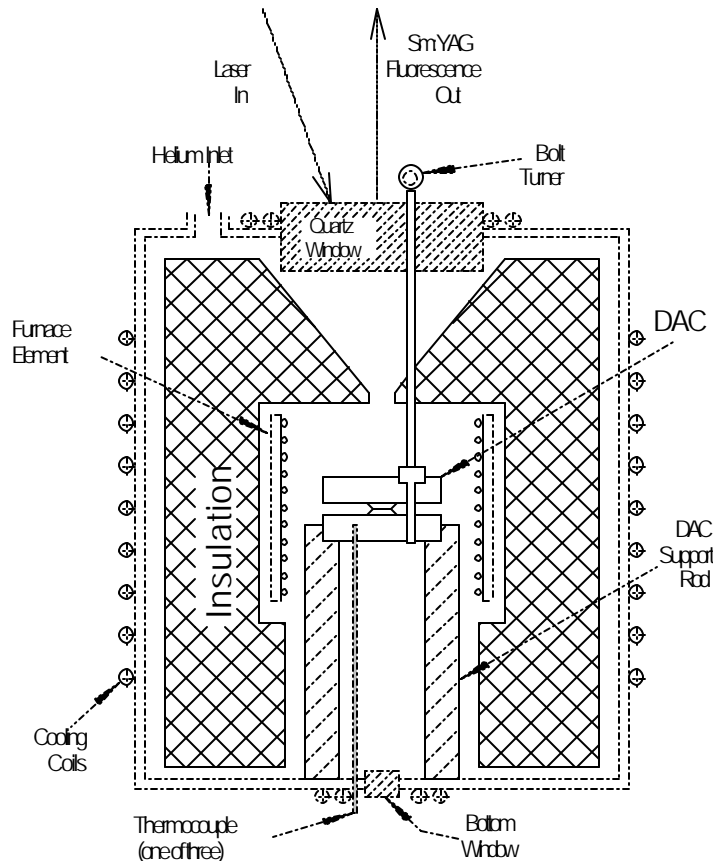
The stream of liquid argon cools down the DAC and then begins to fill the Plexiglas cup. A thermocouple is used as an indicator to check when the liquid argon fills the cup. At that time the cell is opened by means of the three bolt turners, argon fills the pressure chamber and then the cell is shut and the bolts tightened to seal the argon and generate pressure.



{tc "Figure 0.6. Cryogenic Argon Loader." \f}Figure 0.7. Cryogenic Argon Loader.

4.4.3 Furnace

A schematic of the furnace is shown in Fig. 4.7. The furnace is constructed from stainless steel with water cooling coils on the outside. The insulation is constructed from alumina fiber boards and alumina wool. The heating element is a spiral of Kanthal heating wire mounted on the inside wall of a tube of furnace cement and alumina fiber. The insulation is shaped to allow optical access to the DAC. In its current configuration the furnace can operate at 1000 °C while dissipating about 600 W. It is designed to be used at temperatures up to 1100 °C.



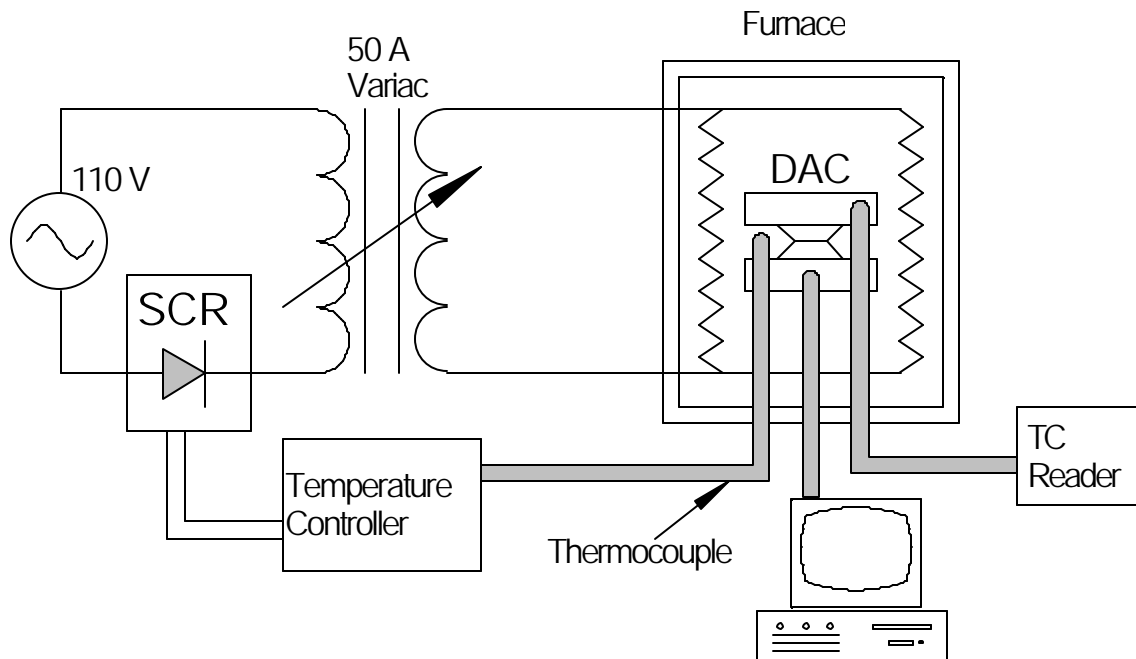
{tc "Figure 0.7. Furnace." \f}Figure 0.9. Furnace.

The furnace is operated with an inert gas atmosphere by pumping the air out and introducing helium at 3 psi over-pressure. The over-pressure allows a

simpler construction of the furnace by not requiring that all seals be completely gas tight. Helium is used instead of argon because it has a very low refractive index and its convection currents do not interfere with the optical access to the DAC. A tube of titanium sheeting inside the element tube provides gettering for any remaining oxygen or water, and acts a heat shield to homogenize the heat from the element.

The DAC sits on hard alumina rods that provide structural support at temperature and prevent rotation when the bolt is tightened. One of the bolts of the DAC is connected to a bolt turner that can be operated from outside while the furnace is operating.

The furnace has two windows, the main one on top and a smaller window at the bottom. The large window in the top provides the optical access to the DAC that is needed measure the pressure at temperature. Pressure is measured by directing a laser into the DAC and measuring the resulting Sm:YAG fluorescence. The details of pressure measurement are described in section 0. The bottom window allows transmitted illumination from below for optical alignment of the pressure measurement system.

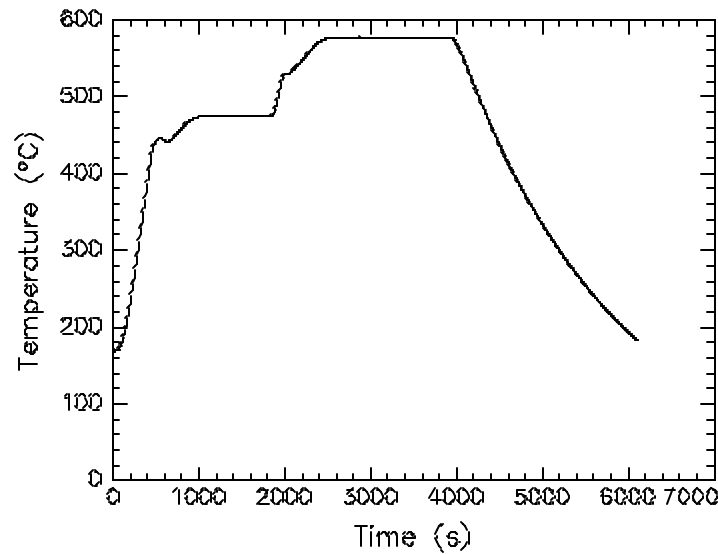


{tc "Figure 0.8. Furnace Temperature Control." \f}Figure 0.10. Furnace Temperature Control.

A schematic of the furnace temperature control and measurement apparatus is shown in {tc "Figure 0.8. Furnace Temperature Control." \f}Figure 0.10. The temperature in the furnace is monitored by three thermocouples at the same radial distance from the central axis. They extend into the DAC. One reads the temperature of the bottom plate, another reads between the plates and a third reads the top plate. By adjusting the insulation and the element in the furnace, the top and bottom thermocouples are made to read within 3°C of each other, with the middle thermocouple reading falling in between them. The temperature repeatability is within 1°C . The thermocouples used are K type (Chromel Alumel) with Inconel sheaths and ungrounded tips purchased from Omega Engineering.

The temperature is controlled by a digital PID controller connected to a silicon controlled rectifier (SCR). The SCR operates in a phase angle control mode for a fine control of the furnace current. The furnace element is a $1.7\ \Omega$

Kanthal wire spiral and is operated at 40 V and 25 A at full power. This setup allows the furnace to climb the final 100 °C in 10 minutes or less without a significant overshoot of the temperature. One of the thermocouples is monitored by computer so that the complete temperature profile can be used in data analysis. Fig. 4.9 shows a typical temperature profile



{tc "Figure 0.9. Typical Temperature Profile." {f}Figure 0.11. Typical Temperature Profile.

Fig. 4.9 shows that the time intervals for the temperature rise and fall are not negligible compared to the anneal time. Therefore D should be treated as time dependent, because it is temperature dependent and temperature depends on time. From Crank⁵⁵, when $D(t)$ is a function of time only then

$$\frac{\partial c}{\partial t} = D \frac{\partial^2 c}{\partial x^2} \quad (0.1)$$

becomes

$$\frac{\partial c}{\partial t} = D \frac{\partial^2 c}{\partial x^2} \quad (0.2)$$

where D_{ann} is the time independent diffusion coefficient at the anneal temperature and t_{eff} is the effective time given by

$$t_{eff} = \frac{1}{D_{ann}} \int_0^t D(t') dt' \quad (0.3)$$

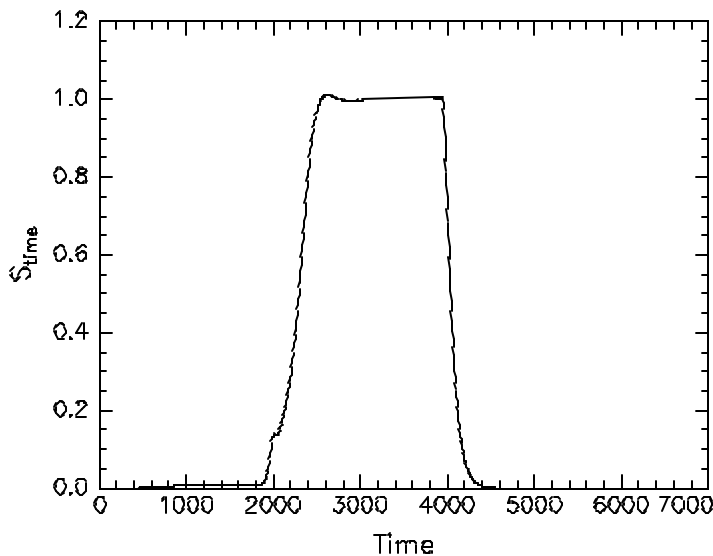
Eq. 4.2 is the linear diffusion equation, with time variable replaced by an effective time variable. Using Eq. 2.14, the Arrhenius form of the diffusion coefficient, we get

$$S_{time}(t) = \frac{D(t)}{D_{ann}} = \frac{\exp\left(-\frac{\Delta H^*}{kT(t)}\right)}{\exp\left(-\frac{\Delta H^*}{kT_{ann}}\right)} \quad (0.4)$$

where S_{time} will be called the time scaling factor, ΔH^* is the activation enthalpy and the T_{ann} is the anneal temperature. The effective time becomes

$$t_{eff} = \int_0^t S_{time}(t') dt' \quad (0.5)$$

and can be calculated from the temperature profile if ΔH^* is known. The ambient pressure ΔH^* of 2.51 eV for arsenic diffusion in germanium⁵⁶ was used as an approximation for the high pressure ΔH^* , because of the small $P\Delta V^*$ made the difference negligible at high pressure. Fig. 4.10 shows a plot of the time scaling factor versus time. The area under the plot is the effective time for the anneal.



{tc "Figure 0.10. Plot of effective time." \f}Figure 0.12. Plot of effective time.

4.5 *Measuring Pressure*

4.5.1 **Goals**

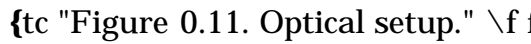
In most high pressure devices the pressure is computed from the applied force. The pressure inside the DAC must be directly measured because gasket deformation makes the pressure impossible to calculate from the applied force. Therefore, unlike other high pressure devices the typical DAC does not even track the applied force. The most common method of measuring pressure is to calculate it from the fluorescence of a piece of ruby inside the pressure chamber^{Error! Bookmark not defined.}. The fluorescence peaks of ruby change position with pressure in a well-characterized manner and have been calibrated⁵⁷. For high temperature high pressure experiments, the ruby fluorescence is useful as a pressure calibrant only up to 200 °C, above which the peaks become too broad and weak to be accurately measured. An older DAC in this laboratory was designed to overcome this problem by heating only the pressure chamber. The force on the diamonds thus remained constant throughout the anneal and the pressure did not change⁵⁸. However this cell

suffered from serious temperature gradients in the pressure chamber and was limited to operating at 600 °C. The DAC described in Section 0 was designed to overcome these limitations, but it made necessary the use of a high temperature pressure calibrant.

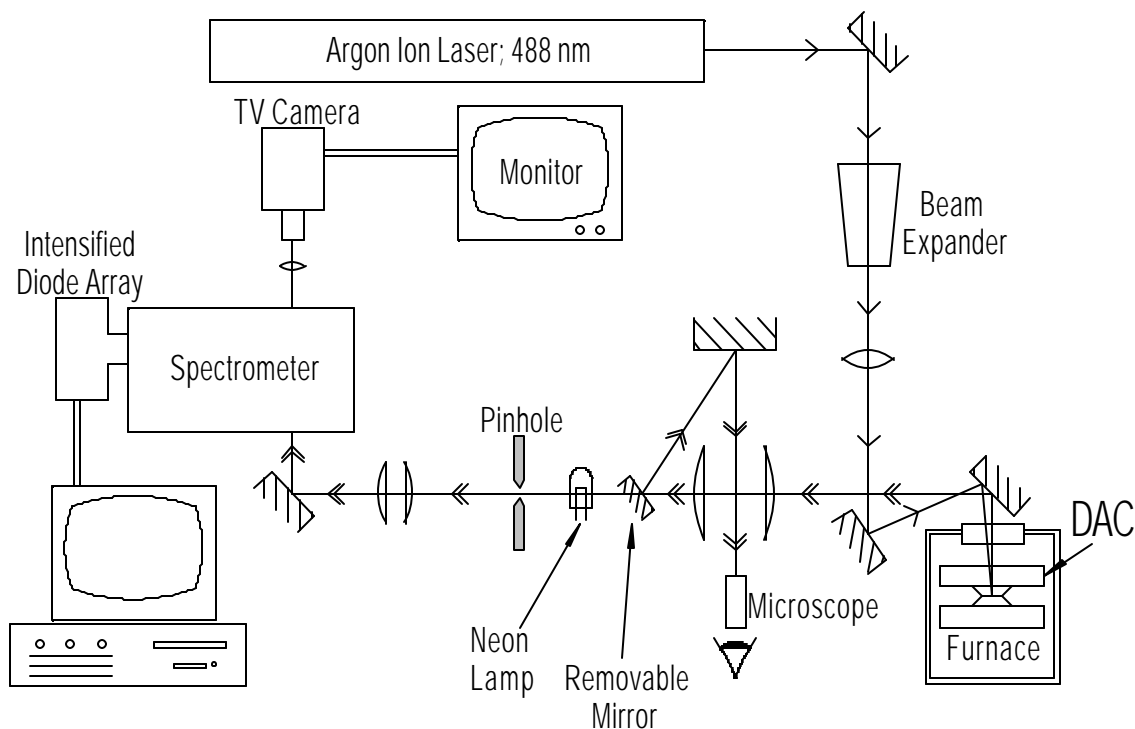
Hess and Schiferl have recently discovered that samarium doped yttrium aluminum garnet (Sm:YAG) can be used as a high temperature pressure calibrant⁵⁹. The relevant peaks are discernible up to 1200 °C and do not show any measurable shift with temperature. However Sm:YAG has rather a weak fluorescence, requiring a sensitive optical detection system. The fluorescence cannot be increased by increasing laser power, because it would result in an unwanted increase in temperature in the pressure chamber. The peak shift for Sm:YAG is 0.31 nm/GPa, therefore the optical system must be capable of detecting peak shifts of 0.06 nm or less.

The optical instrumentation consists of a laser to excite fluorescence and a spectrometer to acquire the spectrum. It is designed such that the laser beam can be exclusively focused on the Sm:YAG piece and spectra acquired exclusively from that piece.

4.5.2 Optical Setup

A schematic of the setup for Sm:YAG fluorescence acquisition is shown in  Figure 0.13. A Coherent Innova 70 argon ion laser is used to excite the Sm:YAG. The 488 nm line is used exclusively, with the output power set at 150 mW or less. The laser beam is expanded before focusing in order to achieve a tighter focus and is directed into the furnace at slight angle from the principal axis of the furnace. The slight angle

of incidence of the laser beam obviates the need for a two way mirror in the system and prevents laser reflections from the diamonds and furnace windows from traveling up the fluorescence beam path. A removable mirror in the fluorescence beam path allows the operator to see the pressure chamber through a microscope and then align the laser spot on to the Sm:YAG piece. This mirror is removed during spectrum acquisition.



{tc "Figure 0.11. Optical setup." \f}Figure 0.13. Optical setup.

The Sm:YAG fluorescence is directed into the spectrometer through two pairs of achromat lenses and a pinhole. Each pair of achromats functions as a single lens operating with a conjugate ratio of unity, that is equal object and image distances. The commercially available cemented doublet achromats used here are optimized for operating at infinite conjugate ratios, and hence are used in pairs to maintain image integrity. The first pair of lenses provides an image plane on the pinhole that is used to select out only the Sm:YAG

fluorescence to be sent into the spectrometer. A 200 μm pinhole was found to be adequate and has been used for all spectrum acquisition. A neon lamp, in a permanently fixed location in the beam path, is used for wavelength calibration. It is too small to disturb the image but provides sufficient illumination for acquiring neon spectra.

The spectrometer is an Aries FF250 0.25 m focal length single grating instrument with a 1200 groove/mm grating and two exit ports. One exit port is connected to an EG&G 1462 intensified diode array and the other to a sensitive TV camera. The spectrometer can send an undispersed image of the incoming light into the TV camera, allowing the operator to visually identify the source of the spectrum to be acquired. The spectrum is acquired by directing the dispersed image onto the diode array. This diode array has 1024 elements, each 25 μm wide with the central 750 elements intensified and it typically counts one in four photons. All the spectra were acquired using a 30 μm entrance slit because, with 25 μm elements smaller slits will not increase the resolution. The acquired spectra are transferred into a computer for analysis and the determination of pressure.

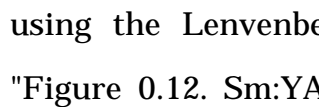
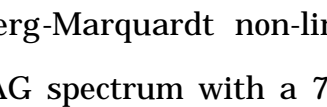
Based on our experience in Schiferl's laboratory we have found it necessary to design the system for faster acquisition of spectra such that a single spectrum is acquired in 5 minutes or less. It was deemed necessary to get multiple pressure measurements during an anneal in order to track pressure changes. Fast spectra acquisition, achieved by collecting more light, is made possible by using a short focal length spectrometer and large lenses in the beam path, resulting in two undesired side effects. Smaller focal length for the spectrometer resulted in a lower dispersion giving a separation of 0.07 nm

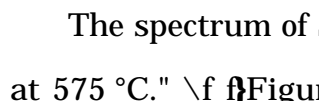
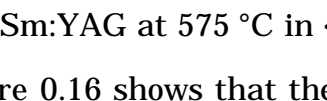
in wavelength space for each diode array element. The larger lenses have resulted in a poorly controlled beam path that gives spurious wavelength shifts when optical components are moved for routine alignment. Both of these issues have been successfully dealt with and are discussed in greater detail in Section 0.

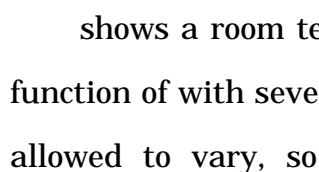
4.5.3 Sm:YAG Spectrum Analysis

The shape of a typical fluorescence peak shape is the Lorentzian function⁶⁰

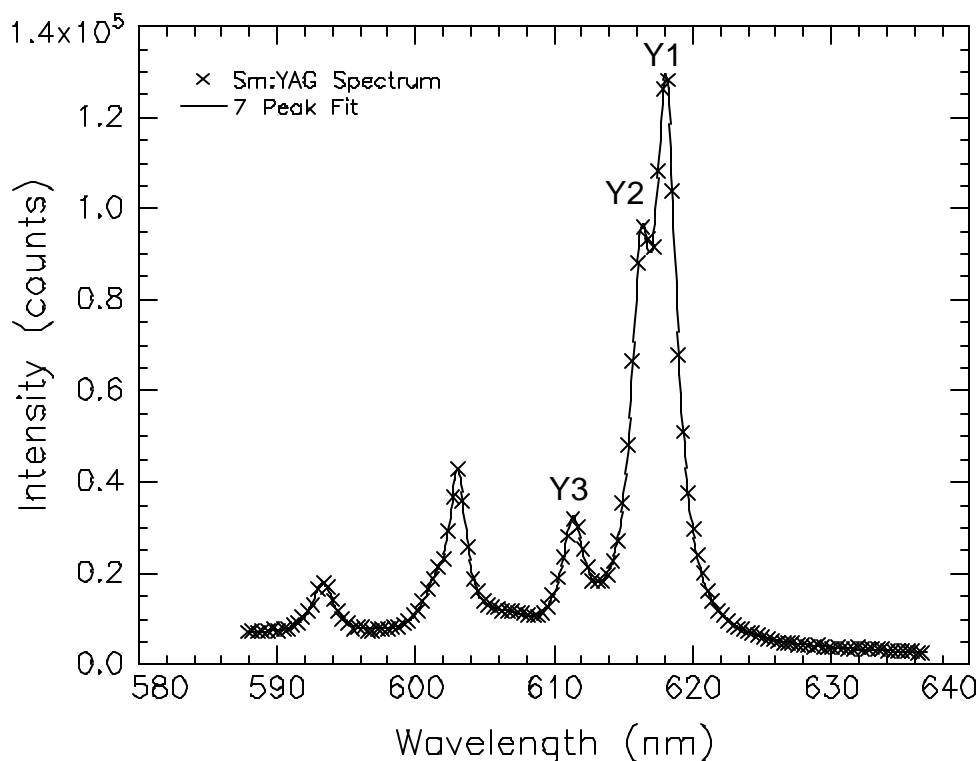
$$lor(x; a, w, h) = \frac{hw^2}{4(x - a)^2 + w^2} \quad (0.6)$$

where h is the height, w is the width and a is the position of the peak. The peak positions are determined by fitting Lorentzians to the peaks in a spectrum using the Levenberg-Marquardt non-linear least squares algorithm.  

The spectrum of Sm:YAG at 575 °C in   shows that the individual peaks have merged at this temperature. Peaks Y1 and Y2 are indistinguishable and the intensity from peak Y3 also contributes to the apparent height of the combined Y1 and Y2 peak. It was found that fits where all the parameters of Y1 and Y2 were allowed to vary did not converge to unique solutions. To avoid this problem a model for robust fitting was developed.

 shows a room temperature ambient pressure Sm:YAG spectrum fit with function of with seven peaks and linear background. All the parameters were allowed to vary, so the resulting fit had 25 free parameters. Hess and

Schiferl^{Error! Bookmark not defined.} have calibrated the peak position shifts with pressure for the peaks marked Y1 and Y2. They found that the shifts in the peak positions are linear with pressure up to 20 GPa. They also found that the peak positions have a negligible shift with temperature up to 550 °C. The calibrations were done against ruby fluorescence and nitrogen vibron Raman spectra as their basis. Work is currently in progress to determine the position shifts with pressure for all the peaks shown in Fig. 4.12.

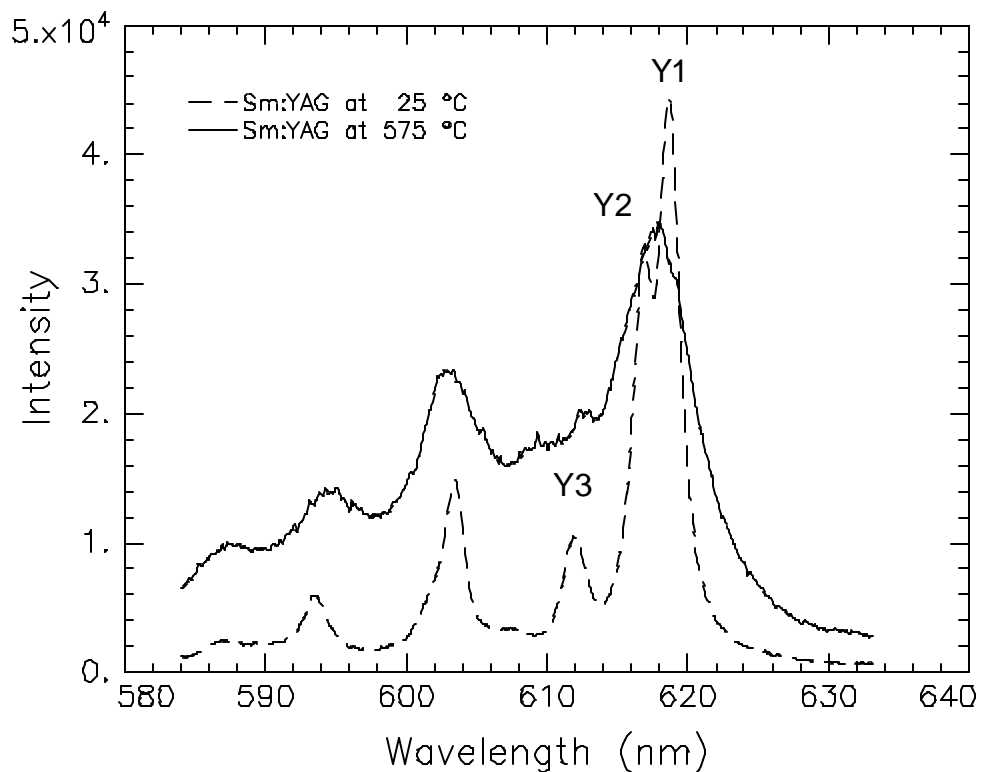


{tc "Figure 0.12. Sm:YAG spectrum with a 7 Lorentzian fit." \f f}Figure 0.15. Sm:YAG spectrum with a 7 Lorentzian fit.

The spectrum of Sm:YAG at 575 °C in {tc "Figure 0.13. Sm:YAG Spectrum at 575 °C." \f f}Figure 0.16 shows that the individual peaks have merged at this temperature. Peaks Y1 and Y2 are indistinguishable and the intensity from peak Y3 also contributes to the apparent height of the combined Y1 and

Y2 peak. It was found that fits where all the parameters of Y1 and Y2 were allowed to vary did not converge to unique solutions. To avoid this problem a model for robust fitting was developed.

The first step in developing a robust fitting technique was to calibrate the pressure shift for Y3. This was done by fitting a 7 peaks plus a slopign background, a 25 free parameter function, to ambient temperature spectra at different pressures acquired at Los Alamos. Spectra from Los Alamos were used because their optical system has greater resolution and a robust optical path that does not give spurious wavelength shifts. Using Hess and Schiferl's calibration for Y1 and Y2 we calibrated Y3.



{tc "Figure 0.13. Sm:YAG Spectrum at 575 °C." \f}Figure 0.16. Sm:YAG spectrum at 575 °C.

The pressure was determined by fitting the high temperature Sm:YAG spectra to the three peaks Y1, Y2 and Y3 with the following constraints. The heights of the Y2 and Y3 peaks are fixed relative to Y1. The widths of Y2 and Y3 had a fixed offset relative to the width of Y1. The peak positions are then allowed to vary with a single pressure variable, each peak moving due to its pressure coefficient. The model also assumed that the peak positions do not change with temperature. The fitting function is

$$\begin{aligned} \text{Fit}(x) = & \text{lor}(x; a_1 + c_1P, w_1, h_1) + \text{lor}(x; a_2 + c_2P, w_1 + d_2, h_1r_2) + \\ & \text{lor}(x; a_3 + c_3P, w_1 + d_3, h_1r_3) + mx + b \end{aligned} \quad (0.7)$$

where a_1 , a_2 and a_3 are the ambient pressure peak positions, c_1 , c_2 and c_3 are the pressure coefficients, w_1 is the width, h_1 is the height, d_2 and d_3 are the width offsets and r_2 and r_3 are the height ratios of their respective peaks, m and b are a linear slope and background and P is the pressure. The function in Eq. 4.7 is fit with only five variables being allowed to vary, the pressure P , height h_1 , width w_1 and the linear background variables m and b . All the spectra were fit in the region between 612 nm to 634 nm, because light from only the Y1, Y2 and Y3 peaks contributed to the spectrum in this region. All the other uncalibrated peaks were far enough away that their contribution was considered negligible. The resulting fits were robust, and always converged to unique and physically reasonable values.

The pressure coefficients c_1 and c_2 are from Hess and Schiferl's calibration, and c_3 was determined from the seven independent peak fit described above. The other constants, the width offsets d_2 and d_3 , and the height ratios r_2 and r_3 were determined by fitting to ambient pressure 575 °C spectra with the peak positions fixed. The resulting widths and the ratio r_2 are comparable to the

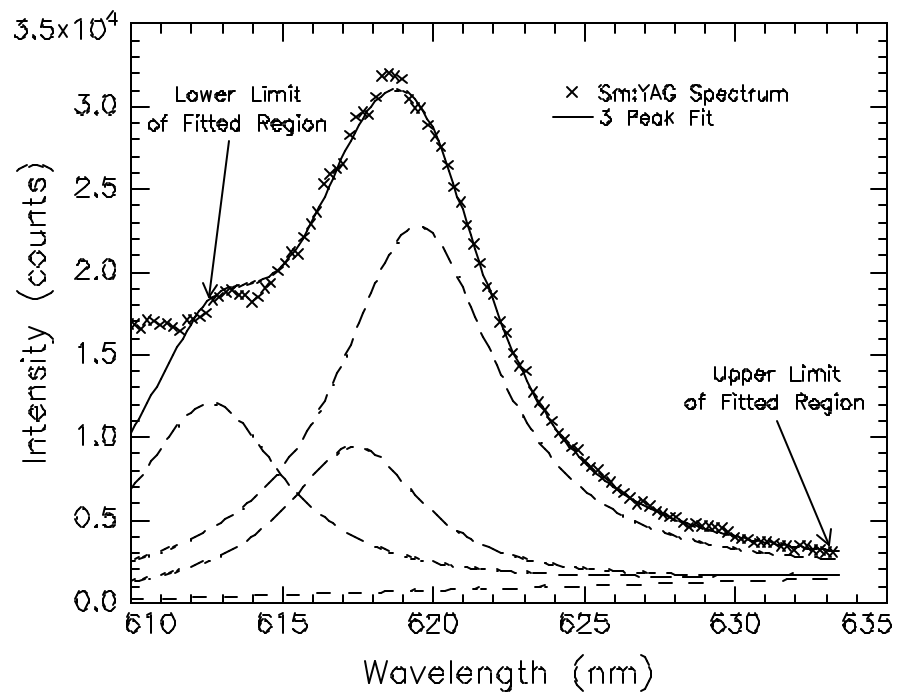
values reported by Hess and Schiferl. A fit to a spectrum at 575 °C is shown in Fig 4.14. It was found that these model parameters always resulted in excellent fits except for r_3 which occasionally needed to be changed. The change needed in r_3 to achieve a good fit resulted in a pressure that was typically only 0.1 GPa different from when the spectrum was fitted with the usual value of r_3 . Because the error in the pressure from alignment errors of the optical system is 0.3 GPa, the changes needed in r_3 were ignored and all the fits were done using the same values of r_3 . The values of the constants used for fitting are shown in Table 4.1.

Constant	Value
c_1	0.3148 nm/GPa
c_2	0.2493 nm/GPa
c_3	0.2866 nm/GPa
d_2	-1.0 nm
d_3	-0.5 nm
r_2	0.4
r_3	0.55

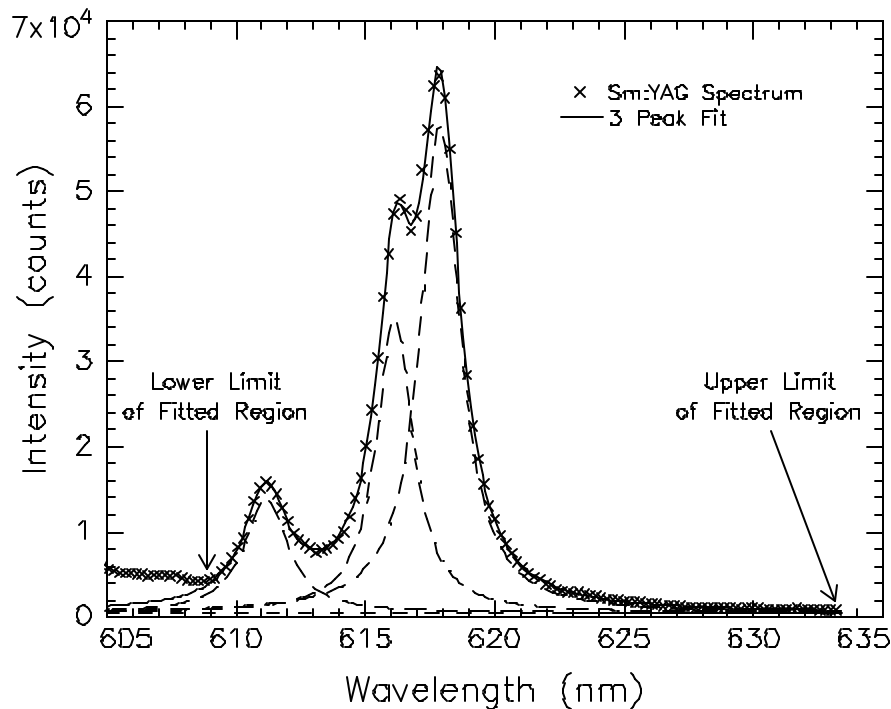
{tc "Table 0.1. Constants used in the model to fit spectra." \f t}Table 0.1. Constants used in the model to fit spectra.

This fitting method also assumes that the height ratios and width offsets are pressure independent. This was confirmed for ambient temperature fits where all the peaks can be fit independently. For high temperatures this has not rigorously confirmed but work is in progress to do independent peak fits at as high a temperature as is possible. However a qualitative visual check suggests that shape of the fluorescence spectrum is independent of pressure. Hence the pressure dependence of the height ratios and width offsets should have a negligible dependence on pressure. A high temperature spectrum and the 3 peak, 5 parameter model fit is shown in Fig. 4.14.

As described in Section 0, the optical system used for this thesis can produce spurious wavelength shifts when the optical components are moved for alignment. This limitation was overcome by the following technique. First a spectrum was acquired from a piece of Sm:YAG at ambient pressure. Then without any realignment of the optical system, a spectrum of Sm:YAG was acquired from inside the DAC. Both of these spectra were fit with a 3 independent peak fit in the wavelength region encompassing all three peaks. A typical fit is shown in Figure 0.15. Sm:YAG at 25 °C with a 3 peak fit in the region 609 nm to 634 nm. Figure 0.19. From these two fits the pressure in the DAC at room temperature was calculated. The DAC was then closed inside the furnace. Enclosing the DAC inside the furnace entails substantial optical realignment. Another spectrum was immediately acquired from the DAC inside the closed furnace but still at room temperature. By assuming that the pressure inside the DAC has remained constant during the 20 minutes it takes to close the furnace, the spurious wavelength shift that occurred during the optics realignment was determined. This shift ranged from 0.3 nm to -0.3 nm; typically it was 0.1 nm. Adding this shift to the peak positions for the ambient pressure Sm:YAG spectrum calculated before the furnace closing gave the effective ambient pressure peak positions with the furnace closed. The furnace is then heated and high temperature spectra from the DAC are acquired without any realignment of the optical system. Hence each high temperature spectrum has its own effective ambient pressure peak positions that were used to calculate the pressure.



{tc "Figure 0.14. Sm:YAG at 575 °C fit to a 3 peak 5 parameter model in the region 612 nm to 634 nm." \[f
f}Figure 0.14. Sm:YAG at 575 °C fit to a 3 peak 5 parameter model
in the region 612 nm to 634 nm.



{tc "Figure 0.15. Sm:YAG at 25 °C with a 3 peak fit in the region 609 nm to 634 nm." \f}Figure 0.19.
Sm:YAG at 25 °C with a 3 peak fit
in the region 609 nm to 634 nm.

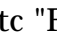
4.6 *Measuring Diffusion.*

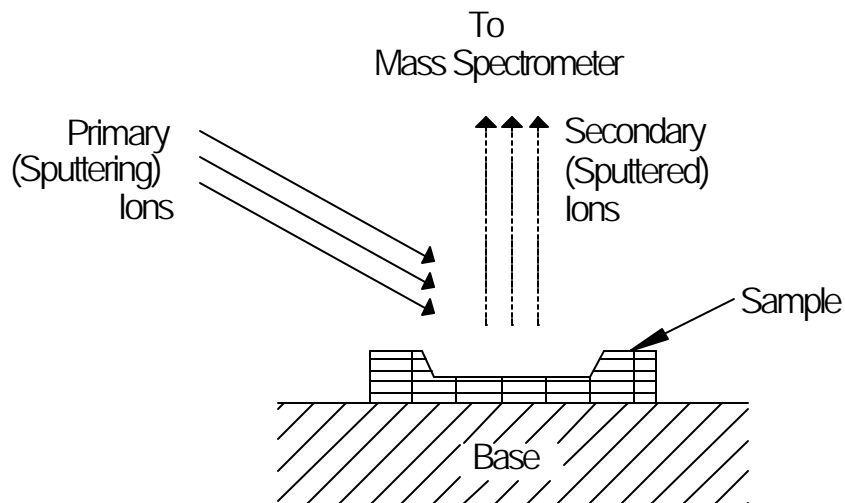
4.6.1 **Goals**

The diffusivity is determined by measuring impurity concentration versus depth ("depth profiles") for annealed and unannealed samples and then using Eq. 2.4 to calculate the diffusion coefficient. One direct method for measuring depth profiles is by depth sectioning the sample and measuring the concentration of the diffusing species in each section. For this project the samples are smaller than 200 μm by 200 μm in size and have a peak arsenic concentration of less than 0.02 atomic percent. The long term goals of this project require depth profiles for many different elements in silicon, and germanium including different isotopes of the matrix. Hence the depth profiling technique needs to section very small samples, measure very low

concentrations and do so for a variety of elements including different isotopes of the matrix. All of these requirements can only be fulfilled by using an ion beam for sputter sectioning and using a mass spectrometer to measure concentrations from the sputtered ions. This is a widely used technique for materials characterization and is called Secondary Ion Mass Spectrometry (SIMS). For this project we have developed a protocol to measure depth profiles by using SIMS on the arsenic in germanium samples that were annealed in the DAC.

4.6.2 SIMS

SIMS is well-characterized technique used widely in research and commercial materials characterization⁶¹. A schematic of the basic SIMS technique is shown in Figure 0.16. A beam of energetic primary ions removes the surface and near surface material from the sample by sputtering. The sputtered material comes off as a mixture neutral and charged molecular and atomic species, called secondary ions, which are electrostatically collected and directed into the mass spectrometer for analysis. The mass spectrometer selects the desired ion species and sends them through to an ion detector. A depth profile is acquired by setting the mass spectrometer to the desired ion species and counting the ions as the primary beam sputters into the sample, digging a crater. If the crater maintains a flat bottom and vertical walls, the instantaneous count rate is linearly related to the concentration at the crater depth at that instant. The raw data that come out as ion counts versus time can then be converted into concentration versus depth.



{tc "Figure 0.16. SIMS Technique." \f f}Figure 0.16. SIMS Technique.

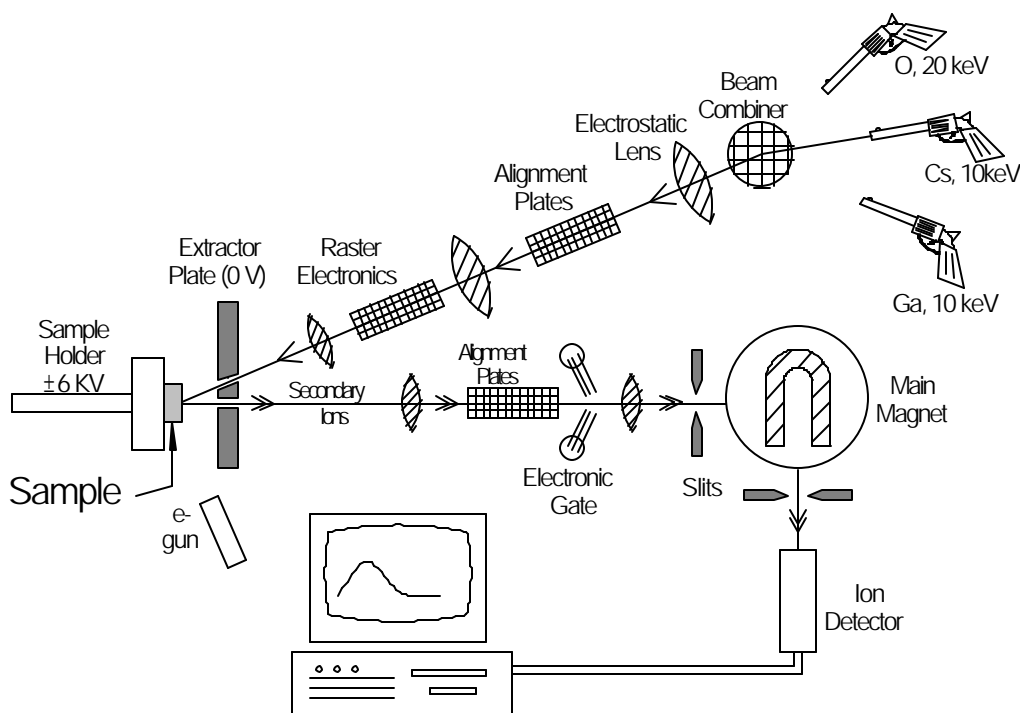
Despite the apparent simplicity, the SIMS technique is complicated to use because the theory of the sputtering process has not been developed to a point where detailed numerical models are available. Secondary ion creation depends on a variety of factors other than the concentration of the element, such as the matrix composition and primary beam parameters. Instrument and sample independent formulae to convert raw data into depth profiles are not available. However, the strengths of the SIMS technique have led to a large body of empirical knowledge which can be used in developing highly accurate protocols for characterizing materials. Depth profiling is a common use of the SIMS technique and the phenomenology has been extensively studied and is described by Wilson, Stevie and Magee⁶². We have used this work to develop a robust protocol for getting accurate depth profiles from our samples and is described below in this section.

The SIMS instrument used in this project is a VG Ionex 1170S, a three gun magnetic sector instrument with depth profiling and imaging capabilities. A schematic of this SIMS instrument is shown in {tc "Figure 0.17. The VG Ionex 1170S SIMS Instrument. " \f f}Figure 0.18. It has three sources of

primary ions. The beam combiner unit allows any one of the three ion guns to be selected. The oxygen and cesium guns are used for depth profiling and the gallium gun is used for imaging. The primary ions are directed onto the sample by ion optics that also focus and raster the ion beam. The primary beam hits the sample at an 60° angle of incidence from the normal. The sample holder is held at a potential of -6 kV to drive off the negative ions into the mass spectrometer. This holder may also be held at a positive potential for positive ion collection. An electron flood gun can be used to neutralize charge buildup on insulating samples. The grounded extractor plate located next to the holder directs the secondary ions into the secondary ion optics. The secondary ions are aligned, focused, and directed into the main magnet of the mass spectrometer. The mass spectrometer sends the desired ion species into the ion detector. Data is sent into a computer for processing. The secondary ion optics are also connected to a video monitor (not shown) that displays a total ion image created by a technique analogous to that used in a scanning electron microscope (SEM). The quality of this image is not comparable to a that produced by a SEM but it is adequate to precisely position the analysis crater.

The chemical nature of the primary beam affects the production of secondary ions. An ion beam of an electropositive element such as cesium enhances the formation of negative secondary ions. Arsenic, an electronegative element, is likely to form negative ions; hence the cesium beam enhances the arsenic detection limit of the system. Similarly, the oxygen beam is used when looking for electropositive elements such as metals. The primary ion energy is an empirically determined compromise between reducing ion beam mixing of the surface layers and enhancing the secondary

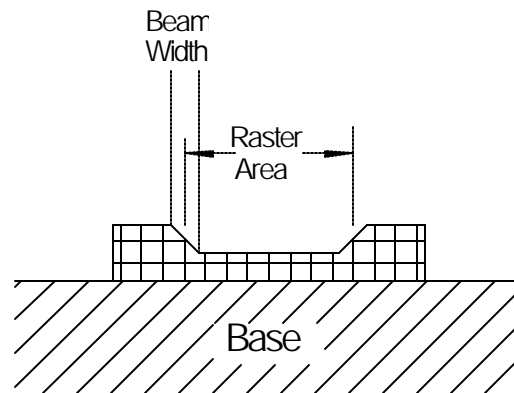
ion yield. A 10 keV Cs^+ primary beam was used to analyse all the samples in this study. Adding the holder potential resulted in an effective primary beam energy of 16 keV which is a typical energy used for cesium primary beams in commercial systems analyzing semiconductors⁶³. The 60° angle of incidence built in to this instrument is designed to improve the ion yield without increasing ion mixing.



{tc "Figure 0.17. The VG Ionex 1170S SIMS Instrument. " \f f}Figure 0.18. The VG Ionex 1170S SIMS Instrument.

Under typical conditions, the sputtering rate is linearly proportional to the primary ion beam current. For accurate depth profiling the crater bottom must remain flat and parallel to the original surface during sputtering. This requires that the average ion intensity be uniform over the analysis area. The simplest technique to achieve uniform ion intensity is to focus and raster the primary beam over the analysis area. The non-zero width of the focused beam creates the crater shape shown in Fig 4.18 with the projected width of the

walls being equal to the beam width. The secondary ions are generated from the crater walls as well as the crater bottom. Hence if all the secondary ions are counted, the instantaneous ion count will come from differing depths, distorting the depth profile. To remove the effect of the crater wall on the detected signal only the secondary ions generated from the central region of the raster are counted. This gating of the secondary ions is achieved by electronically stopping the secondary ion count when the primary beam is off the gated area.



{tc "Figure 0.18. Crater Shape." \f f}Figure 0.20. Crater Shape.

The two types of gating modes used for the data collection are shown in {tc "Figure 0.19. Sample Gating." \f f}Figure 0.21. The commonly used mode shown in {tc "Figure 0.19. Sample Gating." \f f}Figure 0.21 (a) has a raster area smaller than the sample with the gated area adjusted to preclude ions from the crater walls. For very small samples the mode shown in {tc "Figure 0.19. Sample Gating." \f f}Figure 0.21 (b) is used. A rastered area is used which is bigger than the sample, and the gated area that is adjusted to preclude ions from off the sample. In the latter mode, the net area sampled is a larger fraction of the sample and hence the sample is used more efficiently.

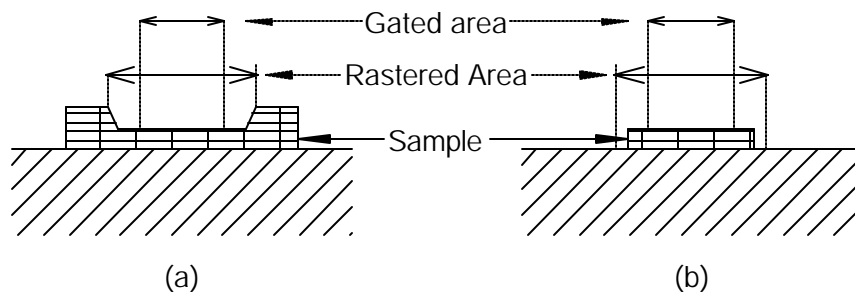


Figure 0.19. Sample Gating. Figure 0.21. Sample Gating.
 (a) Raster larger than sample. (b) Raster smaller than sample.

The cesium gun in the VG instrument produces a primary ion beam width of 10 to 15 μm at typical beam currents. The first gating mode was used on samples with linear dimensions of 150 μm to 200 μm , with a raster size of approximately 60 μm by 50 μm . The gated area had to be set at 5% to 10% of the rastered area to overcome the crater wall effects. For smaller samples, better statistics were obtained in the second gating mode with a raster size of 100 μm by 90 μm and a gate of 20% of the raster size.

Primary beam currents of 2 to 4 nA were used for the smaller raster and 8 to 15 nA for the larger raster, resulting in sputter rates between 0.4 nm/sec and 0.8 nm/sec. The sputter rates were empirically determined from the depth profiles of unannealed samples by using the peak depth determined from TRIM89, a program that calculates the depth distribution resulting from ion implantation. During all the SIMS analysis, the acquisition of depth profiles of annealed samples was alternated with the acquisition profiles of unannealed samples. This was used to check and measure any changes in the sputter rate that may have arisen from changes in the primary beam current.

The AsGe^- ion is known to return the best statistics for tracking arsenic concentration in bulk germanium and is used for all the data collection⁶⁴. Arsenic has only one isotope of mass 75 a.m.u. but germanium has isotopes of

masses 70, 72, 73, 74 and 76 a.m.u. The sputtering process also produces Ge_2 ions that may have the same mass number as an AsGe ion. At the sensitivities needed for depth profiling, the mass spectrometer only resolves integer mass numbers. Hence all the data was collected by using the $^{75}\text{As}^{76}\text{Ge}^-$ because it is the only AsGe ion that does not have a mass number conflict with any Ge_2 ion.

The typical relation between the count rate of an ion and the underlying elemental concentration is given by:

$$\text{Ion Counts} = \text{Concentration} \times a + b \quad (0.8)$$

where a and b are constants that depend on the physical characteristics of the sample and instrumental parameters⁶⁵. However, these constants do not change during an uninterrupted ion count profile from a single sample. The offset b is determined by collecting data at a depth where concentration can be assumed to be zero. The constant of proportionality is empirically determined by comparing a known standard with the sample. This procedure would be very difficult for small irregular samples. However, for this experiment, we have assumed a linear diffusion coefficient for reasons described in Section 0. Linear diffusion obviates the need for determining absolute concentrations, because in this case the diffusion coefficient is concentration independent. The height of the depth profile peak is treated as an adjustable parameter and the ion count profile can be substituted for the depth profile for data analysis. No attempt was made to determine the absolute concentrations from the raw SIMS data. The depth profiles shown in this thesis are made by normalizing the ion integrated count depth profile to the ion implantation dose.

The linear relationship between the ion count rate and the concentration breaks down near the surface. This phenomenon is called the surface transient

of the depth profile. During the sputtering process, the primary ions implant into the material just below the surface, thus changing its composition. Before a steady state develops between the implanting and sputtering, some material has already been sputtered off. Hence the first secondary ions come from the unimplanted matrix that has different characteristics from the implanted matrix following. Because the secondary ion generation is dependent on the matrix characteristics, the ion count will change with the matrix and overshadow any changes due to concentration. The extent of the surface transient is determined by tracking a matrix ion such as the Ge^- or Ge_2^- ion and noting the depth at which their ion count profile flattens out. For a 16 keV Cs^+ primary beam sputtering germanium, the surface transient lasts for approximately 30 nm. However more than 30 nm of surface are used up in secondary ion tuning described below.

The very small samples used in this experiment create another limitation that prevents the near surface depth profile from being available. Technical limitations on design of the SIMS instrument force the acceptance area for secondary ions to be very small. The acceptance area is moved around the sample surface by tuning the secondary ion optics. To acquire a depth profile, the acceptance area must be located over the primary beam raster position. Due to the instrumental limitations, the acceptance area moves relative to the primary beam raster position every time a new sample is brought into the raster area, a phenomena called secondary ion shadowing. For large samples, the secondary ion optics are tuned on one location on the sample and data is collected from a fresh location, but this is not possible for the small samples. Hence the secondary ion optics were tuned while collecting data and up to 100 nm of depth are used up in this manner. The depth profiles for the data in this

thesis start at between 30 and 120 nm depth but this shortcoming is overcome in the data analysis described in Section 0

4.6.3 Analysis of SIMS Data

The unannealed, as implanted concentration profile for arsenic is very well approximated by a Gaussian function

$$gaus(x; h, a, \mathbf{s}) = h \exp\left(-\frac{(x-a)^2}{4\mathbf{s}^2}\right) \quad (0.9)$$

where a is the peak position, \mathbf{s} is the width and h is the height. This was established by doing non-linear least squares fit to SIMS depth profiles of unannealed samples. It was further supported by doing the same fit to a depth profile created by a Monte Carlo simulation of the ion implantation done with the TRIM89 computer program. Gaussian functions are solutions of the linear diffusion equation, Eq. 2.4. For both boundaries at infinity, a depth profile that starts as a linear combination of Gaussian functions will remain that way, with only the widths and the heights changing. From Eq. 2.4 it can be shown that for Gaussian concentration profiles the diffusion coefficient D is given by

$$D = \frac{1}{t} (\mathbf{s}_f^2 - \mathbf{s}_i^2) \quad (0.10)$$

where \mathbf{s}_i is the initial width, \mathbf{s}_f is the final width and t is the time duration of the anneal. Hence D is calculated by measuring the initial and final widths of the depth profile. Because the implanted profile is close the surface, Eq. 2.4 must be solved using reflective boundary conditions at the surface. This problem is equivalent to the infinite boundary problem described above with two Gaussians, the original and a mirror image across the surface, as shown in Figure 0.20. Function used to fit SIMS data." \f Figure 0.23. Hence the annealed profiles are fit with a double Gaussian function

$$Fit(x) = gaus(x; h, a, \mathbf{s}) + gaus(x; h, -a, \mathbf{s}) \quad (0.11)$$

to get s_f . The unannealed profile is fit with a single Gaussian to get s_i and then Eq. 4.10 is used to calculate D .

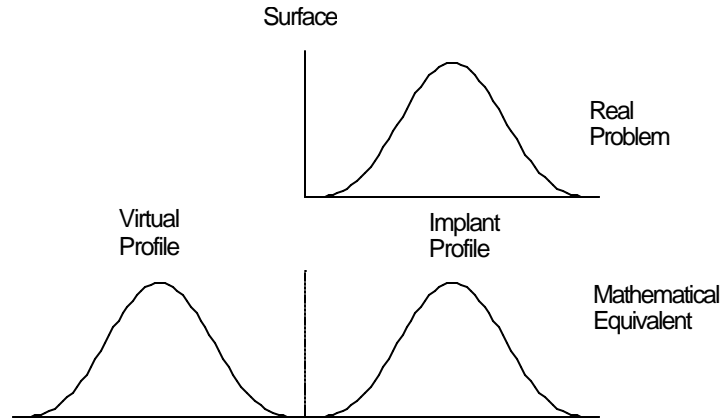
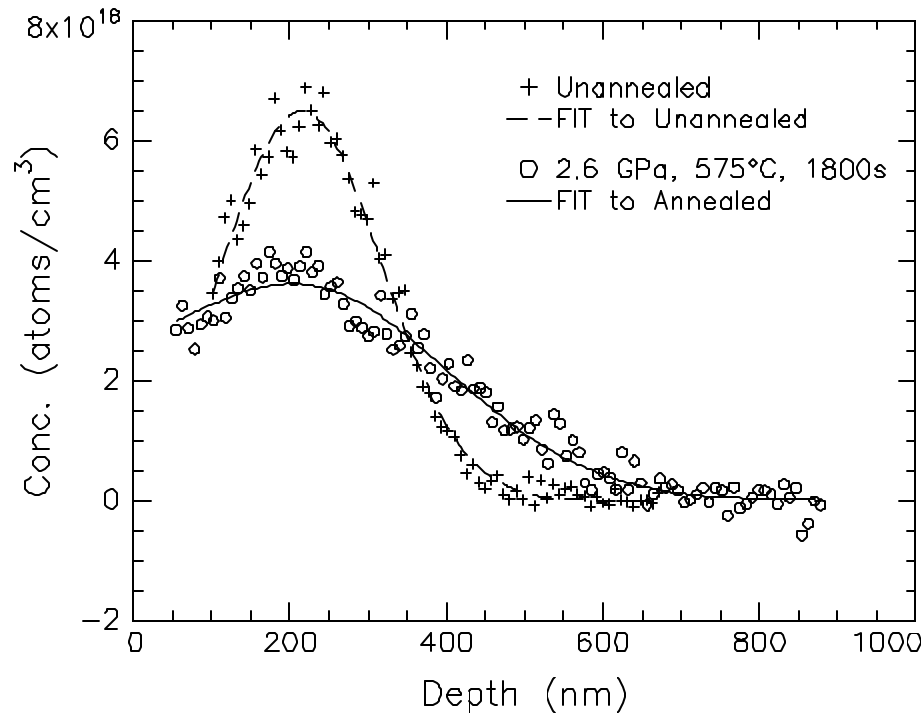


Figure 0.20. Function used to fit SIMS data. Figure 0.23. Function used to fit SIMS data.

Due to the limitations of the SIMS technique and the sample design, it is not possible to determine the exact location of the surface. The principal reason for this is that the SiO_2 layer on the surface is poorly characterized. Its sputtering behavior also changes after the high pressure anneal. Efforts to empirically characterize it have failed because the surface and near surface depth profiling data is unavailable due to surface transients and efforts to reduce secondary ion shadowing. This limitation was overcome by using the fact that the peak position of the Gaussian function does not move during linear diffusion. Hence during fitting the peak of the real Gaussian was forced to match the depth of ion implant peak. Figure 0.21. SIMS Depth Profiles of Annealed and Unannealed Samples. Figure 0.25 shows an unannealed depth profile with a single Gaussian fit and an annealed profile with a double Gaussian fit. Note that the unannealed profile is fit with a *single* Gaussian because the as implanted profile is best described by the single Gaussian. However, the fit for annealed profile requires the second virtual Gaussian to account for the reflective boundary conditions at the surface.



{tc "Figure 0.21. SIMS Depth Profiles of Annealed and Unannealed Samples." \f}Figure 0.25. SIMS Depth Profiles of Annealed and Unannealed Samples.

4.7 *Future Directions.*

Experimental designs are never complete and the experimental setup used for this thesis is no exception. A brief outline of the proposed enhancements for this apparatus and the experimental technique are presented in the following sections. These enhancements are geared towards two goals: the routine operation of the DAC at its maximum design temperature of 1100 °C, and the reduction of uncertainty in the individual data points. A maximum operation temperature of 1100 °C will allow this experiment to be repeated for all the dopants in silicon and germanium, including silicon self-diffusion. Reduction of uncertainty in the data will allow us to study the more subtle effects of pressure on diffusion that may now be buried in the noise.

4.7.1 Improvements in Sample Preparation and Analysis

Reducing the uncertainties in the diffusivity of each data point will come from reducing the uncertainties in the SIMS data. One source of uncertainties in the SIMS data comes from the physical damage of high pressure annealing on the surfaces of the sample. As described in Section 0, a thin film of SiO_2 on the surface was used to prevent the implanted region of the sample from being completely eroded away during the anneal. Nevertheless the sample surfaces are still slightly damaged by the anneal, adding significantly to the uncertainty in the SIMS profiles. One possible solution would be to reduce the chemical reactivity of the pressure medium, and this is discussed in the next section. However, better surface protection would also be very useful, and for the anneals at higher temperatures it may prove to be mandatory. A thicker SiO_2 film may be a possible solution but would cause other problems because as an insulator, SiO_2 would charge up during the SIMS analysis. Each sample would then need to have its SiO_2 film removed before the SIMS analysis. Such a procedure would be tedious for DAC sized samples. Another possible solution is a thick sacrificial layer of poly-crystalline silicon or germanium on the surface. Some of the material will erode away and the remainder can be easily sputtered through. Note that an epitaxial protection layer, though probably better than the unprotected surface, is not as desirable as a poly-crystalline layer because it may inject point excesss defects chemically created at its surface into the implanted region.

Another source of the uncertainty in the SIMS data comes from the width of the unannealed dopant profile. It can be shown that for a given instrumental broadening, typically 5 to 10 nm, a narrow initial depth profile will allow more accurate measurement of diffusivity than a wider initial depth

profile. Narrow implant profiles can only be created by making them shallower. Shallow profiles are not desirable because they are more susceptible to any type of effect from the crystal surface. Even with a protection layer the proximity of the crystal surface can have unforeseen side effects such as the dopant preferentially migrating into the protection layer via grain boundary diffusion. A possible solution is to grow an epitaxial layer on top of the implanted crystal, thus extending the crystal surface away from the implanted layer. The protection layer would then go on top of the epitaxial layer. However this approach can be further extended by doing away with the implant step altogether and introducing narrow dopant profiles during epitaxial growth. If the crystal can be grown with several equally spaced very narrow dopant profiles it would have two additional advantages over the current scheme. The first advantage would be an internal check to see whether the point defect concentration has reached equilibrium. Each dopant peak will give a measurement of the diffusivity at its depth, thus allowing the diffusivity to be measured as a function of depth. It can be shown that an out of equilibrium point defect concentration will not have a uniform depth distribution. Thus the diffusivity of the dopant will vary with depth and a non-equilibrium defect concentration will be picked up by this type of sample geometry. The second advantage of this sample geometry would be an internal check to establish if during SIMS analysis the primary beam has remained constant, achieved by comparing the sputter time between the different peaks. Changes in the SIMS primary current during analysis will result in spurious diffusivities being calculated. An added bonus would be an automatic sputter rate measurement for each sample.

4.7.2 Enhancements to the Pressure System

The basic design of the pressure generation and pressure measurement system has been determined to be sound and hence only incremental design changes are proposed.

The main body of DAC has been designed to operate at temperatures up to 1100 °C. The bolts are the most highly stressed components in the DAC. At about 800 °C for 10 GPa with diamonds with 1 mm culet diameter the stresses across the cross section of bolts, made of Haynes 230, are expected to exceed the yield strength of the material. Thus they should be replaced with bolts made out of stronger material such as rhenium. Rhenium is probably the strongest ductile material available and will easily handle the load at the elevated temperatures. Rhenium has an additional advantage in that it does not gall with nickel based super-alloys⁶⁶; Haynes 230 being nickel based is expected to gall to itself at a temperature of approximately 700 °C. If a loaded cell with Haynes 230 bolts is taken up to 700 °C, the bolts will probably have to be drilled out. We note that the Rhenium bolts for this diamond cell have already been constructed but have not been used except for test runs.

The cryogenic loading system described in Section 0 is designed to load clean oxygen free argon into the DAC pressure chamber. This is achieved by introducing the liquid argon into the DAC inside a sealed box that is evacuated before starting the argon loading. Nevertheless annealed samples still showed signs of chemical activity on the surface and further efforts to keep the argon clean should be considered. A major improvement could result from redesigning the argon loading box such that a bakeout is possible during evacuation. The bakeout temperature need only to be at approximately 150 °C

to effectively remove moisture from the environment. The present cryogenic loader is constructed from aluminum plates sealed shut with super glue, with the DAC being held inside a Plexiglas cup. The function of the Plexiglas cup is to serve as heat insulation, but it may be a major source of contamination for the argon. The proposed loader would be made of stainless steel parts that are welded shut. The lid and bolt turners would be sealed with Viton gaskets. All the insulation would be on the outside of the loader such that it could be removed for a bakeout. Such a loader could easily be baked out on a hot plate. An added advantage would be that it could be cooled in a liquid nitrogen bath before starting the argon load, thus speeding up the loading process.

The final enhancement to the system concerns with the improvement in the accuracy of pressure measurement. The principal source of error in measuring the pressure comes from flex in the optical path from the DAC to the spectrometer. Very small changes in the angle by which the Sm:YAG fluorescence enters the spectrometer can cause large and spurious changes in the measured pressure. The procedure developed to overcome this problem has been described in Section 0. This problem may be completely eradicated if optical realignment to direct the Sm:YAG image into the spectrometer is achieved by moving the furnace itself rather than the present practice of moving various mirrors. The present furnace is probably too large and heavy to be effectively mounted on some type of a translation stage. It may be cost effective to redesign a smaller and lighter furnace. Such a redesign is possible because the large size of the furnace was result of an attempt to avoid the need for water cooling. But this attempt failed and water cooling had to be added. The new furnace would still be a Kanthal element, sealed helium atmosphere furnace driven with the present power supply and temperature control system.

The redesign would allow the addition of several other features. The water cooling could be better integrated with the main body of the furnace. The single bolt turner currently available could be replaced with three, allowing finer control of the pressure. The insulation inside the present furnace generates copious quantities of dust and it could be replaced with solid heat shields.

5. Results and Discussion

The final data set used in this thesis is presented in Table 0.1. Diffusion Coefficient of Arsenic in Germanium at 575 °C." Table 0.1 in reverse chronological order of acquisition. The pressure and diffusion coefficient columns are used in the final analysis. The data set consists of two different anneal times, nominally 4200 and 1800 seconds. Because we do not have complete control over the anneal duration, the effective anneal times calculated using the technique in Section 0 are used for calculating the diffusion coefficient. Two different anneal times are used to establish whether there is any time dependence of the diffusion coefficient. All anneals were done using rhenium as gasket material except for the final three, which were done using Inconel. Rhenium gaskets could not maintain high pressure for the longer duration anneals, and therefore Inconel gaskets were substituted. The Inconel gaskets did succeed in maintaining the high pressures but at the cost of damaging the diamonds. After three runs one of the diamonds was damaged to the point that it had to be sent out for repair. The switching of the gasket material is not expected to have any effect on the diffusion coefficient. Argon of 99.998% purity from Matheson Gases of Waltham Massachusetts was used for the all the anneals except for those marked as alternate argon. The gas for these anneals was also nominally 99.998% but came from a different vendor, Igos of Somerville, Massachusetts.

The data are presented as a log plot in Fig. 5.1. The pressures are typically known to within 0.3 GPa. The errors in the pressure measurement are due to the wavelength shift in the optical system that leads to inaccuracies in the peak positions of Sm:YAG. The diffusivities are typically known to 40% of their

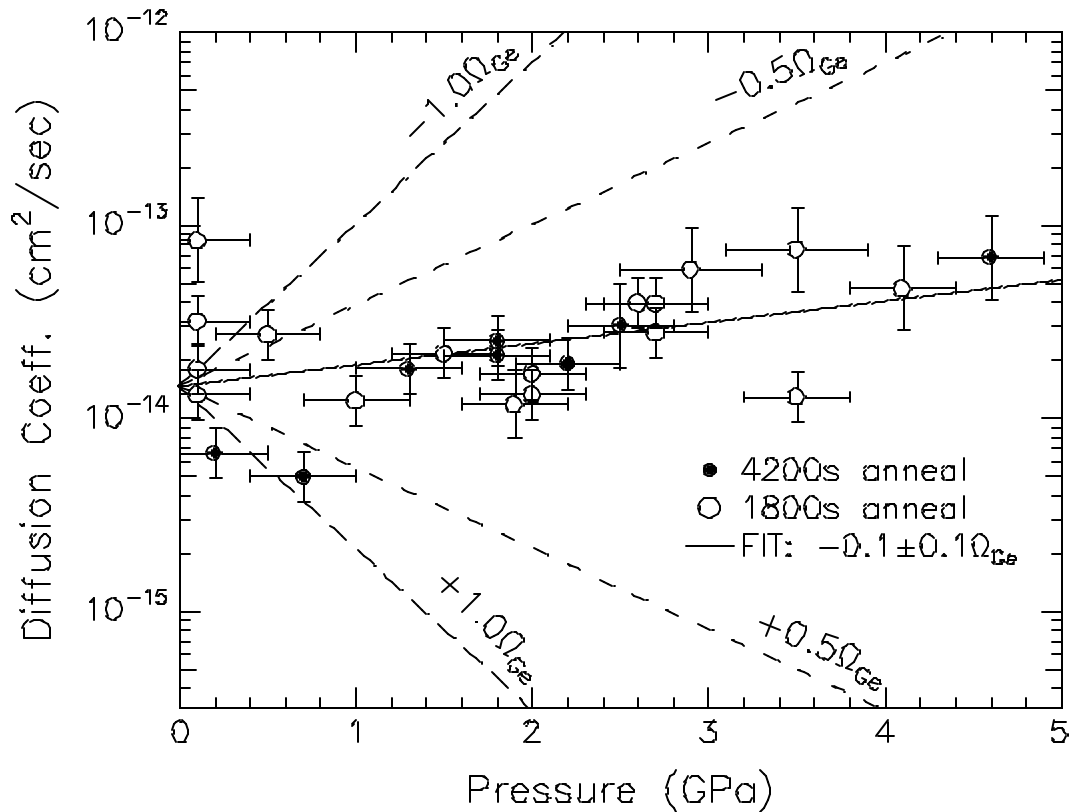
value. The errors in the diffusivity are due to the noise in the SIMS depth profiles that lead to inaccuracies in fitting. The error bars for both axes represent 60% confidence intervals.

Pressure (GPa)	Diffusion Coefficient (10^{-14} cm ² /sec)	Effective Time (sec)	Gasket	Notes
3.5	7.48	1698	Inconel	
2.5	3.04	4104	"	
4.6	6.84	4104	"	
2.7	2.77	1704	Rhenium	
2.7	3.94	1710	"	
2.6	3.96	1704	"	
1.8	2.13	4212	"	
4.1	4.69	1704	"	
2.9	5.91	1710	"	
1.3	1.81	4212	"	
0.1	1.32	1812	"	
0.1	8.34	1812	"	
2.2	1.91	4212	"	
2.0	1.33	1812	"	
2.0	1.70	1812	"	
1.8	2.52	4212	"	
1.0	1.23	1812	"	
0.1	1.80	1812	"	
0.7	0.50	4788	"	Alternate Ar
0.2	0.66	4914	"	Alternate Ar
1.9	1.18	2106	"	
0.5	2.71	2106	"	
1.5	2.16	2100	"	
0.1	3.18	2124	"	
3.5	1.29	1986	"	

{tc "Table 0.1. Diffusion Coefficient of Arsenic in Germanium at 575 °C." \f t}Table 0.1. Diffusion Coefficient of Arsenic in Germanium at 575 °C.

Using Eq. 2.20 the activation volume for arsenic diffusion is calculated by fitting a straight line to the plot in Fig. 5.1. The result is an activation volume of -1.7 ± 1.4 cm³/mole or -0.12 ± 0.1 Ω_{Ge} , where Ω_{Ge} is the atomic volume of germanium at 1 atmosphere pressure and room temperature. The fit was done using a weighted linear least squares technique and by fitting to both offset and slope. For comparison, calculated slopes for activation volumes of $\pm 0.5 \Omega_{Ge}$ and $\pm 1.0 \Omega_{Ge}$ are also shown in Fig. 5.1. The offset, 1.3×10^{-14} cm²/sec, is the

ambient pressure diffusivity of arsenic in germanium at 575 °C and it agrees well with the value of 1.0×10^{-14} cm²/sec that was calculated from published activation enthalpies and D_0 **Error! Bookmark not defined.**



{tc "Figure 0.1. Diffusion of Arsenic in Germanium at 575 °C." {f f}Figure 0.1. Diffusion of Arsenic in Germanium at 575 °C.

If diffusion is point defect mediated, the calculation for the activation volume is valid only if the point defect concentrations are at their equilibrium levels. In defect free crystals point defects are created or annihilated at the free surface. Hence the duration of the anneals needs be long enough for the point defects to travel well beyond the region of interest. From dimensional analysis the expected distance traveled is

$$dist \approx \sqrt{D_{pd}t} \quad (0.1)$$

where D_{pd} is the diffusion coefficient of the point defects and t is the anneal time. For point defect diffusion the probability that the defect is next to a jump site is always unity. Hence from arguments similar to those in Section 0 the diffusion coefficient for point defects is

$$D_{pd} = D_{pd0} \exp(-DH^*/kT) \quad (0.2)$$

and the pre-exponential factor D_{pd0} is

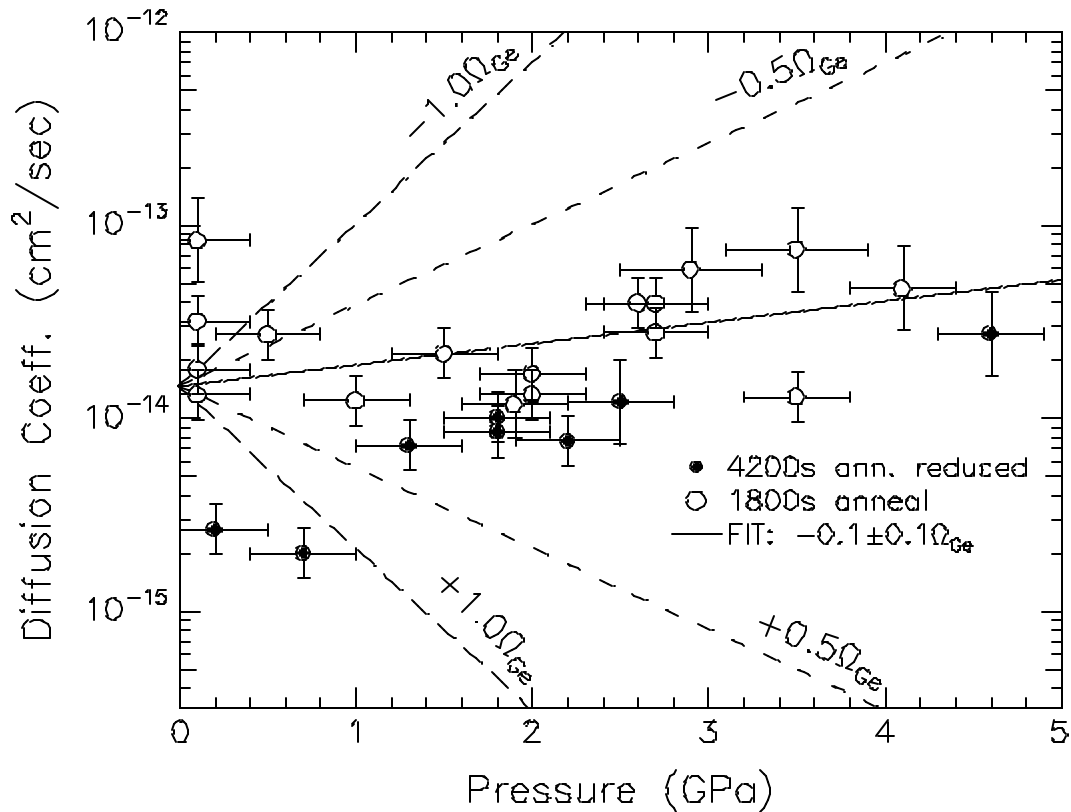
$$D_{pd0} = gn^2 \exp(DS_m/k) \quad (0.3)$$

where DH_m and DS_m are the migration enthalpy and entropy respectively for the impurity diffusion. Using Eq. 2.15 and Eq. 5.3

$$D_{pd0} = (D_0/f) \exp(DS_f/k) \quad (0.4)$$

where DS_f is the entropy of formation, D_0 is exponential prefactor of the impurity diffusion coefficient and f is the correlation coefficient from the dopant diffusion equation. For this calculation if we assume no binding between the dopant and defect then f is of order unity. In silicon the vacancies created by irradiation have DH_m ranging from 0.18 eV to 0.45 eV^{67,68,69}. Measuring the decay rate of swirl defects in silicon gives an approximate interstitial migration enthalpy of 1.7 eV⁷⁰. Scaling with the bond strength ratios of germanium to silicon gives vacancy migration energies of less than 0.4 eV and an interstitial migration energy of 1.3 eV for germanium. The formation entropies for both interstitials and vacancies are thought to range from $3k$ to $10k$ in silicon and are based on estimates of defect concentrations^{71,72}. In a worst case scenario we use $f = 1$ in Eq. 5.4 and a formation entropy of $10k$ in germanium yielding a minimum approximate travel distance of 6×10^5 nm for vacancies and 1.2×10^3 nm for interstitials. The peak of the depth profile is at 215 nm. Note that the correlation coefficient, f , for dopant diffusion via the vacancy mechanism calculated in Appendix A is less than unity and consequently its inclusion would increase the travel

distances for vacancies. For a travel distance of less than 200 nm the point defect would need a migration enthalpy of greater than 1.7 eV.



{tc "Figure 0.2. Diffusion of arsenic in germanium with the diffusion coef. for 4200s anneals reduced by a factor of 2.3." \f f}Figure 0.2. Diffusion of arsenic in germanium with the diffusion coef. for 4200s anneals reduced by a factor of 2.3.

If the travel distances of the point defects are comparable to the depth of the peak of the profile then the point defect concentrations would change during the anneal. The diffusion coefficient is proportional to the defect concentrations and these changes in the defect concentration would result in a time dependence of the diffusion coefficient. From Fig. 5.1 the diffusivities for the long and short anneals are statistically indistinguishable. This can be seen by estimating what the plot would look like if all diffusion stopped after 1800 s.

This would be an approximation of the effect of diffusion mediated by, for example, a transient enhanced interstitial concentration that was being reduced with time as vacancies generated from the surface were annihilating them to reach equilibrium concentration. D for the long anneals would then be reduced by a factor of 2.3 and the resulting plot is shown in

{tc "Figure 0.2. Diffusion of arsenic in germanium with the diffusion coef. for 4200s anneals reduced by a factor of 2.3." \f f}Figure 0.2: the long anneals begin to separate from the short anneals. Within the resolution of our experiment the diffusion coefficient is time independent and so, therefore, is the point defect concentration. The time independent concentration implies that the travel distance is long enough for the point defects to reach equilibrium in the region important for the measurement of the depth profile. It can also imply that the travel distance is so short that no newly created point defects from the surface have reached the region of diffusion, but this would require implausibly high migration energies.

Our results yield an activation volume of $-0.12 \pm 0.1 \Omega_{Ge}$ for arsenic diffusion in germanium at 575 °C. The only other measurement of activation volume for diffusion in germanium is by Werner *et al.* **Error! Bookmark not defined.** They have measured the activation volume for self-diffusion under various conditions. Lu *et al.* **Error! Bookmark not defined.** have measured the activation volume of SPEG in germanium. These results are compared in {tc "Table 0.2. Comparison of Activation volumes in Germanium." \f t}Table 0.2. Werner *et al.* have also determined that the negative vacancy is responsible for 77% of the transport for self-diffusion in germanium at 700 °C. Their experimental and analysis techniques were described in Section 0.

Process	Activation volume (Ω_{Ge})	Temperature ($^{\circ}\text{C}$)	Author
SPEG in Ge	-0.46	350	Lu <i>et al.</i>
As diffusion in Ge	-0.1 \pm 0.1	575	this work.
Self-diffusion in Ge	+0.24	603	Werner <i>et al.</i>
"	+0.41	813	"
S-d with negative vacancy	+0.28	700	"
S-d with neutral vacancy	+0.56	700	"
Calculated vacancy formation volume in silicon is $0.75 \Omega_{\text{Si}}$			Antonelli <i>et al.</i>

Table 0.2. Comparison of Activation volumes in Germanium.

The activation volume measured for arsenic diffusion in germanium is negative and small in magnitude. Because the activation volume is the sum of the volumes of migration and formation, additional information is needed to separate them and to deduce the diffusion mechanism. Below we explore the consequences of three different assumptions for the relative contributions of formation and migration terms to the measured activation volume.

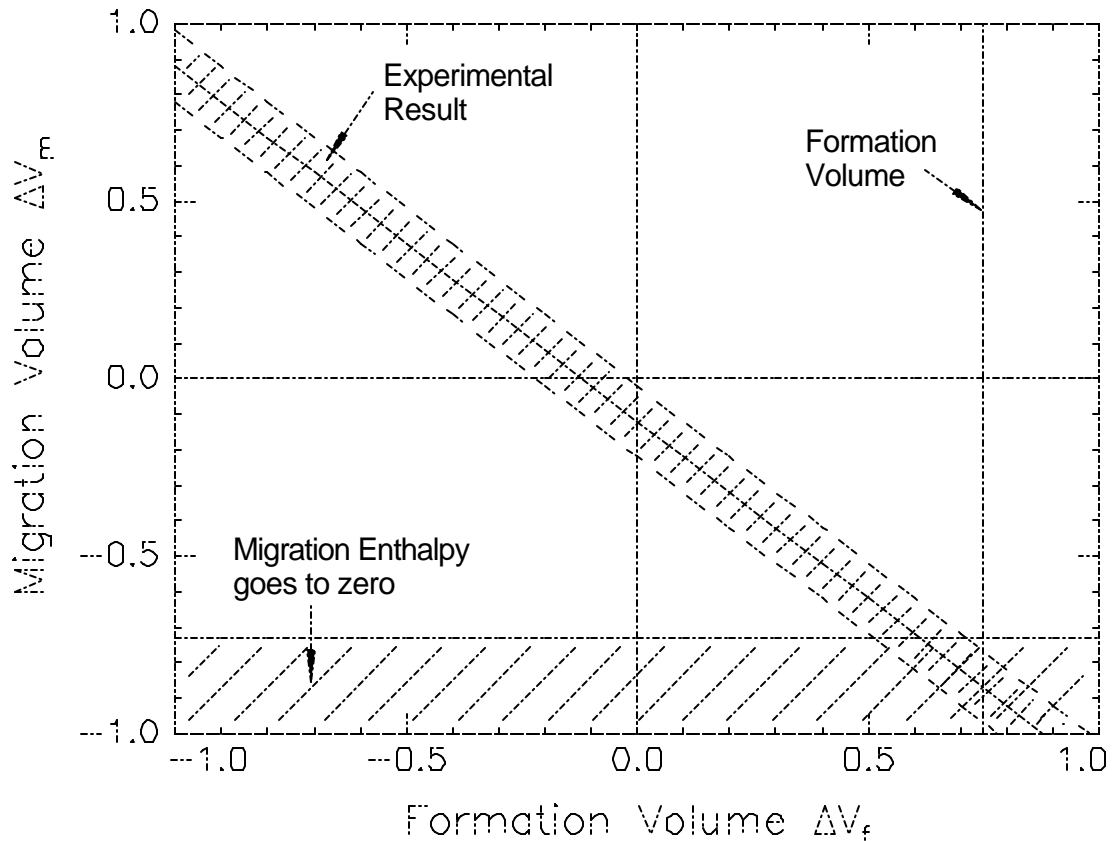
Werner *et al.* assumed that the migration volume is small and used the activation volume as an approximation for the formation volume. With positive activation volumes they concluded that the vacancy is the predominant point defect mediating self diffusion. By assuming that the migration volumes are small, our results imply a formation volume of $-0.1 \Omega_{\text{Ge}}$. This would be consistent with a direct interchange mechanism **Error!** **Bookmark not defined.** because it does not involve a point defect and consequently would have formation volume of exactly zero. Werner *et al.* base their assumption of small migration volumes on studies of self diffusion in gold⁷³. Gold is a close-packed metallic solid whereas germanium is 4-fold coordinated open covalent structure and hence the assumption of small migration volumes may not be valid for germanium.

Lu *et al.* have measured large negative activation volumes for SPEG and suggest that the mediating defect has a small volume of formation and therefore their measured activation volume of $-0.46 \Omega_{\text{Ge}}$ is approximately equal to the migration volume. By assuming that the migration volumes for SPEG and diffusion processes in 4-fold coordinated networks are comparable, a migration volume as large and negative as $-0.4 \Omega_{\text{Ge}}$ for diffusion in germanium is plausible. (However other reasons may preclude such a large and negative migration volume, see next paragraph.) A 100% contribution to transport from a vacancy mechanism in our case would then require that the vacancy mediating arsenic diffusion have a formation volume of $+0.3 \Omega_{\text{Ge}}$. Such a small formation volume implies a very large relaxation volume for the vacancy. For comparison, first principles calculations for silicon give a formation volume of $+0.75 \Omega_{\text{Si}}$ **Error! Bookmark not defined.** and there is no reason to expect such a large difference between silicon and germanium vacancy formation volumes.

Finally if we assume the volume of formation for a germanium vacancy is approximately $+0.75 \Omega_{\text{Ge}}$ in accordance with the theoretical result for silicon then the migration volume calculated from our result is $-0.85 \Omega_{\text{Ge}}$. The difference between enthalpy of migration at ambient pressure and at high pressure is $P DV_m$. For a pressure of 4 GPa and a DV_m of $-0.85 \Omega_{\text{Ge}}$ this product is -0.48 eV. In silicon the migration enthalpies for vacancies range from 0.18 eV to 0.45 eV for different charge states **Error! Bookmark not defined.,Error! Bookmark not defined.,Error! Bookmark not defined.,Error! Bookmark not defined.** . Scaling with the bond strength ratios gives germanium vacancy migration enthalpies ranging from 0.14 eV to 0.36 eV. Adding the $P DV_m$ term to these numbers results in the migration enthalpy going to zero at a critical pressure ranging

from 1.2 GPa to 3 GPa. At this pressure we would expect some kind of break in the slope as the barrier to migration vanishes, precluding a further reduction in the barrier. Such a break is not observed in Fig. 5.1.

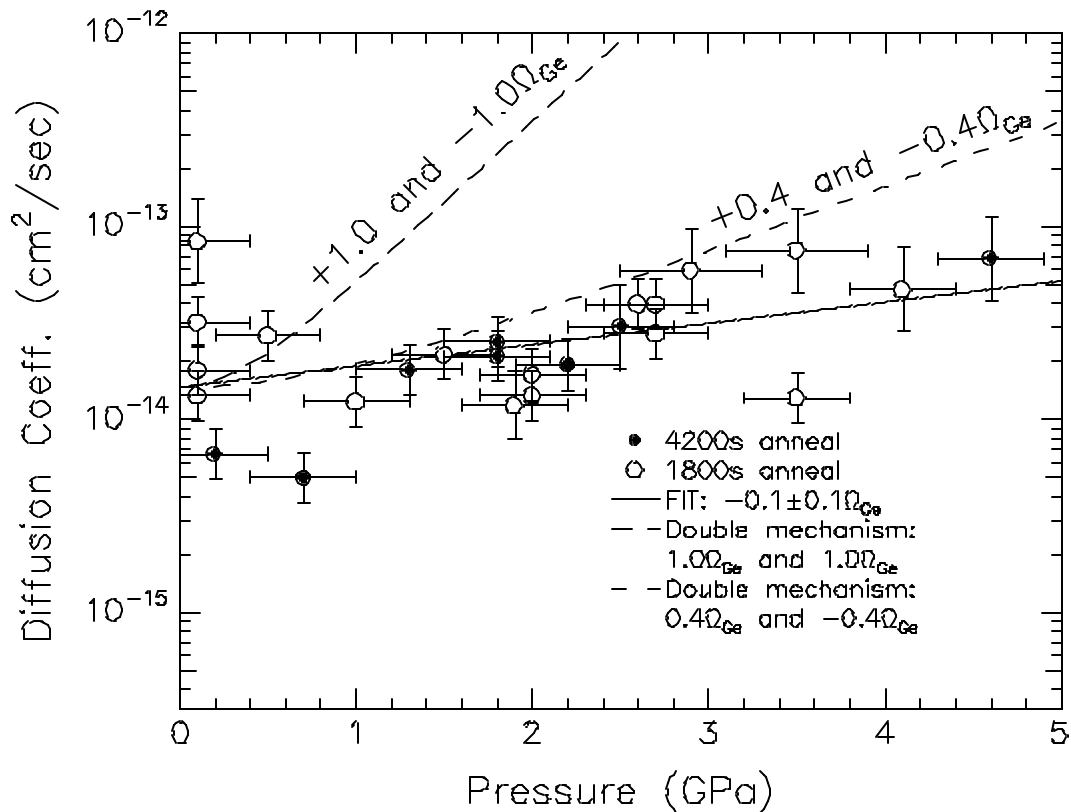
Fig. 5.3 graphically summarizes the arguments presented in the preceding three paragraphs on a plot of DV_m vs. DV_f . The experimental result, $DV_f + DV_m = -0.12 \pm 0.1 \Omega_{Ge}$, is shown as the diagonal region. Assuming a migration enthalpy of 0.36 eV and a limit on the critical pressure of 3.5 GPa (from Fig. 5.1) requires that the migration volume be greater than $-0.73 \Omega_{Ge}$. This region, marked as the region where migration enthalpy goes to zero, can be excluded from consideration. Therefore a formation volume of $+0.75 \Omega_{Ge}$ for a vacancy would require the migration volume to be in the excluded region. A



{tc "Figure 0.3. Plot to exclude regions in DV_f and DV_m space for the vacancy mechanism." \f}Figure 0.4. Plot to exclude regions in DV_f and DV_m space for the vacancy mechanism.

migration volume of zero, assumed by Werner *et al.*, would require the formation volume to be too small for a vacancy mechanism. Therefore we conclude that our experimental results cast serious doubt on a 100% vacancy mechanism.

However, multiple diffusion mechanisms may be operating in parallel. Fig. 5.4 shows a plot of the data compared to predictions for a pair of diffusion mechanisms with defects that have activation volumes of $+1.0 \Omega_{\text{Ge}}$ and $-1.0 \Omega_{\text{Ge}}$. The exponential prefactors D_0 have been adjusted such that at ambient pressure each defect contributes 50% to the transport and the total diffusion coefficient is equal to the experimental value. The plot clearly shows that our data are inconsistent with a double defect mechanism where the activation volumes are large and of opposite signs. However double mechanisms with activation volume magnitudes of less than about $0.4 \Omega_{\text{Ge}}$ and opposite signs cannot be clearly ruled out. Note that the relative contribution from the point defect with a positive activation volume rapidly decreases with pressure. Hence if the defect with the positive activation volume is making the major contribution to diffusion at ambient pressure then the activation volume plot will have a negative slope at very low pressure. This low pressure negative slope may not be visible due to the noise in the data. However at higher pressures the contribution from the defect with the negative activation volume will dominate. At higher pressures the data do not support a large positive slope; therefore we can clearly rule out any significant contribution from a diffusion mechanism that has a large and negative activation volume of magnitude greater than about $0.4 \Omega_{\text{Ge}}$.

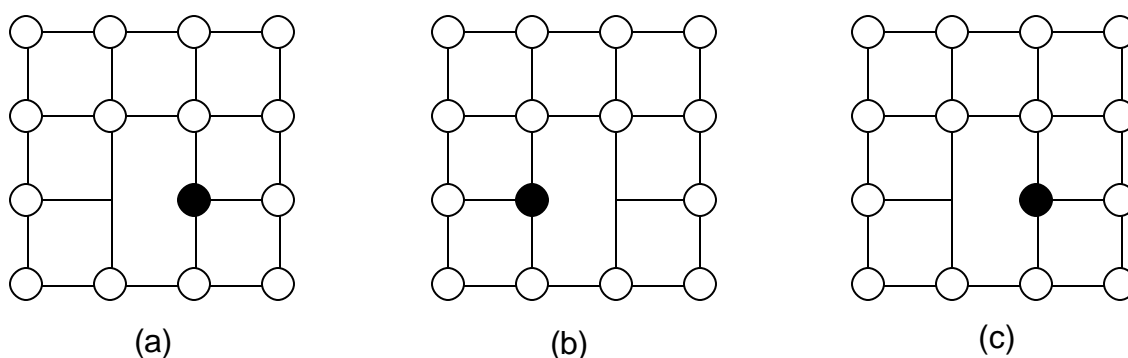


{tc "Figure 5.4. Double defect diffusion mechanism compared with data." \f}Figure 5.5. Double defect diffusion mechanism compared with data.

The experiment by Werner *et al.* is the principal evidence for the predominance of the vacancy mechanism in germanium. Their positive activation volume shows that the vacancy is the principal defect mediating self-diffusion in germanium. They also show that the negative vacancy is predominant and has a smaller activation volume. Because arsenic is a donor, an arsenic atom on the substitutional site in the lattice will be positively charged. Hence it would attract and bind to the negative vacancy. This binding would be stable because the arsenic would take the electron from the charged vacancy, form a lone pair, and become 3-fold coordinated. Calculations in silicon show that such binding results in the formation of

stable arsenic-vacancy complexes⁷⁴. Experiments in silicon also suggest a strong binding between arsenic atoms and vacancies^{Error! Bookmark not defined.,Error! Bookmark not defined.}. Hence we assume that negative vacancies in germanium and arsenic atoms on substitutional sites will attract and then form complexes. As shown in Section 0 the diffusion of arsenic and other donors is much faster than acceptor and self-diffusion in germanium. Because the negative vacancy is the predominant defect in germanium and should be strongly attracted to the donor atoms it has been suggested that it enhances their diffusion^{Error! Bookmark not defined.}⁷⁵. The dominance of the negative vacancy is further enhanced because the donor atoms increase the Fermi level, thereby increasing the concentration of negative vacancies. However in diamond cubic structures, the increased association of a vacancy with an impurity atom due to binding should not cause a large increase in the diffusivity of that impurity by the normal vacancy mechanism. This is because in diamond cubic structures the nearest neighbors do not share any other nearest neighbors. Therefore, for a vacancy on a lattice site next to an arsenic atom, any jump other than exchanging position with the arsenic atom will cause the dissociation of the vacancy arsenic pair. If there is any binding (and there are strong indications that there is) then the lowest energy jump will be for the arsenic and the vacancy to exchange positions. Hence the arsenic vacancy pair will be trapped, as they continue to exchange positions. A two dimensional schematic of this situation is shown in Fig. 5.5 and it is treated quantitatively in the Appendices. In Appendix A we develop a model to calculate a correlation factor that incorporates vacancy impurity binding and in Appendix B we use these results to calculate the effects of binding on impurity diffusivity via the vacancy mechanism. Our model shows that at 575 °C attractive binding of any magnitude will cause the diffusivity to be

enhanced at most by a factor of 2. At this temperature the diffusivity of arsenic in germanium is 3 orders of magnitude greater than self-diffusivity which is thought to be mediated by vacancies. Therefore it is unlikely that arsenic is diffusing via a normal vacancy mechanism. We note that the calculation of the correlation factor in Appendix A does not apply to delocalized or 'amorphous' vacancies proposed by Frank^{Error! Bookmark not defined.} and therefore they have not been ruled out.

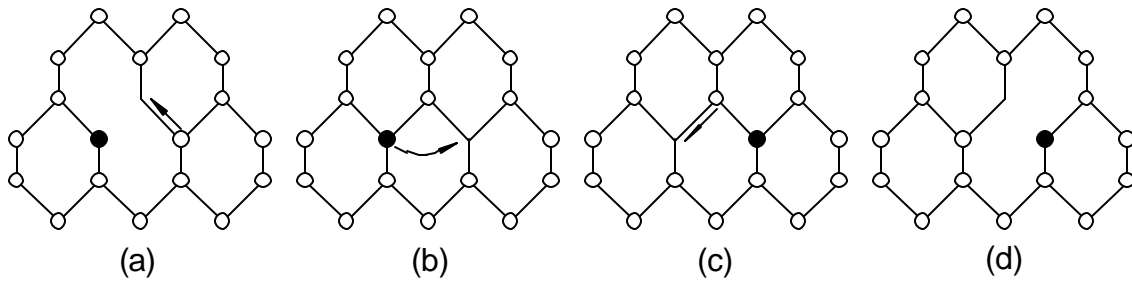


{tc "Figure 5.5. 3-Fold arsenic trapped in a 4-fold germanium lattice." \f f}Figure 5.6. 3-Fold arsenic trapped in a 4-fold germanium lattice.

Werner *et al.* have concluded that self-diffusion in germanium is mediated by vacancies. Copper has been shown to be diffusing in germanium via the Frank-Turnbull dissociative mechanism^{Error! Bookmark not defined.}. Based on these results, Frank^{Error! Bookmark not defined.} argued that the interstitial concentrations in germanium are much lower than the vacancy concentrations, and that the ratio of interstitial to vacancy concentrations falls with temperature. But because we have ruled out 100% transport by vacancies then interstitials by default may mediate diffusion. But in germanium donors are faster diffusers than acceptors or self diffusion. An interstitialcy diffusion mechanism for self-diffusion in germanium must be slower than the vacancy mechanism, or Werner *et al.* would have seen it. If we assume that the interstitialcy mechanism predominates for arsenic diffusion then there must

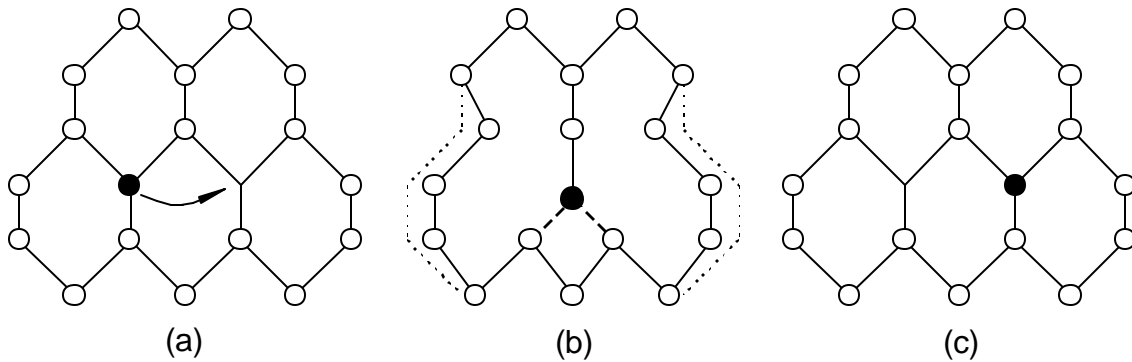
be some explanation why it is not the predominant mechanism for self-diffusion. One solution proposed by Frank⁷⁶ is that negative interstitials may be mediating arsenic diffusion in germanium. In such a case the preceding objections can be overcome. Increased association with interstitials does not reduce diffusivity in the diamond cubic structure because interstitials can move among interstitial sites while remaining adjacent to a substitutional impurity. Negative interstitials would then enhance the diffusion of donors with respect to self diffusion.

It is also possible that a more complex mechanism is operating with jumps between lattice sites that are not nearest neighbors. Based on bond counting arguments Kaxiras⁷⁷ has described such a vacancy assisted exchange mechanism which can lead to long range transport of arsenic. A schematic is shown in Fig. 5.6 with the arsenic atom in black. The six fold rings are projections of the (110) plane in the germanium lattice. Consider a vacancy arsenic complex in which the vacancy and arsenic have been exchanging frequently. On rare occasions a germanium atom moves into the vacancy as shown in (a), making the arsenic atom 4-fold coordinated and less stable. In this state it can perform a 'long' jump as shown in (b), where it is still 4-fold coordinated and subsequently a germanium atom jumps into the vacancy as shown in (c). The resulting state in (d) has the arsenic atom next to its vacancy. Because of the impurity atom 'swings' on single bond to make the jump Theiss⁷⁸ has proposed that it be called the Tarzan mechanism. It will be referred to as the *direct Tarzan mechanism*. Note that the vacancy makes a second nearest neighbour jump. However first principles calculations of the energetics involved are required to check the feasibility of such mechanisms.



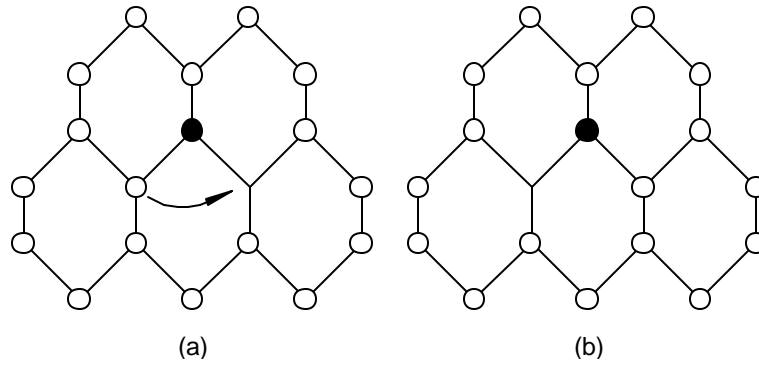
{tc "Figure 5.6. Direct Tarzan mechanism." \f}Figure 5.7. Direct Tarzan mechanism.

To assist the arsenic atom in making the jump to the next nearest neighbor, the germanium lattice may have to collapse down as is shown in Fig. 5.7. Hence we might expect a negative migration volume for the direct Tarzan mechanism.



{tc "Figure 0.7. Migration volume of the direct Tarzan mechanism." \f}Figure 0.8. Migration volume of the direct Tarzan mechanism.

Once next nearest jumps are considered then Aziz⁷⁹ has proposed that the presence of arsenic may allow an occasional next nearest jump for germanium as is shown in Fig. 5.8. This mechanism would permit the long range transport of the arsenic vacancy pair without dissociation. This mechanism will be referred to as the *indirect Tarzan mechanism*. However, like the previous case, first principles calculations have to be done on this mechanism to check its feasibility.



{tc "Figure 0.8. Indirect Tarzan mechanism." \f}Figure 0.9. Indirect Tarzan mechanism.

We conclude that the normal vacancy mechanism with only nearest neighbor jumps cannot be the predominant diffusion mechanism of arsenic diffusion in germanium. The interstitialcy and direct interchange mechanisms cannot be ruled out and some explanation is needed for the fast diffusion of donors in germanium. However some more complex mechanism may be operating.

6. Summary

The goal of this project was to design build and execute an experiment to measure the activation volume of arsenic diffusion in germanium. We have designed and developed an externally heated high temperature diamond anvil cell system. The pressure medium is liquid argon, which provides a chemically inert and hydrostatic environment. External heating allows for accurate control and measurement of the temperature. The pressure is measured at high temperatures using the shift in the peak positions of Sm:YAG fluorescence. We developed an optical system to acquire the Sm:YAG spectra. The optical system is designed for fast and efficient acquisition of the rather faint Sm:YAG fluorescence spectra. A protocol was developed for accurate and robust determination of pressure from the Sm:YAG spectra. The diffusivity was measured from sputter sectioning using a SIMS. A protocol was developed for doing SIMS analysis on very small samples.

For arsenic diffusion in germanium at 575 °C we measure an activation volume of $-0.12 \pm 0.1 \Omega_{\text{Ge}}$ where Ω_{Ge} is the atomic volume of germanium. Werner *et al.* **Error! Bookmark not defined.** have measured activation volumes for self-diffusion in germanium. Their results range from $+0.41 \Omega_{\text{Ge}}$ at 813 °C to $+0.24 \Omega_{\text{Ge}}$ at 603 °C. They conclude that germanium self diffusion occurs via the simple vacancy mechanism. The small and negative activation volume for arsenic diffusion in germanium, however, seems inconsistent with a simple vacancy diffusion mechanism. Werner *et al.* also show that neutral and negative singly charged vacancies mediate self-diffusion, and at 700 °C diffusion mediated by the negative vacancy predominates. The diffusion of donors in germanium is faster than that of acceptors or self diffusion. From

this it has been concluded **Error! Bookmark not defined.** that the attraction between donors and the negative vacancies is responsible for their faster diffusion. We show, however, that in diamond cubic lattices any binding between a vacancy and an impurity should not strongly enhance the impurity diffusion. Hence, we conclude that the simple vacancy mechanism is unlikely to mediate arsenic diffusion in germanium.

Appendix A

The Correlation Factor for Vacancy Mechanism in Diamond Cubic Structures with Vacancy Impurity Binding

The correlation factor for an impurity or tracer diffusion is given by⁸⁰

$$f = \frac{1 + \overline{\cos Q}}{1 - \overline{\cos Q}} \quad (\text{A.1})$$

where Q is angle between the direction vectors of two successive jumps of the diffusing atom. The average of the cosine of the angles is given by

$$\overline{\cos Q} = \sum_{k=1}^z P_k \cos Q_k \quad (\text{A.2})$$

where k are all the possible sites that the diffusing atom can reach in the next jump and P_k is the probability that the next jump is to site k . For diffusion mediated by a vacancy, the vacancy must first reach the designated site k and then exchange positions with the diffusing atom. Hence for vacancy diffusion

$$P_k = \sum_i P_{ki} \quad (\text{A.3})$$

where i are all the possible paths by which the vacancy can reach site k and P_{ki} is the probability that the vacancy travels the path i and then exchanges positions with the diffusing atom.

Consider a vacancy and an impurity atom held together with the standard free energy of binding DG_b . The vacancy can move by either exchanging lattice sites with the impurity atom or by exchanging with a neighboring matrix atom. From Fig. 5.4 we see that, in a diamond cubic crystal, if the vacancy exchanges lattice sites with a matrix atom then it must move away from the impurity atom. All exchanges with a matrix atom must then result in the breaking apart of the vacancy impurity complex. Assuming equal energy barrier heights for both these vacancy jumps, then

$$\frac{w_{mV}}{w_{dV}} \approx \exp\left(\frac{-DG_b}{kT}\right) \quad (\text{A.4})$$

where w_{dV} is the rate at which the vacancy exchanges lattice sites with the impurity atom and w_{mV} is the rate at which the vacancy exchanges lattice sites with a matrix atom. The probability that a vacancy exchanges sites with impurity atom is

$$P_{dV} = \frac{w_{dV}}{w_{dV} + 3w_{mV}} = \frac{1}{1 + 3B} \quad (\text{A.5})$$

where

$$B = \exp(-DG_b/kT). \quad (\text{A.6})$$

The probability that it exchanges sites with a particular matrix atom is

$$P_{mV} = \frac{w_{mV}}{w_{dV} + 3w_{mV}} = \frac{B}{1 + 3B}. \quad (\text{A.7})$$

We also assume that after the vacancy moves away from the impurity atom its motion becomes entirely random, which implies that the vacancy impurity binding operates only when they are on adjacent lattice sites.. Therefore the probability for any other vacancy jump is 1/4.

Consider an impurity atom d shown in Fig A.1 that has just moved from site $k = 1$. The vacancy that mediated its move is now located at site $k = 1$. For the atom to move into any site other than $k = 1$ will require the vacancy to come around to that site and then exchange with d . This process will require at least five steps for the vacancy. Using Eq. A.6 and A.7 the probability for all the paths with the vacancy moving up to five steps is calculated. The results are tabulated in Table A.1. Paths with an even number of steps do not move d . Note that paths with a greater number of steps become less probable but do not introduce terms with higher orders of B . B is only introduced into the calculation at the beginning and end of a path therefore all paths (except for the 1 step path) have the term $B/(1 + 3B)^2$.

Path	Probability d reaches $k = 1$ ($Q = 180^\circ$)	Probability d reaches $k = 2,3,4$ ($Q = 71^\circ$)
Vacancy Steps = 1	$\frac{1}{1+3B}$	0
Vacancy Steps = 3	$\frac{3}{4} \frac{B}{(1+3B)^2}$	0
Vacancy Steps = 5	$\frac{9}{64} \frac{B}{(1+3B)^2}$	$\frac{2}{64} \frac{B}{(1+3B)^2}$

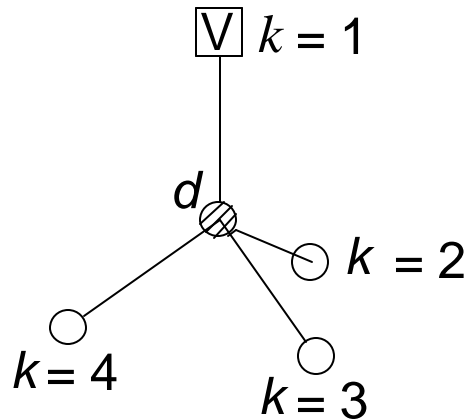
{tc "Table A.1 Calculation of Probabilities for different Diffusion Paths." \f t}Table A.1 Calculation of Probabilities for different Diffusion Paths.

Using the results in Table A.1 and Eq. A.2

$$\overline{\cos Q} = -\left(\frac{1+3.86B}{(1+3B)^2}\right) \quad (\text{A.8})$$

and then using Eq. A.1 gives

$$f = \frac{2.14B+9B^2}{2+9.86B+9B^2}. \quad (\text{A.9})$$



{tc "Figure A.1 Sites next to diffusing atom." \f f}Figure A.1 Sites next to diffusing atom.

If there is no binding between the impurity and the vacancy then $B = 1$ and we get $f = 0.53$. This number agrees very well with the reported calculated correlation factor for diamond cubic structures, $f = 0.5^{81}$. The implications of this correlation factor are discussed in Appendix B.

Appendix B

The effect Vacancy Impurity Binding on Vacancy Mediated Diffusivity in Diamond Cubic Structures.

For a vacancy impurity complex with a standard free energy of binding of $\mathbf{D}G_b$, the formation energy for the vacancy next to the defect becomes $\mathbf{D}G_f^0 - \mathbf{D}G_b$. Therefore the probability that the vacancy is next to the impurity is⁸²

$$P = \exp\left(\frac{-\mathbf{D}G_f^0 + \mathbf{D}G_b}{kT}\right) = \frac{\exp(-\mathbf{D}G_f^0/kT)}{B} \quad (\text{B.1})$$

where

$$B = \exp(-\mathbf{D}G_b/kT). \quad (\text{A.6})$$

Note that the probability of finding a vacancy next to the impurity has been enhanced by a factor of $\exp(\mathbf{D}G_b/kT)$.

By using the equation for diffusivity from Section 2.3,

$$D = fgnl^2 \exp(-\mathbf{D}G^*/kT), \quad (\text{2.5})$$

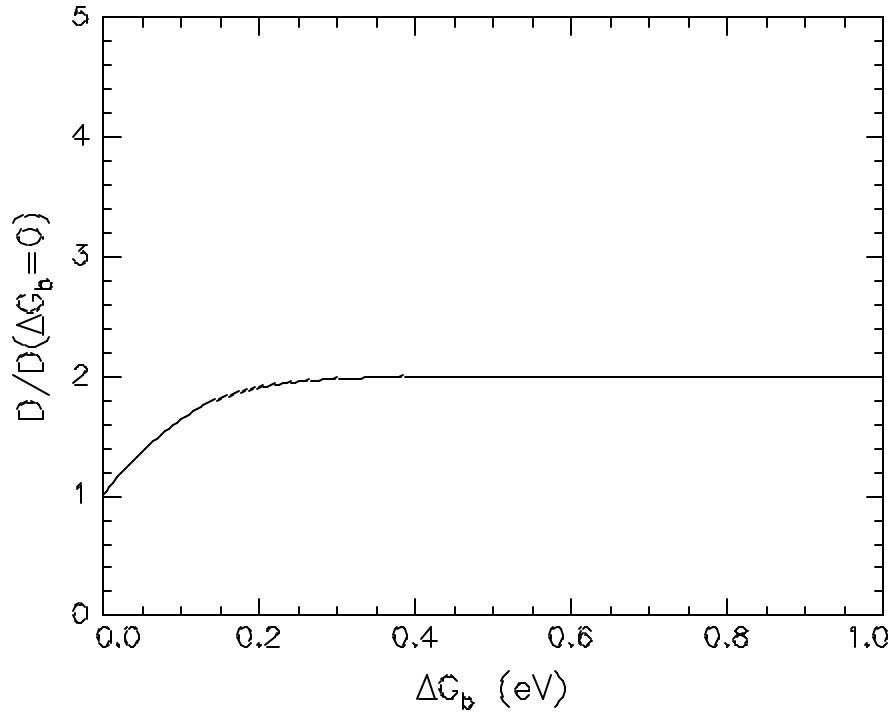
and using Eq. B.1 the diffusivity with vacancy impurity binding becomes

$$D = fgnl^2 \frac{\exp(-\mathbf{D}G^*/kT)}{B}. \quad (\text{B.2})$$

Incorporating the correlation factor determined in Appendix A (Eq. A.9) we get

$$D = gn l^2 \exp(-\mathbf{D}G^*/kT) \frac{2.14 + 9B}{2 + 9.86B + 9B^2}. \quad (\text{B.3})$$

The enhancement of diffusivity versus binding energy at 575 °C is plotted in Fig B.1. We conclude that, for the model used in Appendix A, attractive vacancy impurity binding cannot enhance diffusivity by more than a factor of 2 at this temperature.



{tc "Figure B.1. Enhancement to diffusivity from vacancy impurity binding at 575 °C." \f f}Figure B.1.
Enhancement to diffusivity from vacancy impurity binding at 575 °C.

By using the equation for the activation volume from Section 2.4,

$$DV^* = -kT \frac{\int \ln D}{\int p} \Big|_T + kT \frac{\int \ln(fgnl^2)}{\int p} \Big|_T, \quad (0.6)$$

and using the diffusivity from Eq. B.3 the activation volume with vacancy impurity binding becomes

$$DV^* = -kT \frac{\int \ln D}{\int p} \Big|_T + kT \frac{\int}{\int p} \ln \left(gnl^2 \frac{2.14 + 9B}{2 + 9.86B + 9B^2} \right) \Big|_T. \quad (B.4)$$

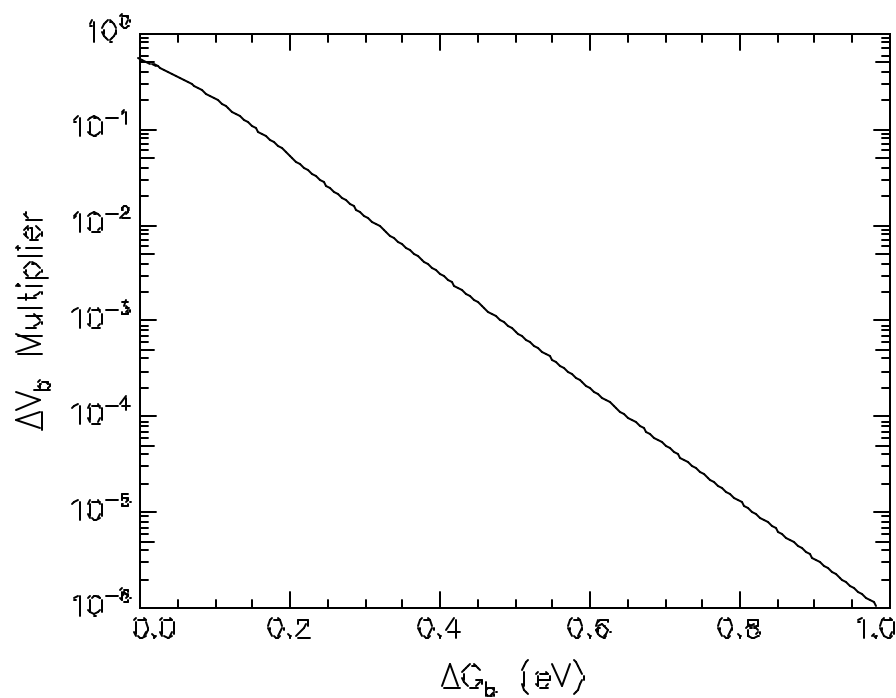
In Section 2.4 we show that the pressure dependence of n , g and l is negligible therefore Eq. B.4 simplifies to

$$DV^* = -kT \frac{\int \ln D}{\int p} \Big|_T + \left(\frac{9B}{2.14 + 9B} - \frac{9.86B + 18B^2}{2 + 9.86B + 9B^2} \right) DV_b \quad (B.5)$$

where

$$DV_b = \frac{\int DG_b}{\int p} \Big|_T \quad (B.6)$$

will be called the *binding volume*. It is due to the relaxation of the crystal as the vacancy and impurity come together but does not include the formation volume of the vacancy. Therefore no lattice point is created or annihilated in the formation of the impurity vacancy complex and the magnitude of the binding volume can be reasonably be expected to be substantially smaller than one lattice volume. The second term in Eq. B.5 will be called the *correction to the activation volume*, i.e. the product of the binding volume and its multiplier. This multiplier to the binding volume at a temperature of 575 °C is plotted in Fig. B.2. We see that this multiplier decays rapidly with increasing free energy of binding. Because the magnitude of the volume of binding will be of order unity or less, the correction to the activation volume will be negligible except for complexes with very low binding energies and large volume of binding.



{tc "Figure B.2. Multiplier to the binding volume vs. free energy of binding at 575 °C." \f f}Figure B.2.
Multiplier to the binding volume vs. free energy of binding at 575 °C.

For this thesis the correction to the activation volume can be considered significant only if it is equal to or greater in magnitude than the experimental error, i.e. $0.1 \Omega_{Ge}$. Fig. B.3, on a plot of DV_b versus DG_b , shows the region where the magnitude of this correction is less than $0.1 \Omega_{Ge}$ at 575 °C. For the model for diffusion used in Appendix A and any physically reasonable DV_b the correction to the activation volume is negligible for $DG_b > 0.15$ eV at 575 °C.

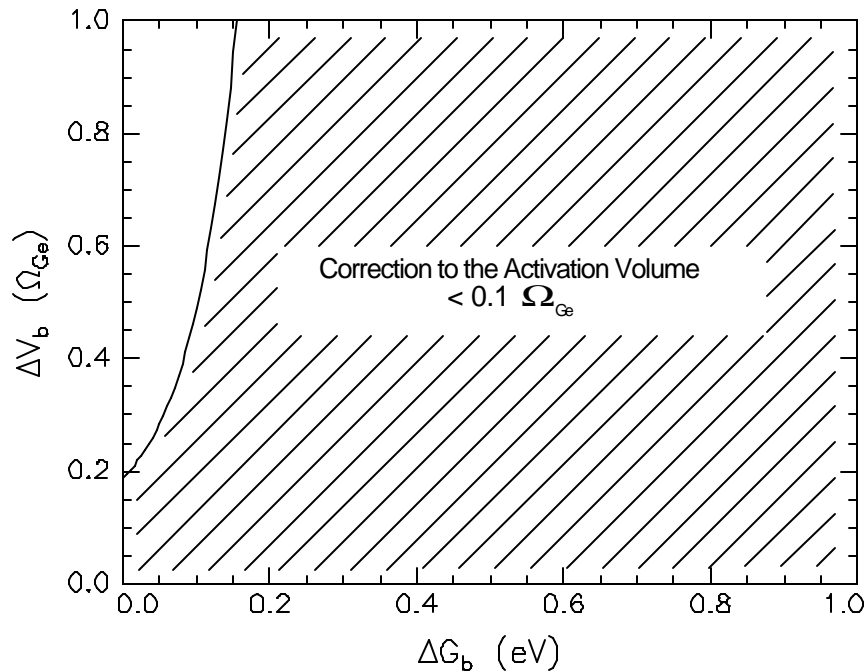


Figure B.3. Region in DG_b vs. DV_b space where the correction to the activation volume is insignificant at 575 °C.

For arsenic diffusion in silicon an experimental lower limit of 1.2 eV for the *binding enthalpy* has been reported^{Error! Bookmark not defined.,Error! Bookmark not defined.}. Scaling with the bond strength ratios of germanium to silicon gives a lower limit of 0.91 eV for the binding enthalpy of an arsenic vacancy complex in germanium. No estimates for the entropy of binding have been reported, therefore we will use vacancy formation entropy as an approximation for the entropy of binding. It should be noted that vacancy formation is probably a

more energetic event than the formation of a vacancy arsenic complex and therefore the vacancy formation entropy is probably an upper limit for the entropy of binding. The formation entropy for vacancies is thought to range from $6k$ to $10k$ in silicon and is based on estimates of defect concentrations **Error! Bookmark not defined.** Using an entropy of binding of $10k$ and the enthalpy lower limit of 0.91 eV gives a lower limit of 0.21 eV for the free energy of binding for an arsenic vacancy complex in germanium at 575 °C. We therefore conclude that the correction to the activation volume is probably insignificant at 575 °C.

References

- ¹ R. J. Borg and G. J. Dienes, *An Introduction to Solid State Diffusion*. (Academic Press, San Diego, 1988), p. 198.
- ² C. S. Nichols, C. G. Van de Walle and S. T. Pantelides, *Phys. Rev. B*, **40**, 5484 (1989).
- ³ P. M. Fahey, P. B. Griffen and J. D. Plummer, *Rev. Mod. Phys.* **61**, 289, (1989).
- ⁴ H. Mehrer and A. Seeger, *Crys. Latt. Def.* **3**, 1 (1972).
- ⁵ R. H. Dickerson, R. C. Lowell and C. T. Tomizuka, *Phys. Rev.* **137**, A613 (1965)
- ⁶ J. N. Mundy, *Phys. Rev. B*, **3**, 2431 (1971).
- ⁷ M. Werner, H. Mehrer and H. D. Hochheimer, *Phys. Rev. B*, **32**, 3930 (1985).
- ⁸ E. Nygren, M. J. Aziz, D. Turnbull, J. M. Poate, D. C. Jacobson and R. Hull, *Appl. Phys. Lett.* **47**, 105, (1985).
- ⁹ M. J. Aziz, E. Nygren, W. H. Christie, C. W. White and D. Turnbull, in *Impurity Diffusion and Gettering in Silicon*, edited by R. B. Fair, C. W. Pearce and J. Washburn, *Materials Research Symposia Proceedings*, Vol. 36 (Materials Research Society, Pittsburg, PA, 1985), p. 101.
- ¹⁰ U. Södervall, M. Friesel and A. Loddding, *J. Chem. Soc. Faraday Trans.* **86**, 1293 (1990).
- ¹¹ P. G. Shewmon, *Diffusion in Solids*, (J. Williams Book Company, Jenks OK, 1983), p. 2.
- ¹² K. C. Pandey, *Phys. Rev. Lett.* **57**, 2287 (1986).
- ¹³ P. Haasen, *Physical Metallurgy*, 2nd ed. (Cambridge University Press, Cambridge UK), p. 170.
- ¹⁴ W. Frank in *Crucial Issues in Semiconductor Materials and Processing Technologies*, edited by S. Coffa, (Kluwer Academic Publishers, The Netherlands, 1992), p. 383.
- ¹⁵ W. Frank , U. Gösele, H. Mehrer and A. Seeger, in *Diffusion in Crystalline Solids*, edited by G.E. Murch and A.S. Norwick (Academic Press, Orlando, FL, 1984), p. 63.
- ¹⁶ F. C. Frank and D. Turnbull, *Phys. Rev.* **104**, 617 (1956).
- ¹⁷ U. Gösele, W. Frank, A. Seeger, *Appl. Phys. A*, **23**, 361 (1980).
- ¹⁸ P. G. Shewmon, *Diffusion in Solids*, (J. Williams Book Company, Jenks Oklahoma, 1983), p. 52
- ¹⁹ G.H. Vinyard, *Phys. Chem. Solids*, **3**, 121 (1957).
- ²⁰ D. Lazarus in *Solid State Phys.* **10**, 190 (1960).

- ²¹ R. J. Borg and G. J. Dienes, *An Introduction to Solid State Diffusion*, (Academic Press, San Diego, 1988), p. 66.
- ²² R. N. Jefferey and D. Lazarus, *J. Appl. Phys.* **41**, 3186 (1970).
- ²³ F.P. Larkins and A.M. Stoneham, *J. Phys. C*, **4**, 143 (1971); **4**, 154 (1971).
- ²⁴ G.A. Baraff, E.O. Kane and M. Schluter, *Phys. Rev. B*, **21**, 5662 (1980).
- ²⁵ U. Lindefelt, *Phys. Rev. B*, **28**, 4510 (1983).
- ²⁶ M. Scheffler, J.P. Vigneron and G.B. Bachelet, *Phys. Rev. B*, **31**, 6541 (1985).
- ²⁷ R. J. Borg and G. J. Dienes, *An Introduction to Solid State Diffusion*, (Academic Press, San Diego, 1988), p. 187.
- ²⁸ S. M. Hu, *Mat. Sci. and Eng. Repts.* **13**, 105 (1994).
- ²⁹ N. A. Stolwijk, W. Frank, J. Hölzl, S. J. Pearton and E. E. Haller, *J. Appl. Phys.* **57**, 5211 (1985).
- ³⁰ H. C. Casey, Jr. and G. L. Pearson, in *Diffusion in Semiconductors*, Vol. 2, edited by J. H. Crawford and L. M. Slifkin (Plenum Press, New York, 1975), p. 163.
- ³¹ W. Frank and N. A. Stolwijk, *Mater. Sci. Forum*, **15-18**, 369 (1987).
- ³² E. I. Blount, *J. Appl. Phys.* **30**, 1218 (1959).
- ³³ G. D. Watkins, R. P. Messmer, C. Weigel, D. Peak and J. W. Corbett, *Phys. Rev. Lett.* **27**, 1573 (1971).
- ³⁴ G. D. Watkins, J. D. Troxwell, A. P. Chatterjee, *Inst. Phys. Conf. Ser.* **46**, 16 (1979).
- ³⁵ G. D. Watkins in *Defects in Semiconductors*, edited by J. Narayan and T. Y. Tan (North Holland, New York), p. 21.
- ³⁶ S. Mizuo and H. Higuchi, *Jpn. J. Appl. Phys.* **21**, 281 (1982).
- ³⁷ S. M. Hu, *J. Appl. Phys.* **45**, 1567 (1974).
- ³⁸ M. Hirata, M. Hirata and H. Saito, *J. Phys. Soc. Jpn.* **27**, 405 (1969).
- ³⁹ A. Antonelli and J. Bernholc, *Phys. Rev. B*, **40**, 10643 (1989).
- ⁴⁰ G. Rein and H. Mehrer, *Philos. Mag. A*, **45**, 467 (1982).
- ⁴¹ W. Shockley and J. Last, *Phys. Rev.* **107**, 392 (1957).
- ⁴² U. Södervall, A. Lodding and W. Gust, *Defect and Diffusion Forum*, **66-69**, 415 (1989).
- ⁴³ F. R. Boyd and J. L. England, *J. Geophys. Res.* **65**, 741 (1960).
- ⁴⁴ C. Agee (private communication).
- ⁴⁵ G. L. Olsen and J.A. Roth, *Mat. Sci. Reports*, **3**, 1 (1988).
- ⁴⁶ G. Q. Lu, E. Nygren and M.J. Aziz, *J. Appl. Phys.* **70**, 5323 (1991).
- ⁴⁷ D. A. Young, *Phase Diagrams of the Elements*, (U. of California Press, Berkeley, 1991).
- ⁴⁸ M. J. Aziz, P. C. Sabin and G. Q. Lu, *Phys. Rev. B*, **44** 9812, (1991).
- ⁴⁹ A. Jayarman, *Rev. Mod. Phys.* **55**, 65, (1983).
- ⁵⁰ David Schiferl (private communication).
- ⁵¹ L. Merrill and W. A. Bassett, *Rev. Sci. Instrum.* **45**, 290 (1974).
- ⁵² Parts fabricated from Inconel have to be annealed at approximately 750 °C for approximately 10 hours to achieve their optimal strength. Further annealing at higher temperatures reduces their strength. See e.g. *The*

- Metals Handbook, Vol 1*, 10th ed. (American Society for Metals, Cleveland OH, 1990).
- ⁵³ Manufacturer's Specifications; Haynes International Inc. Kokomo, Indiana.
- ⁵⁴ D. M. Adams and A. G. Christy, *High Temp. High Press.* **24**, 1, (1992).
- ⁵⁵ J. Crank, *The Mathematics of Diffusion*, 2nd ed. (Clarendon Press, Oxford), p. 104.
- ⁵⁶ W.C. Dunlap Jr. *Phys. Rev.* **94**, 1531 (1954).
- ⁵⁷ R. A. Forman, G. J. Piermarini, J. D. Barnett and S. Block, *Science*, **176**, 284 (1972).
- ⁵⁸ G. Q. Lu, Ph.D. thesis, Harvard University, 1990.
- ⁵⁹ N. Hess and D. Schiferl, *J. Appl. Phys.* **71**, 2082 (1992).
- ⁶⁰ A. Yariv, *Quantum Electronics*, 2nd ed. (John Wiley & Sons, New York, 1975), p. 154.
- ⁶¹ J. C. Vickerman, in *Secondary Ion Mass Spectroscopy; Principles and Applications*, edited by J.C. Vickerman, A. Brown and N. M. Reed (Clarendon Press, Oxford, 1989), p. 1.
- ⁶² R. G. Wilson, F.A. Stevie, C.W. Magee, *Secondary Ion Mass Spectrometry; A Practical Handbook for Depth Profiling and Bulk Impurity Analysis* (John Wiley & Sons, New York, 1989).
- ⁶³ *ibid.* p. 1.2-1.
- ⁶⁴ *ibid.* p. App. F.2.
- ⁶⁵ *ibid.* p. 3.1-1.
- ⁶⁶ D. Schiferl, (Private Communication).
- ⁶⁷ G. D. Watkins, in *Lattice Defects in Semiconductors, 1974*, edited by F. A. Huntley (Institute of Physics Conference Series, **23**, London, 1974) p. 1.
- ⁶⁸ G. D. Watkins, J. R. Troxell and A. P. Chatterjee, in *Defects and Radiation Effects in Semiconductors, 1978*, edited by J. H. Albany (Institute of Physics Conference Series, **46**, London, 1978) p. 16.
- ⁶⁹ J. L. Newton, A. P. Chatterjee, R. D. Harris and G. D. Watkins, *Physica (Utrecht)*, **116B**, 219 (1983).
- ⁷⁰ A. Seeger, H Föll and W. Frank in *Radiation Effects in Semiconductors, 1976*, edited by N. B. Urli and J. W. Corbett (Institute of Physics Conference Series, **31**, London, 1976) p. 12.
- ⁷¹ F. Morehead, in *Defects in Electronic Materials*, edited by M. Stavola, S. J. Pearton and G. Davies (Materials Research Society Symposium Proceedings, **104**, 1987) p. 99.
- ⁷² S. Dannefaer, P. Mascher and D. Kerr, *Phys. Rev. Lett.* **56**, 2195 (1986).
- ⁷³ R. M. Emrick, *Phys. Rev.* **122**, 1720 (1961).
- ⁷⁴ E. Kaxiras, (private communication).
- ⁷⁵ R. J. Borg and G. J. Dienes, *An Introduction to Solid State Diffusion*. (Academic Press, San Diego, 1988), p. 196.

⁷⁶ W. Frank (private communication).

⁷⁷ E. Kaxiras (private communication).

⁷⁸ S. D. Theiss (private communication)

⁷⁹ M. J. Aziz (private communication).

⁸⁰ A. D. Le Claire and A. B. Lidiard, *Phil. Mag.* **1**, 518 (1956).

⁸¹ R. J. Borg and G. J. Dienes, *An Introduction to Solid State Diffusion*. (Academic Press, San Diego, 1988), p. 72.

⁸² S. M. Hu, *Phys. Rev.* **180**, 773 (1969).